VIGNETTES ON PRESERVATION, PREPARATION, AND PALEOECOLOGY

A Dissertation presented to the Faculty of the Graduate School

at the University of Missouri – Columbia

In Partial Fulfillment of the Requirements for the Degree

Doctor of Philosophy

by

Gabriel Shai Jacobs

Dr. John Warren Huntley

Doctoral Advisor

JULY 2022

The undersigned, appointed by the Dean of the Graduate School, have examined the dissertation entitled

VIGNETTES ON PRESERVATION, PREPARATION, AND ECOLOGY

presented by Gabriel S. Jacobs,

a candidate for the degree of Doctor of Philosophy,

and hereby certify that, in their opinion, it is worthy of acceptance.

Professor John W. Huntley

Professor Sarah M. Jacquet

Professor Tara Selly

Professor James D. Schiffbauer

Professor Kenneth G. MacLeod

Professor Kevin M. Middleton

DEDICATIONS

I thank my parents, Paul M. Jacobs and Susan J. Dickman, for their patient and loving support of my personal and academic ambitions, through times joyous and trying. I thank my step-parents, Helen Crowley and Dr. Adrian Gross, for their kind words of guidance and encouragement, and am proud to call them family. I thank my siblings, Amit M. Jacobs and Noam V. Jacobs, for their fraternal love and goodwill, and hope I have not been too difficult with them. I honor the memories of my grandparents: Mort Jacobs, Helen Jacobs, Dr. Maurice Dickman, and Sylvia Dickman, and hope that this achievement does their legacy proud.

I thank my fiancée, Kyana Williams, for her devotion, patience, and humor throughout my years of graduate school, far-flung by geography but brought close by bonds of love.

I thank the members of my masters committee: Dr. Jesse R. Carlucci, Dr. Jonathan D. Price, Dr. Raymond E. Willis, and Dr. C. Matthew Watson, for their input and mentorship that has helped me to reach this point. I likewise thank my current committee members, especially Dr. John W. Huntley, for their moral support and patience. I thank my fellow graduate students: Y. Ranjeev Epa, Laura E. Speir, Kimberly D. Moore, Jeremy L. Webb, and Jeffrey S. Snowden among too many others to list, for their friendship and camaraderie through the ordeals of graduate education (for many, during a pandemic).

I would like to acknowledge the following artists, whose music has lifted my spirits during the long hours of experimentation and writing: REM, Emerson Lake & Palmer, the Grateful Dead, Digital Underground, the Quintette du Hot Club de France, Here Come The Mummies, ЯUSSKAJA, Rush, Talking Heads, The Ocean Collective, TWRP, Gorillaz, Genesis, Yes, Frank Zappa and the Mothers of Invention, Sophus Alf Agerbæk-Larsen, Dire Straits, Mcbaise, and Das Racist.

ACKNOWLEDGMENTS

I am grateful to Dr. John W. Huntley, Dr. Sarah M. Jacquet, Dr. Tara Selly, Dr. James D. Schiffbauer, Dr. Kenneth G. MacLeod, and Dr. Kevin M. Middleton for their assistance in designing the studies making up this dissertation, in sample preparation and imaging, and in general guidance throughout my PhD.

Dr. Jesse R. Carlucci graciously provided field notes for the Strasburg Junction site. Y. Ranjeev Epa assisted with identification of bivalves.

Radiocarbon dating services were provided by Darrell Kaufman and Jordon Bright at the Northern Arizona University Amino Acid Geochronology Lab.

L.G. Huntley assisted with field work and data collection. B. Kort (Island County Mapping Center) granted access to the shaded relief map of Whidbey Island.

This research is supported by NSF EAR CAREER (1650745), by the Alexander von Humboldt Stiftung, by a Yochelson Student Research Award from the Paleontological Society, by a Graduate Student Research grant from the Geological Society of America, and by a graduate student research grant and the Leonard Harris and Maurice Mehl scholarship funds of the University of Missouri Department of Geological Sciences.

TABLE OF CONTENTS

LIST OF FIGURES

LIST OF TABLES

ABSTRACT

Preservation exercises strong control over what can be observed and interpreted from the fossil record. The research projects presented here seek to examine the ways in which certain preservational types clarify some aspects of the paleoenvironments they chronicle while obscuring others. From the Holocene of the Salish Sea, the pristine condition of original bivalve shell material tells a story of parasitic interactions usually obliterated in older fossils by the coarsening effects of diagenesis. Drawing on this well-preserved material, we hope to characterize how parasitism pressure in coastal bivalves has changed during the Holocene. Meanwhile, Upper Ordovician rocks from the Shenandoah Valley of Virginia contain a preservational double-bill, with fine-detailed silicification and incomplete pyritization cropping up side-by-side with potentially starkly different taxonomic and body-size biases and biogeochemical requirements. Based on the simultaneous presence of these two preservational types, we ask: what kinds of organisms are preserved through one pathway or the other, and which survive preparation? And how do different preparation styles affect paleobiological interpretation of a deposit? Rather than a single cohesive program of research, I present three vignettes on preservation, preparation, and paleoecology.

Chapter 1: Introduction

Themes

The "preservational window" in paleoecology

All aspects of paleontology are defined and bounded by the incompleteness of the fossil record. Where neontologists may pick and choose for focused study any spot on the expansive vista of the natural world, paleontologists are limited to tightly restricted glimpses through the inky veil of the vanished past. This field is one of accommodations and workarounds, of extracting the most information from the limited material available to us, and of refining methods of interpreting that information.

A judicious look through one of these "preservational windows" can reveal a great deal of what lies beyond it; a handful of shells and the marks left on them by predators and parasites may be enough to reconstruct the teeming network of fauna within a lagoon, and a thin layer of exceptionally preserved sediments can breathe life and color into the conceptual sketch of an ancient ocean. But as always, it is important to consider the limits of what is accessible to the observer and what blind spots might lie within it, to consider the unknown unknown and beware that which lies just out of the frame of view. All reconstructions of the past must bear in mind the potential for bias introduced by the vagaries of preservation and the particulars of preparation, and when possible, account for known sources of bias.

The importance of quantitative approaches

The reconstruction and interpretation of past ecosystems is particularly vulnerable to biases and limitations of the fossil record. Ecosystems of the present and of the past are

complex, and even small errors can affect study conclusions in unpredictable ways. The projects in this program of research have focused on questions of paleoecological relevance, harnessing modern computing methods to provide quantitative answers with statistical rigor.

Goals

Characterization of parasitism regimes in glaciomarine sediments with comparison to modern settings

Parasites are important components of modern ecosystems, modulating the flow of resources through trophic webs throughout the biosphere, and this is generally understood to be true of past environments as well. However, most parasites are soft-bodied and have almost no preservation potential, limiting their fossil record to traces left on their more durable hosts. With this limitation in mind, documenting such traces when a taphonomic window allows is crucial to reconstructing host-parasite dynamics of past ecosystems for comparison to modern analogues. This goal underlies the first study in this work, an assessment of the prevalence and distribution of digenean parasites in bivalve hosts in latest Pleistocene and Recent Puget Sound.

Assessment of biases in descriptive and quantitative paleobiology/paleoecology associated with preparation type

The second and third studies turn to biases in preservation and preparation of silicified fossils, quantifying differences in interpretation of fauna and paleoenvironments between two preparation methods. Silicified fossils in limestone are commonly extracted using acid maceration, a chemical preparation technique, which may result in differential

recovery of fossils based on body size or taxonomic affinity. By pairing this form of destructive preparation with a non-destructive 3-D X-ray imaging method, it is possible to compare the results of the two methods in order not only to characterize the advantages and drawbacks of the methods with regard to recovery of information from samples, but also to quantify the biases of each and their effects on interpretation of paleoecology of the site.

Chapter 2: Taphonomy, ecology, and parasitism of coastal bivalve assemblages – Whidbey Island, Salish Sea, US

Introduction

Parasites play major roles in modulating energy flow through many ecosystems today, exerting selective forces on their hosts and frequently shaping community structure (Hudson et al., 2006; Kuris et al., 2008; Mouritsen & Poulin, 2002, 2005). While it is likely that they have had similar importance throughout the Phanerozoic, most obligate parasites are soft-bodied (due to their lack of a free-living habit) and have low preservation potential, leaving them generally absent from the fossil record (de Baets et al., 2021; Leung, 2017; Morris, 1981).

Additionally, body fossils of parasites record little of their life habit if not found with their hosts, leaving their paleoecological significance ambiguous (Walossek et al., 1994). When obligate parasites are preserved separately from their hosts it is by definition an atypical and displaced condition for the organism, which interferes with documentation of its life habit and interactions.

These two issues can be addressed simultaneously through study of the characteristic traces left by parasites on the hard parts of their hosts, recording not only the presence of the parasite but its interaction with other organisms (de Baets & Huntley, 2021a, 2021b; Zhang et al., 2020). A key example of such interactions in the fossil record is the distinctive pits left on the shells of bivalves by the metacercaria-stage larvae of digenean trematodes of the family Gymnophallidae (Huntley et al., 2021; Huntley & de Baets, 2015; Ruiz & Lindberg, 1989). These parasitic flatworms are widely known today

as infesters of infaunal bivalves, with both ecological and aquacultural importance (Cremonte & Ituarte, 2003; Paladini et al., 2017). Since their definitive hosts are shorebirds, gymnophallids (and other digeneans with similar life habits) often alter the burrowing behavior of infested hosts to increase the likelihood of predation and therefore improve their own chances of reproduction (Addino et al., 2010; Mouritsen & Poulin, 2005). Despite their diminutive size and low preservation potential, these parasites can have outsize effects on coastal food webs and nutrient cycling, effects that go unrecognized in the past if their agents are not detected in the fossil record.

Fortunately, bivalve shells with excellent preservation can preserve the pits characteristic of trematode infestation. Traces reliably attributable to gymnophallids are present as far back as the Cretaceous, a first appearance consistent with the emergence of their definitive hosts (shorebirds) between the Cretaceous and Eocene (de Baets et al., 2015; Rogers et al., 2018; Todd & Harper, 2011). The Cenozoic record of these traces remains patchy, however, as they are easily obliterated or degraded beyond recognition by taphonomic forces (Huntley & de Baets, 2015).

The record of gymnophallid-bivalve parasitic interactions is best in the recent (Pliocene and younger) past (Huntley & de Baets, 2015; Ruiz & Lindberg, 1989), including fossiliferous deposits of Pleisto-Holocene age from Whidbey Island in Puget Sound, Washington. These sediments apparently record rapid transgression during the last glacial retreat, though reworking by mass wasting makes their true age difficult to definitively constrain (Domack, 1983). Previous studies suggest that transgressive episodes may increase the prevalence of trematode parasitism in coastal environments (Huntley et al., 2014; Huntley & Scarponi, 2012, 2015; Scarponi et al., 2017); since the

taxa present in the sediments are found also in adjacent modern environments, live-dead comparisons can be used to test for this possible effect.

Our central question is: how have shallow-marine ecosystems in the Salish Sea changed throughout the Holocene? How do modern parasitism regimes affecting bivalves compare to those of the geologically recent past? Does sea level change play a major role in parasite-host population dynamics?

Materials and Methods

Sample collection and preparation

Eleven ~3.75 l bulk samples of beach death assemblages and *in situ* shell beds were collected on Whidbey Island, WA in October 2017 (Figure 1). Three bulk samples (EL17-1, EL17-2, and EL17-3) were collected from a previously unmapped, 10–15 cm thick shell bed that directly underlies an unconsolidated conglomerate unit mapped as Late Pleistocene to Holocene mass wasting deposits (Qmw) at the EL17 location near Ebey's Landing (Polenz et al., 2005). The shell bed is located on the beach southeast of the parking area where Hill Road begins its ascent uphill toward the southeast. Bivalves in the shell bed display a high degree of disarticulation and fragmentation and the bed is overlain by cobbles resting in concave-up valves. The three samples were collected along a 10 m traverse of the exposure. Three shell bed bulk samples (OHSB-1, OHSB-2, and OHSB-3) and three beach death assemblage bulk samples (OHDA-1, OHDA-2, and OHDA-3) were collected near Monroe Landing. The shell bed is approximately 20 cm thick and has a high degree of disarticulation for bivalves that are generally concave up. This shell bed is overlain by darker, shell-poor pebbly sand. The shell bed is laterally continuous for tens of meters. The death assemblage has the appearance of a fresh

accumulation of valves, with periostracum still apparent on many individuals, and has a high abundance of mytilids. These bulk samples comprise the upper 2-3 cm of a 1 m^2 surface. This location has been mapped as Late Pleistocene to Holocene beach (Qb) and marsh (Qm) deposits (Polenz et al., 2005). Two death assemblages bulk samples were collected along the strandline at Double Bluff, an outcrop which primarily comprises Pleistocene glacial and non-glacial deposits (Polenz et al., 2006). The shell concentrations were much less dense at Double Bluff than at the previous two locations. DBDA-1 is composed of every shell and fragment from the surface of an approximately 2

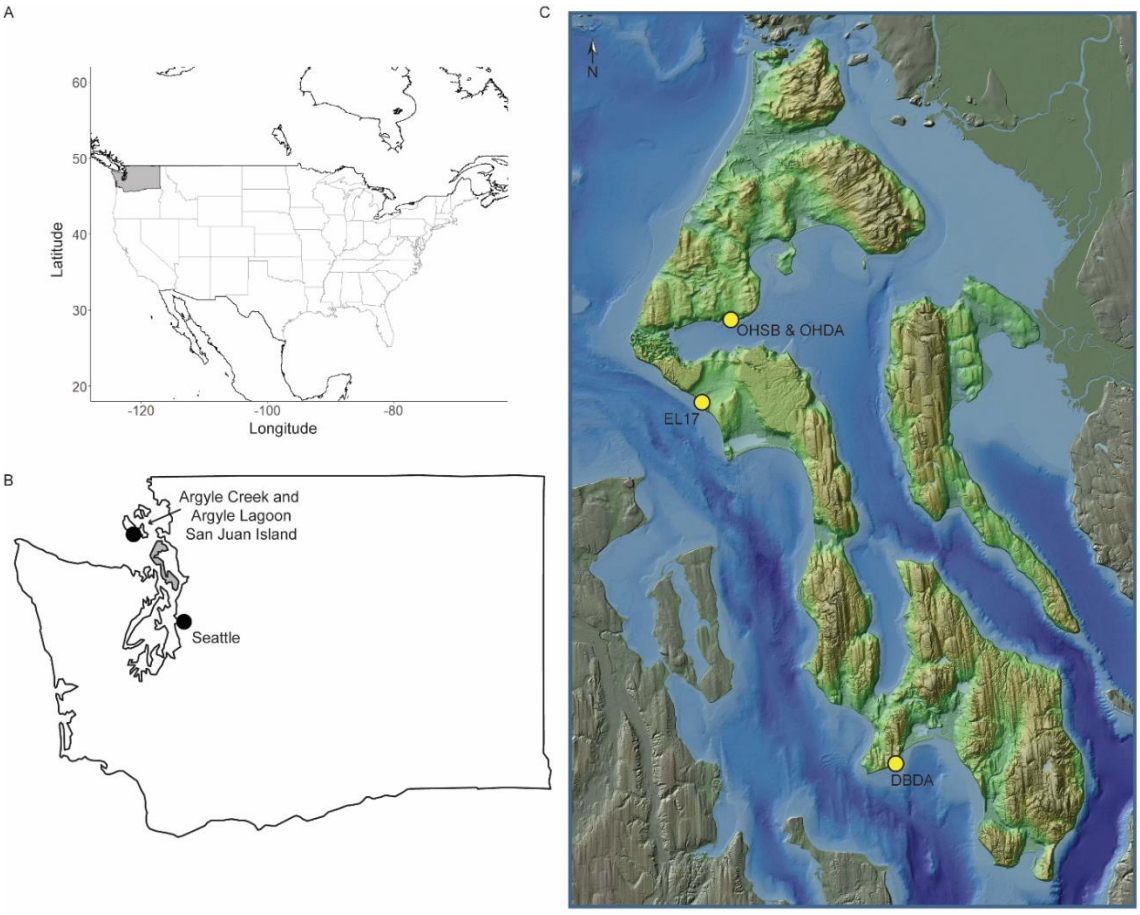

Figure 1: Location map of study area

(A) US map, (B) map of Washington, (C) relief map of Whidbey Island

Shaded relief map made available from the Island County Mapping Center (https://www.islandcountywa.gov/maps/Pages/Home.aspx).

m by 10 m transect running parallel to the shoreline. DBDA-2 comprises every shell and fragment on the surface from a 2 m by 20 m transect also parallel to the shoreline.

All samples were washed on a 2 mm sieve and all whole valves and unique, identifiable fragments were identified (Kozloff, 2000). Material within each subsample was sorted by taxon, with mollusks being identified to the species level. Each taxon was counted for minimum number of individuals, with paired articulated valves counted as 1 individual and isolated disarticulated valves counted as 0.5 individuals for bivalves. Valves were counted only if they contained the umbo, and were classified as non-unique fragments (and not counted towards taxon abundance) otherwise. For gastropods, each valve was counted as 1 individual; for polyplacophorans, every 8 valves were counted as 1 individual. For echinoids, crustaceans, and osteichthyans, all material was treated as fragmentary and non-unique. Taxon abundance for each subsample was scored as either absent (0 individuals, no fragmentary material), present (0 individuals, fragmentary material identified), or by number of individuals.

Low-precision radiocarbon dating

Well-preserved bivalve specimens without evidence of corrasion, encrustation, and boring were selected evenly across sampling locations and species for low-precision radiocarbon dating. These specimens were typically identifiable, non-unique fragments.

Sample preparation at Northern Arizona University Amino Acid Geochronology Laboratory followed the protocols modified from Bush et al. (2013). Blanks, standards, and unknowns were sonicated in deionized distilled water (DDI water; 16.7 Mohm*cm), rinsed three times with DDI water, leached with 2N ACS grade hydrochloric acid, and

then finally rinsed three times with DDI to remove surface contaminants before being dried in a 50° C oven overnight. Samples for direct carbonate ^{14}C analysis were ground to a fine powder using an agate mortar and pestle and manually mixed with 6.0 to 7.0 mg of niobium powder (Alfa Aesar Puratronic, -325 mesh, 99.99%) in Kimble borosilicate glass culture tubes (6 mm OD x 50 mm) that were pre-baked at 500° C for 3 hours. Powdered carbonate sample masses ranged between 0.30 and 0.50 mg, which equates to 36 to 60 µg of carbon, respectively. The culture tubes were flushed with N_2 gas to reduce contamination from atmospheric carbon and capped with Supelco plastic column caps (1/4" OD) until the carbonate-niobium powder mixture was pressed into targets.

The carbonate-niobium mixtures were pressed into pre-drilled (4.1 mm depth) aluminum targets at 400 psi, rotated 90°, and pressed again at 400 psi. The pressed targets were sent to UCI for AMS 14C analysis (Southon & Santos, 2007). Radiocarbon concentrations are given as percent of the Modern (pMC) standard following the conventions of Stuiver & Polach (1977). Sample preparation backgrounds have been subtracted based on measurements of ^{14}C-free calcite (IAEA C1) using an isotope mixing calculation (Donahue et al., 1990). All graphite ^{14}C determinations have been corrected for isotopic fractionation according to conventions of Stuiver & Polach (1977) with $\delta^{13}C$ values measured on prepared graphite using the AMS spectrometer.

Taphonomic analyses

All whole valves and unique identifiable fragments from all samples were scored for taphonomic analyses. The scoring was conducted for the following variables: disarticulation, fragmentation, internal corrasion, internal bioerosion, internal encrustation, external corrasion, external bioerosion, and external encrustation. Higher

scores correspond to poorer preservation but see Table 1 for an explanation of the scores for the individual variables. A total taphonomy score was calculated by the summing the scores of the previous eight taphonomic variables; possible scores ranged from zero to 13.

Variable name	0	1	2
Disarticulation	Articulated	Disarticulated	-
Fragmentation	Whole	>50% present	Fragmentary
Internal corrasion	Pristine	Dulled	Chalky/pitted/stained
Internal bioerosion	Absent	Present	-
Internal encrustation	Absent	<20% area	>20% area
External corrasion	Pristine	Texture smoothed	Texture obliterated
External bioerosion	Absent	Present	-
External encrustation	Absent	<20% area	>20% area

Table 1: Taphonomic variables with criteria for scores

Multivariate ordinations

Non-metric Multidimensional Scaling (nMDS) ordinations were conducted on: 1) a matrix of taphonomic variable values of individual valves and 2) two matrices of taxonomic composition of samples (minimum number of individuals and relative abundance values). The relative abundance scoring for number of individual valves is as follows: 0 = Absent, 1 = 1-5 valves, 2 = 6-15 valves, 3 = 16-30 valves, and 4 < 30 valves. The nMDS ordinations were conducted using the *metamds* function in the *vegan* package in *R* and *RStudio* freeware (Dixon, 2003; Oksanen et al., 2022; R Core Team, 2017).

Paleoparasitological analyses

Trematode prevalence was calculated as the proportion of valves of a taxon within a sample that had at least one trematode-induced pit. Intensity was calculated as the mean number of trematode-induced pits per valve within a sample, including valves with no pits. Aggregation of trematode pits was measured as the slope of the least-squares regression model between $\log_{10}$-transformed mean intensity and $\log_{10}$-transformed variance of intensity. All statistical analyses, line maps, and figures relaying quantitative analyses were performed in *R* and *RStudio* freeware using the following packages: *ggplot2*, *ggthemes*, *viridis*, *ggrepel*, and *lmodel2* (Arnold et al., 2021; Garnier et al., 2021; Legendre, 2018; R Core Team, 2017; Slowikowski et al., 2021; Wickham, 2016; Wickham et al., 2022).

Results

Valve age distributions

Low-precision radiocarbon dates (y BP) were determined for 55 bivalve specimens from the shell beds and death assemblages (Figure 2, Table 2). The median age of death assemblage valves is 335 y BP and 1,030 y BP for shell bed valves, a statistically significant difference ($p_{\text{Wilcoxon}} <<< 0.001$). The variance of ages is significantly higher among death assemblages than shell beds ($p_{\text{F-test}} <<< 0.001$). Ages of specimens were largely consistent between sub-samples of each of the sampling locations (Figure 2).

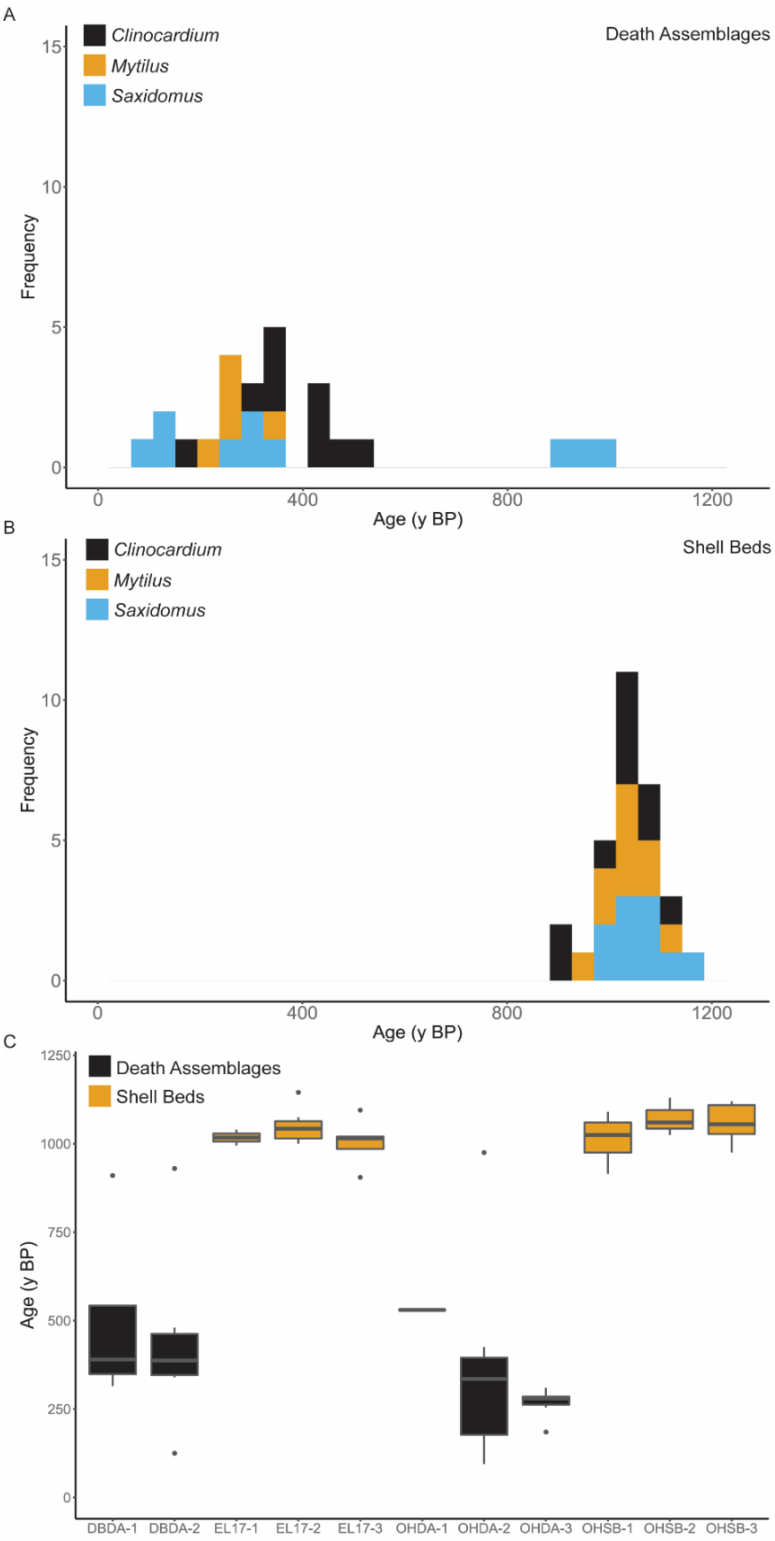

Figure 2: Distribution of radiocarbon ages in (A) death assemblage taxa, (B) shell bed taxa, (C) individual sub-samples

Sample	Deposit	n_{dates}	Minimum age	Mean age	Maximum age
EL17-1	Shell Bed	2	995	1017.5	1040
EL17-2	Shell Bed	8	1000	1048.1	1145
EL17-3	Shell Bed	5	905	1004.0	1095
OHSB-1	Shell Bed	6	915	1014.2	1090
OHSB-2	Shell Bed	3	1025	1071.7	1130
OHSB-3	Shell Bed	6	975	1058.3	1120
DBDA-1	Death Assemblage	4	315	501.3	910
DBDA-2	Death Assemblage	6	125	441.7	930
OHDA-1	Death Assemblage	1	530	530	530
OHDA-2	Death Assemblage	7	95	364.3	975
OHDA-3	Death Assemblage	7	185	267.1	310

Table 2: Summary of low-precision radiocarbon dates of bivalve material.

n_{dates}: the number of individual valves dated.
Age values: y (BP).

Radiocarbon dates were determined for an additional 5 specimens of the purple varnish clam, *Nuttallia obscurata*, from DBDA-1 and DBDA-2. *N. obscurata* is an invasive species introduced to the Pacific Northwest approximately 30 years before present, and so these ages were not included with the analysis of ages from native taxa (Forsyth, 1997; Gillespie et al., 1999). However, reported ^{14}C ages for these samples ranged from 105 to 645 y BP, with a median of 170; this incongruity between the reported radiometric dates and conclusively known ages calls into doubt the reliability of radiocarbon dates from other sampled material.

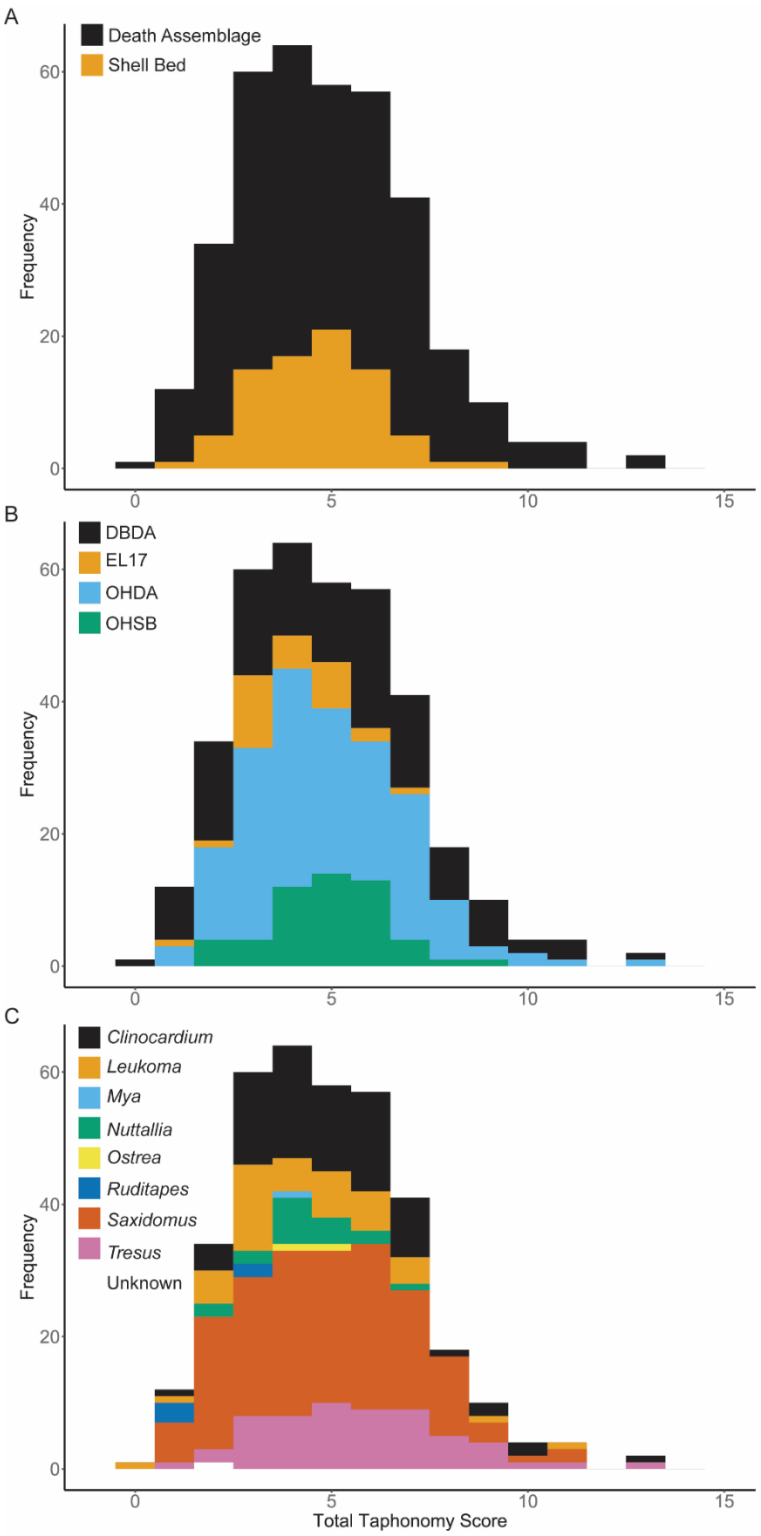

Figure 3: Total taphonomy score distributions across (A) death assemblages and shell beds, (B) sampling locations, (C) taxa

Taphonomy

Total taphonomy scores (TTS) of individual valves ranged from zero to 13 with a mean value of 4.9, a median value of 5, and a standard deviation of 2.2. There was no significant difference in mean TTS between shell beds and death assemblages or between sampling locations (Figure 3A, B and Table 3). There were, however, significant differences in mean TTS values between several genera. Mean TTS of *Ruditapes* was significantly lower than that of *Clinocardium*, *Saxidomus*, and *Tresus*. Similarly, the mean TTS of *Leukoma* was significantly lower than *Tresus* (Figure 3C and Table 3).

Grouping Variables	Values	n	Mean	Variance	Statistical Tests
Deposit Type	Shell Bed	81	4.6	2.3	$p_A = 0.17$
	Death Assemblage	284	5.0	5.5	
Location	EL17	28	3.9	1.8	$p_A = 0.10$
	OHSB	53	4.9	2.3	
	DBDA	122	5.1	7.0	
	OHDA	162	4.9	4.3	
Genus	*Clinocardium*	79	5.0	4.2	$p_A = 0.0009$
	Leukoma	44	4.3	4.5	*Ruditapes*/*Clinocardium*: $p_T = 0.032$
	Mya	1	4	–	*Tresus*/*Leukoma*: $p_T = 0.023$
	Nuttallia	18	4.3	1.7	*Saxidomus*/*Ruditapes*: $p_T = 0.047$
	Ostrea	2	4.5	0.5	*Tresus*/*Ruditapes*: $p_T = 0.003$
	Ruditapes	5	1.8	1.2	
	Saxidomus	156	4.8	4.7	
	Tresus	59	5.7	5.5	

Table 3: Statistical comparisons of Total Taphonomy values between grouping variables

Tukey's Honest Significant Differences (HSD) *p*-values (adjusted for multiple comparisons) are reported for pairs that exhibit *p*-values less than 0.05.

p_A: *p*-value for ANOVA.

p_T: *p*-value for Tukey's Honest Significant T (adjusted for multiple comparisons).

The nMDS of scores of the eight taphonomic variables (Table 1) for individual valves reduced the matrix to three axes using the Bray-Curtis dissimilarity index and resulted in a stress value of 0.106 (Figure 4A). The nMDS1 score negatively corresponds with internal and external encrustation and positively with disarticulation. The nMDS2 score most positively corresponds with fragmentation and internal bioerosion. Overall, taphonomic characters correspond with negative PC1 and positive PC2 values. Shell beds have significantly higher median nMDS1 and median nMDS2 values than death assemblages (Figure 4B).

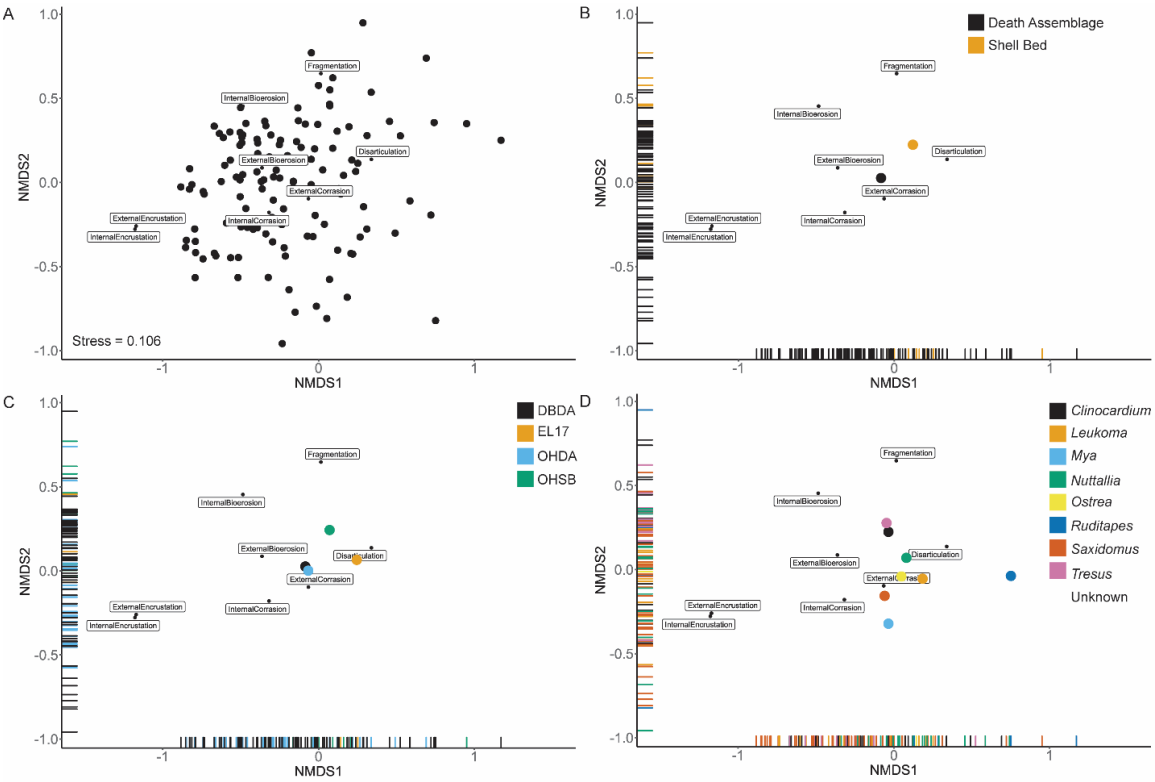

Figure 4: Non-Metric Multidimensional Scaling of taphonomic scores of individual valves

A) Scores of all valves and taphonomic variables.
B) Rug plot and median nMDS1 and median nMDS2 values of death assemblages and shell beds.
C) Rug plot and median nMDS1 and median nMDS2 values of locations.
D) Rug plot and median nMDS1 and median nMDS2 values of taxa.

Sampling location EL17 has a significantly higher median nMDS1 value than locations DBDA and OHDA. Sampling location OHSB has a significantly higher median nMDS2 value than DBDA and OHDA (Figure 4C). *Ruditapes* has a significantly higher median nMDS1 value than *Clinocardium, Saxidomus,* and *Tresus*. *Tresus* has a significantly higher median nMDS2 value than *Saxidomus* and *Leukoma*; *Clinocardium* has a significantly higher median nMDS value than *Saxidomus* (Figure 4D).

Paleoecology and community structure

The following taxa were included in the nMDS ordination: the bivalves *Tresus capax*, *Saxidomus gigantea*, *Leukoma staminea*, *Mytilus trossulus*, *Clinocardium nuttalli*, *Ostrea lurida*, *Mya arenaria*, *Macoma sp.*; the gastropods *Polinices lewisii*, *Nucella lamellosa*, *Collisella pelta*, *Littorina sitkana*, *Littorina sp.*; the polyplacophorans *Lepidochiton dentiens* and *Katharina tunicata*; and the echinoid *Strongylocentrotus* sp. The bivalves *Ruditapes philippinarum* and *Nuttalia obscurata* were not included in the ordinations as they are both introduced species and their inclusion would likely bias the nMDS to primarily reflect temporal changes in taxonomic composition rather than more subtle differences in environment and community structure.

The first nMDS ordination reduced the minimum number of individuals matrix to two axes and had a stress value of 0.129 (Figure 5A). Negative nMDS1 values are associated with taxa common on open rocky coasts (e.g., the oyster *O. lurida* and the chiton *K. tunicata*) while positive nMDS1 values are associated with taxa common in lower energy environments with finer grained sediment (e.g., the bivalves *M. arenaria* and *C. nuttalli*). The gradation between rocky and fine-grained environment taxa is not

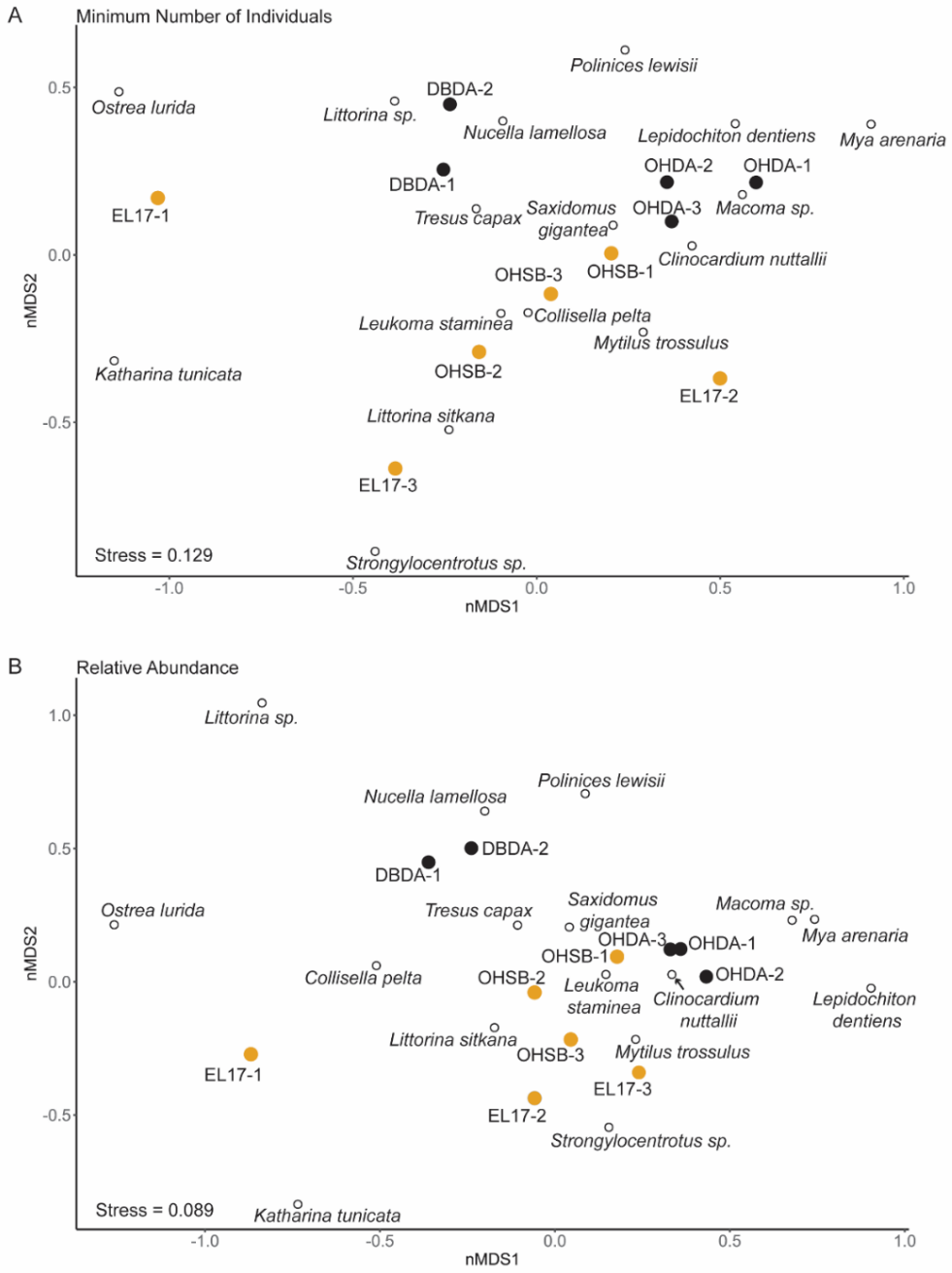

Figure 5: Non-Metric Multidimensional Scaling of taxa

A) minimum number of individuals in sub-samples
B) relative abundance in sub-samples.
Death assemblages in black, shell beds in gold, taxa as open circles.

clearly demarcated along nMDS1, likely due to the common occurrence of cobbles and boulders in quiet bays along this rocky coastline. Among the taxa associated with

environments dominated by fine-grained sediment, positive nMDS2 values are associated with taxa that prefer clean sand (e.g., the predatory moonsnail *P. lewisii*) and negative nMDS2 values correspond to taxa that prefer a mix of mud, sand, and gravel (e.g., the bivalves *L. staminea* and *C. nuttalli*). Death assemblage samples display intermediate (DBDA) to positive (OHDA) nMDS1 values and positive nMDS2 values. Shell bed samples span the range of nMDS1 values and tend toward negative nMDS2 values. Most sub-samples tend to plot close to one another in the nMDS space with the exception of the EL17 shell bed samples, which are dispersed broadly across both axes. The second nMDS ordination reduced the relative abundance matrix to two axes and had a stress value of 0.089. (Figure 5B) Though there is some variation between the two, this second ordination of taxonomic data is consistent with that identified in the first.

Trematode-induced pits, taphonomy, prevalence, and aggregation

Trematode-induced pits were identified on three bivalve taxa from four samples; two samples were shell beds and two were death assemblages (Table 4). The mean TTS for valves with trematode pits (3.6) is significantly lower ($p_{ANOVA} = 0.007$) than the mean TTS for valves with no trematode traces (5.0). Individual valves of *Leukoma*, *Saxidomus*, and *Tresus* with trematode pits tend to plot with positive nMDS1 values and negative nMDS2 in the taphonomy nMDS space and are, therefore, associated with higher quality preservation (Figure 6).

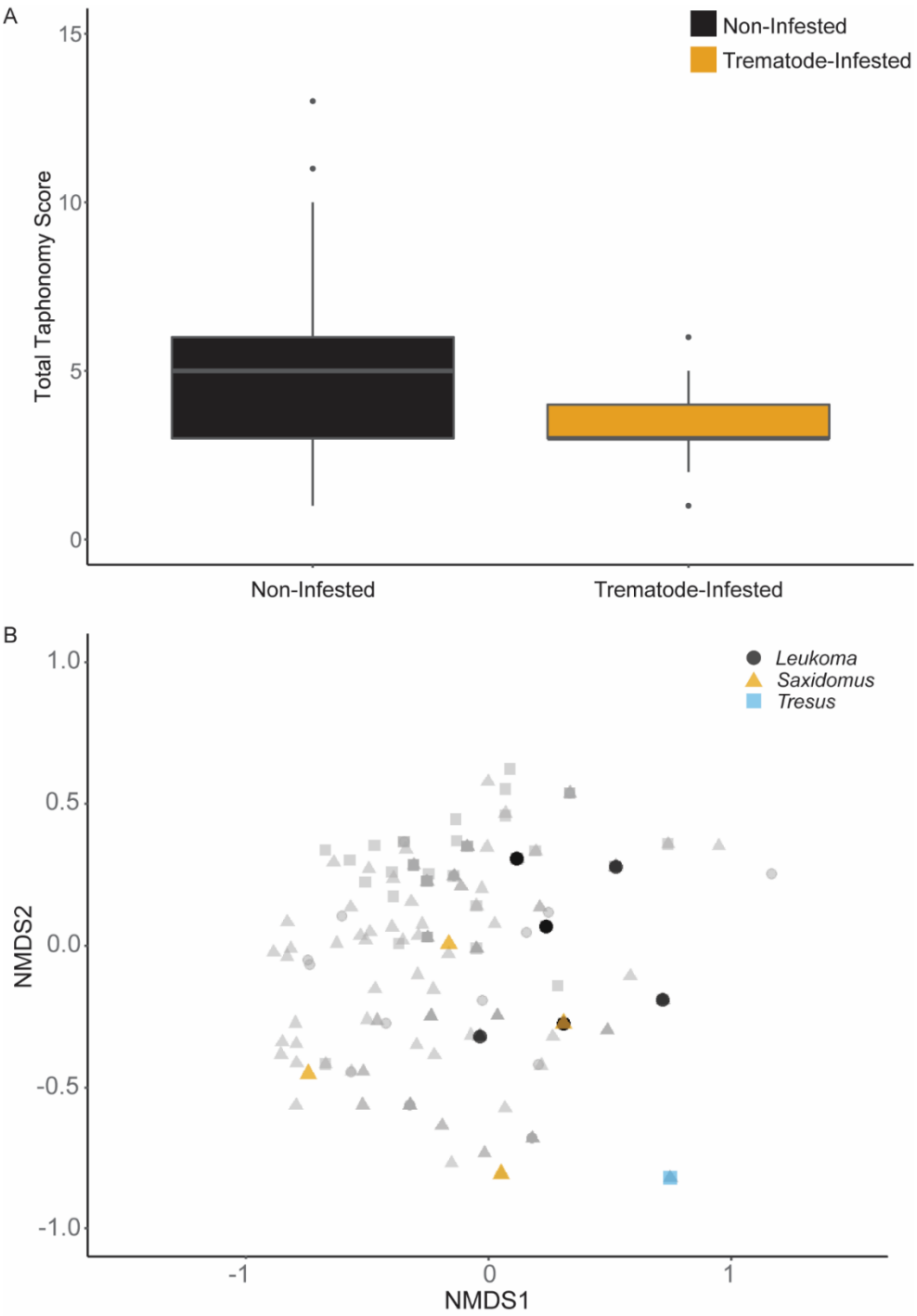

Figure 6: Taphonomy and trematode parasitism

A) Box and whisker plots of Total Taphonomy Score by infested and non-infested bivalves. B) non-Metric Multidimensional Scaling of taphonomic scores of individual valves (see Fig. 5 above) of taxa with trematode-induced pits.
Parasitized individuals plotted in color and non-parasitized individuals plotted in transparent gray. Data from Whidbey Island only.

Trematode prevalence among EL17-3 *L. staminea* (0.650) was significantly higher than that among OHSB-1 *S. gigantea* (0.053), OHDA-1 *S. gigantea* (0.176), and DBDA-2 *T. capax* (0.053). *Leukoma staminea* from shell bed sample EL17-3 is, however, statistically indistinguishable from two 2004 live-collected samples from nearby San Juan Island, WA (Huntley, 2007).

Sample	Genus	n_{Valves}	n_{Pits}	Prevalence	Mean Intensity	Variance Intensity
EL17-3	*Leukoma*	20	13	0.650	4.150	48.660
OHSB-1	*Saxidomus*	19	1	0.053	0.053	0.053
OHDA-1	*Saxidomus*	17	3	0.176	0.667	5.154
DBDA-2	*Tresus*	19	1	0.053	0.158	0.474
Argyle Creek (Huntley, 2007)	*Leukoma*	51	29	0.569	4.350	112.150
Argyle Lagoon (Huntley, 2007)	*Leukoma*	50	34	0.680	3.490	31.970

Table 4: Trematode prevalence and intensity values

n_{Valves}: number of valves of a given taxon in that sample.
n_{Pits}: number of valves of a given taxon in that sample that have at least one trematode-induced trace.
Mean Intensity: the mean number of pits per valve (including valves with no pits).
Variance Intensity: variance of the number of pits per valve (including valves with no pits).

Mean intensity of trematode-induced pits ranged from 0.053 and 4.150 (to 4.350 when including data from Huntley, 2007) and the variance of intensity ranged from 0.053 to 48.660 (to 112.150 when including Huntley, 2007; Table 4). Log_{10}-transformed mean intensity and log_{10}-transformed variance of intensity for all data (including Huntley, 2007) are significantly, positively correlated ($R_{Pearson}$ = +0.992; p = 0.0001). The slope of the least squares regression model between these two variables is 1.57, which is significantly higher than a slope of one and indicates aggregation of parasites among hosts (Figure 7). These patterns remain the same when Huntley (2007) data are not included.

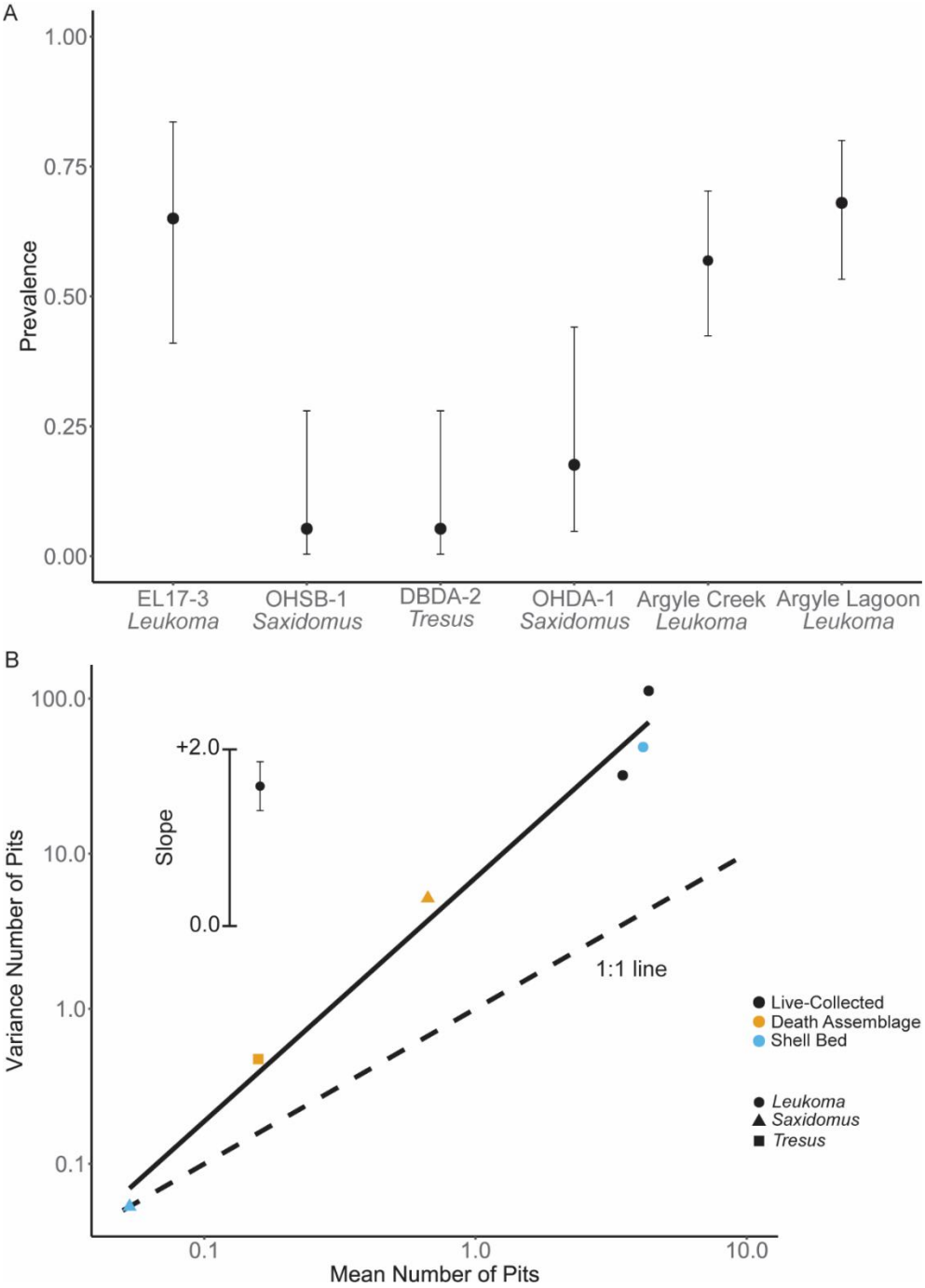

Figure 7: Trematode prevalence and aggregation analyses

A) Prevalence among taxa from this study and live-collected *Leukoma* reported in Huntley (2007).
B) Least-squares regression model of $\log_{10}$-transformed mean intensity and $\log_{10}$-transformed variance of intensity.

Discussion

Patterns of parasitism

The results of this study show a clear taxonomic effect on the prevalence and intensity of digenean parasitic traces; *Leukoma staminea* from shell beds and from modern live-collected individuals have dramatically higher rates of parasitism in terms both of prevalence and intensity and show statistically significant features of aggregation of parasites in host individuals. However, *Leukoma* from death assemblages do not appear to share this high rate of parasitism pressure; whether this is an illusory feature of taphonomic bias or reflects some difference in environmental parameters is unclear.

Trace morphologies

In addition to the simple, rimmed, shallow pits generally associated with digenean metacercariae, inspection of shells in this study revealed further uncommon trace morphologies. Two igloo-type traces were observed, one in *Leukoma* (Figure 8A) and one in *Saxidomus*; these features are thought to represent an extreme host response to the parasite, and consist of a blister-like feature with a single pore connecting an interior opening to the outside of the shell, apparently kept clear against the encroaching shell by the erosive action of the metacercaria. One individual of *Leukoma* from EL17-3 contained 28 individual pits, the highest of any taxon or sample in this study, all with a noticeably raised and inflated rim surrounding a deeply incised center (Figure 8B). These "inflated-incised" pits may represent an intermediate host response between typical pits and igloos (Huntley et al., 2021), and to the best knowledge of the author are not otherwise known from the literature on the topic.

Figure 8: Unusual trace morphologies

A) Inflated-incised pits in *Leukoma*
B) Igloo in *Leukoma*

Mud-blisters and U-shaped borings attributable to commensal or kleptoparasitic polychaete worms were occasionally observed on the exteriors of shells, but cannot usually be definitively called a live-live interaction, since polychaetes are known to bore into non-living substrates as well. One striking exception to this precautionary rule is that of a *Clinocardium* from OHDA-2 (Figure 9) containing a large mudblister extending over a large area between layers of the shell; one shell adductor attachment scar is dramatically reshaped, suggesting pathological growth by the host in an attempt to compensate for the irritation and weakening of the shell.

Figure 9: Large mudblister in *Clinocardium*

Combined transmitted- and incident-light photograph of *Clinocardium* showing the internal extent of a mudblister (darkened area at right-center) caused by polychaete infestation.

Parasitic traces and taphonomy

The association between the presence of parasitic pits and lower TTS raises the possibility that taphonomic degradation plays a role in observed patterns of parasitism. Parasitic traces may not be truly absent from higher-TTS shells, but merely obscured or obliterated by taphonomic effects such as corrasion or bioerosion of the shell interior. This potential confounding effect can be investigated by further sampling and selecting only shells with well-preserved interior surfaces for analysis. For the purposes of identifying traces produced by digenean trematodes infesting the mantle of bivalves, damage purely to the exterior of the shell is irrelevant.

Certain types of traces produced by live-live interactions, such as predatory drillholes and polychaete mudblisters, can have causal interactions with taphonomic variables; if an interaction structurally weakens the skeleton of the host or increases its exposure to shell-crushing predators, shells bearing the traces of the interaction are disproportionately likely to be taphonomically fragmented, causing such traces to be underrepresented in low-TTS collections. However, the simple pits left by digeneans do not have any known effect on the structural strength of their hosts' shells. While digenean infestation can increase the predation pressure on bivalves by impairing their burrowing abilities (Jonsson & Andé, 1992), fragmentary shells from this study do not show any particular signs of durophagous predation.

Ecological groupings

The NMDS of taxonomic abundances within samples appears to associate taxa by ecological habit within the space defined by the first two ordination axes; organisms

associated with high-energy rocky coasts, low-energy sandy environments, and low-energy mixed mud-sand habitats tended to plot separately from each other. While NMDS is an exploratory rather than confirmatory method and these groupings are necessarily tentative, this may be informative of the paleoenvironments that produced the material in the shell beds and how they compare in physical parameters and taxonomic composition to modern environments nearby.

Age constraints and reservoir effects

Reported radiocarbon ages from OHSB and EL17 indicate a Holocene age and possible Native American shell-midden origin for these shell beds, which are considered to be glaciomarine deposits from the latest Pleistocene based on previous work (Domack, 1983). Reported ages from OHDA and DBDA, meanwhile, suggest a high degree of time averaging and reworking of Recent shell accumulations in the study area, with shells routinely persisting near the surface for multiple centuries. However, the discordant dates returned for shells of strictly bounded age (of *Nuttallia obscurata*) indicate that these may not be true ages and are instead the result of an unaccounted-for variable.

A likely culprit for these unreliable ages is the reservoir effect of dissolved inorganic carbon (DIC) in the local seawater. Radiocarbon dating presumes that the sampled organism constantly exchanged carbon with the atmosphere in life, establishing a baseline ratio of carbon isotopic abundances consistent with the well-documented carbon isotopic composition of the atmosphere. While this is generally true of terrestrial biota, it is not always so for marine organisms. Mollusks are known to source carbonate for their skeletons from a variable combination of metabolic carbon from their diet (which, in coastal settings, may derive from terrestrial sources) and DIC (Bauer et al.,

1998; Dillaman & Ford, 1982; Mook & Vogel, 1968; Stuiver et al., 1998; Tanaka et al., 1986). DIC in surface waters is not in near-equilibrium with the atmosphere, and its ratio of ^{14}C to ^{12}C may vary significantly from atmospheric composition due to upwelling of old (^{14}C-depleted) carbon from the deeper ocean. Previous work indicates a "reservoir effect" deviation for the northeastern Pacific in which marine shells tend to date as 800 to 1100 years older than their true radiocarbon age, as determined from comparison of syndepositional shells and wood (Kovanen & Easterbrook, 2002).

While this reservoir effect would explain the anomalously old reported ages for death assemblage material, it would not explain the surprisingly recent ages reported for the shell beds. Putting definitive bounds on the ages of the shell beds will likely require further sampling and mapping of the deposits, work beyond the scope of this study.

Conclusions

This study is best understood as part of a broader program of work investigating parasites of bivalves in the fossil record and the ecological factors affecting parasitism pressure in shallow marine environments (Huntley, 2007; Huntley et al., 2014, 2021; Scarponi et al., 2017). In attempting to untangle modern ecological conditions in environments heavily influenced by the effects of human inhabitation and industry from the historical pre-modern baseline, records of analogous past ecosystems are useful for generalizing the mechanics and bounds of ecological change. The body of evidence available is equivocal on whether or not transgressions are associated with increased parasitism pressure, but building upon the record of parasitism in the recent past can help to clarify this key question.

Ecological change due to deglaciation at the beginning of the Holocene records a recent history of rapid eustatic transgression. As modern warming proceeds due to human influence, further transgression is likely on a geologically rapid timescale. Turnover and stasis in community structure and parasitism regimes across such change in the recent past may hold useful predictions for episodes of similar change in the future.

Chapter 3: Exploration of taphonomic and preparation bias in silicified fossils through paired analyses

Background

Acid maceration

Acid maceration is a common chemical preparation technique used to extract fossils from limestone, relying on the high solubility of calcite in acidic solution and the comparatively low resistance of micritic matrix to alteration or dissolution (Grant, 1989; St. Clair, 1935). Fossils best suited to this method are insoluble in mild acid, typically siliceous, phosphatic, or organic in composition; this may reflect the original mineralogy of the organisms in question (e.g., siliceous diatoms, phosphatic brachiopods, organic graptolites) or replacement of originally calcareous biota. However, it is possible albeit risky to prepare calcareous fossils in this way if textural or compositional differences between fossils and matrix cause the former to dissolve significantly more slowly (Vodrážka, 2009).

Unlike similar methods in vertebrate paleontology, acid maceration for invertebrate fossils is typically applied to whole rock volumes rather than individual fossils (Grant, 1989; Padilla et al., 2010; Toombs & Rixon, 1959). This application is well-suited for research requiring large sample sizes and indiscriminate selection; rather than picking fossils visible on bedding planes or weathering out, bulk samples containing material of interest can be wholly dissolved, and all fossils found in residue retained for analysis. Despite the avoidance of human bias in this stage of sample selection, acid maceration does have its own inherent biases which should not be overlooked.

Silicification

One of the most common applications of acid maceration is to extract silicified fossils from limestone. Fabric-specific replacement of calcareous biota with silica (typically as chalcedony or opal, but sometimes as sparry quartz cement) is fairly common in the fossil record, especially in the early Paleozoic, and is often relatively taxon-independent (Butts, 2007, 2014; Butts & Briggs, 2010). While the fine-scale mechanisms of silicification in limestone remain unclear, the overall pattern is fairly simple: pore fluids containing dissolved silica (whether volcanic, hydrothermal, or biogenic in origin) undergo transport and react with the host rock, causing simultaneous dissolution of calcite and/or aragonite and precipitation of silica through mechanisms involving both pH change and pressure dissolution (Maliva & Siever, 1988). This replacement can be massive or nodular, producing diagenetic cherts, or can proceed to a much smaller degree around suitable sites. Buried skeletal material is especially viable for such replacement, as the residual organic material can nucleate silica deposition and organic acids produced by ongoing decay both increase the solubility of calcite and aragonite and decrease that of silica (Butts & Briggs, 2010).

Because silica remineralization of fossils tends to be simultaneous with the loss of its original calcareous material (rather than moldic deposition following after dissolution), silicification tends to proceed from outer surfaces inwards rather than replacing the entire grain at once (Butts & Briggs, 2010). If silicification is interrupted by a change in pH or by depletion of the silica supply, this can result in partially silicified fossils composed of a calcareous core surrounded by a thin rind of poorly consolidated silica; such fossils rarely survive acid maceration, since the outer layer easily crumbles

once the interior is dissolved away. Since the square-cube law dictates that larger grains have a lower ratio of surface area to volume (and are therefore more likely to retain a sizable calcareous interior volume), this can introduce body size bias into samples prepared through maceration, underrepresenting larger objects. This can then lead to bias in sclerite ratios within a species (skewing some measures of the degree of pre-burial transport), in ontogenetic population structure within a species, and in ecological structure across species (if some taxa have larger mean body size than others).

Silicification can also be taxon-specific under certain circumstances, introducing paleoecological bias directly. Perhaps the best-documented issue stems from the sparry texture of echinoderm ossicles; if early-burial conditions promote calcite precipitation, these skeletal grains tend to develop a syntaxial cement that makes them fairly resistant to further alteration. If the sediment is later partially silicified, the ossicles frequently remain entirely calcitic while other taxa (and even surrounding micrite) are converted to silica (Butts, 2007, 2014; Nebelsick, 2004). For instance, chert nodules in encrinites, such as parts of the Mississippian Burlington Limestone, often contain molds of crinoid columnals that kept their calcite composition even while the rock around them was entirely silicified. This results in a near-total loss of echinoderms when such rocks are prepared through acid maceration.

Preparation biases

Further biases can arise from the washing process itself. Larger fossils may be tumbled against other grains or container walls, leading to abrasion or breakage, while smaller fossils may be crushed beneath larger objects as grains settle. Elongated grains may be more prone to breakage than spheroidal grains of the same volume due to a lower

minimum cross-sectional area, which can lead to taxon or sclerite bias against fossils with rod-like geometry, such as dendroid bryozoans and the spines of some trilobites. These overlapping effects can produce a wide variety of biases in size and shape, and any net bias in body size or taxon is practically impossible to predict from first principles.

The strength of biases associated with washing can be affected by the composition of the host rock as well. Well-cemented rocks can require longer maceration and washing than poorly consolidated ones, while argillaceous rocks may need more thorough washing to drive off insoluble clays, often including sonication. The longer sediment is washed and manipulated, the more breakage tends to occur, making matrix texture an important factor of preparation bias.

If biases in differential preservation and recovery methods go unaccounted for, certain types of analyses can be more severely affected. Systematic descriptions of organisms may be only mildly affected by the underrepresentation of some ontogenetic stages relative to others, but studies of paleoecology or biofacies can suffer in quality due to their reliance on an accurate assessment of what biota are present in the deposit. The near-absence of a guild of predators or the preferential breakage of certain types of shell ornamentation, for example, might drastically alter the interpretation of the food web of a paleoenvironment; similarly, the loss of fossils in a certain size range during preparation can affect conclusions on the energy of the depositional environment or the degree of bioturbation. Because of the potential for these biases to skew studies' conclusions, quantifying or at least constraining them can improve confidence in the results of research relying on this common preparatory method.

Paired analyses

Previous research has attempted to account for preservational and preparation bias in acid maceration of silicified fossils, notably a 2015 paper by Sara Pruss, Jonathan Payne, and Sophie Westacott. In that study, the authors compared two methods for measuring the paleoecological makeup of rocks known for silicified fossils: petrographic thin sections and acid maceration. Hand samples were collected from Triassic-age outcrops, and each was partially digested in buffered acetic acid, with the remaining material processed into a thin section. Dissolved material was washed, sieved and picked for recognizable fossils, and the abundances of three key taxa (bivalves, gastropods, and echinoderms) were calculated. Thin sections were point-counted and taxon abundances were similarly scored. By comparing relative abundances between the two methods for their samples, the authors were able to roughly quantify taxonomic bias in the studied deposit (Pruss et al., 2015).

Two questions not addressed by that study are those of body size bias and breakage patterns. Since thin section analysis can identify fossils by their taxonomic group but gives only an underestimate of their dimensions, detecting differences in body size distribution between thin section grains and fossils recovered in residues is not feasible. Similarly, it is impossible to tell by those methods whether fossils in residues suffered damage during digestion and washing or whether the breakage occurred prior to burial; because thin sections and residues do not record the same fossils but rather disjoint subsets of the total fossils within the hand sample, no true before-and-after comparison can be made. Indeed, since both methods applied in this study are destructive, a single fossil cannot be recorded by both.

This inherent limitation can be avoided, however, by pairing a non-destructive whole-rock imaging/analytical method with acid maceration. X-ray micro-computed tomography (micro-CT or μCT) is well-suited to such an approach, allowing quasi-compositional (density proxy) and textural variation within a sample to be imaged in three dimensions, revealing fossil material within. By then subjecting the sample to acid maceration, individual fossils can be resolved and measured before and after chemical preparation, and any breakage or loss documented.

μCT and its applications

Micro-CT works by passing a focused X-ray beam through a sample and onto an electronic detector (or scintillator-detector pair), which measures incident beam intensity at each pixel location on the detector to produce a measurement of the total X-ray opacity of the sample along the beam direction. The sample is then rotated and imaged again along a different direction, repeating until the full 360-degree arc has been covered to a desired angular density of measurements. (Unlike in medical CT instruments, the sample is rotated while the beam source and detector remain stationary.) Imaging parameters can be varied to better match individual sample characteristics; beam intensity can be adjusted to achieve better contrast depending on sample composition, and the distance between the sample and the detector (proportional to the field intercepted by the detector, due to the divergence of the beam from the source window) can be increased or decreased to the desired magnification. The projections through a sample are then used to interpolate the opacity of each incremental volume within it, typically by proprietary software sold with the instrument, to produce a voxel map of X-ray opacity represented as brightness. This 3-dimensional image, usually in the form of a “stack” of greyscale

images orthogonal to the axis of sample rotation, is then ready for further processing and interpretation (Cnudde & Boone, 2013; Ketcham & Carlson, 2001; Mees et al., 2003).

Modern CT imaging is capable of extremely high magnification, with maximum resolutions far surpassing optical microscopes and comparable to electron microscopes, depending on the specifications of individual instruments. These capabilities do come with certain drawbacks and limitations inherent in the imaging method, which must be taken into account in projects relying on it.

One such caveat relates to resolution, the smallest possible distance between features that can be resolved by an imaging method. Not only is this distance always larger (coarser) than the side length of pixels or voxels making up the image produced, but it depends on the nature of the sample, with more internally complex and heterogeneous materials having larger effective resolution than homogeneous ones (Elkhoury et al., 2019). Resolution can also be coarser and more challenging to measure in three-dimensional imaging than in two. Determining by observation whether adjacent features are connected or distinct in a two-dimensional plane is relatively easy, but due to limitations of how displays and human vision project three dimensions down to two, the equivalent task in three-dimensional volume is more challenging. In practice, this means that features near the theoretical resolution limit of 3D imaging methods are likely to be lost, especially when interpreted by human observers.

CT imaging also suffers from various types of artifacts caused by interactions of the X-ray beam with the sample and by how individual projections are processed into a single image. Many artifacts result from various types of beam hardening, in which lower-energy photons are preferentially attenuated by the sample, leaving behind a

"hardened" beam with higher average energy per photon; this beam more readily passes through the remaining material with fractionally less absorption, causing areas struck by a hardened beam to be interpreted as darker (i.e., more transparent to X-rays). Since the beam is always slightly hardened by passing through the outer surface (lateral to the axis of sample rotation) before reaching the interior of the sample, the interior is always slightly darkened relative to the outermost layer. These are known as cupping artifacts, from the concave-upward graph of relative brightness along a lateral transect through a sample. Since these artifacts are produced predictably based on sample geometry, they can be corrected relatively easily (Abel et al., 2012; Jung et al., 2011; Schladitz, 2011).

Beam hardening can also manifest in more problematic ways in heterogeneous samples. Regions of higher-density material (e.g., iron minerals in sediments, bones in biological samples) can drastically harden beams passing through them, causing dark blotches to appear around bright features within a sample and especially in the spaces between multiple bright features. These artifacts are far more difficult to correct due to their irregular shape, and remain the subject of ongoing research in economic geology and other materials science fields (Bam et al., 2019; Park et al., 2015; Remeysen & Swennen, 2006).

Variances in detector calibration can produce ring artifacts, radial variations in brightness; the algorithms used to reconstruct the 3D image from the stack of 2D projections can also contribute to this. Filtering during pre-processing can reliably correct for these artifacts, but often at the cost of introducing noise along the axis of sample rotation (Kyriakou et al., 2009; Yousuf & Asaduzzaman, 2009).

Samples to be studied

Since X-ray opacity (which micro-CT directly measures) is closely correlated with density, fossiliferous samples well-suited to imaging with this method will have distinct fossil and matrix mineralogy, preferably with high density contrast between phases. Limestones with matrix consisting of calcite ($\rho = 2.7$) with some clay content ($\rho \approx 2.6 – 3.0$) tend to contrast well against both silicified fossils preserved as opal ($\rho \approx 2.1$) and pyritized fossils preserved as a mixture of pyrite and hematite ($\rho \approx 5 – 5.3$). Rocks of this nature are known from the Ordovician-age deposits of the Shenandoah Valley in Virginia, where the black limestones and shales of the Edinburg Formation are exposed.

The Edinburg Formation is a unit of massively bedded black limestone with occasional shaley interbeds, representing deep-ramp to basinal deposition at the northwest of the Taconic foreland basin system after drowning of shallower ramp carbonate facies including the underlying Lincolnshire Limestone. Originally figured as Middle Ordovician, it has since been revised to Upper Ordovician (Mohawkian) in age based on fossil assemblages (Holland & Patzkowsky, 1996). Potassium bentonites derived from Taconic volcanism are sporadically present in the sediments of the foreland basin and have been sampled for radiometric ages, most notably the Millbrig bed, which lies somewhat upsection of the Edinburg in the Martinsburg Formation and has been dated at 452.86 Ma using U-Pb ages (Leslie, 1995; Mitchell et al., 2004; Sell et al., 2013).

Materials and Methods

Field site: Strasburg Junction

All samples in this study were collected from the Strasburg Junction railcut, a well-studied site in the Shenandoah Valley of Virginia (Figure 10). Along the exposure of the Liberty Hall facies of the Edinburg Formation at this site, strata with fossils visible on weathered surfaces were noted; from each of six visibly fossiliferous horizons, in-place material was taken as hand samples and the apparent stratigraphic up direction noted for each. A horizon from the underlying Lincolnshire Formation was also collected but was not included in this analysis.

A total of fifteen cylindrical cores, approximately 2 cm in diameter and ranging from 1 to 4 cm in height, were cut from five of the six sampled horizons using a drill press. Each was cut approximately normal to bedding planes, and hand samples with visible fossils were preferentially cored. Each core was subjected to micro-computed X-ray tomography (μCT) on a Zeiss Xradia 510 Versa X-ray microscope with an isotropic voxel size of approximately 30 μm, producing three-dimensional images of the interior.

All μCT scans were processed using ORS Dragonfly software to reduce imaging artifacts using the Ring Removal and Median filters (*Dragonfly*, 2022). Regions of high brightness (corresponding to high-density ferrous material) and low brightness (corresponding to low-density siliceous material) relative to the local background were thresholded and manually segmented in Dragonfly, excluding regions at the very top and bottom of cores due to persistent boundary artifacts. Due to radial and longitudinal variation in background brightness across the cores, multiple brightness thresholds were

used to segment siliceous material in some cores; in such cases, the total siliceous volume is the union of the volumes from segmentation by the various thresholds.

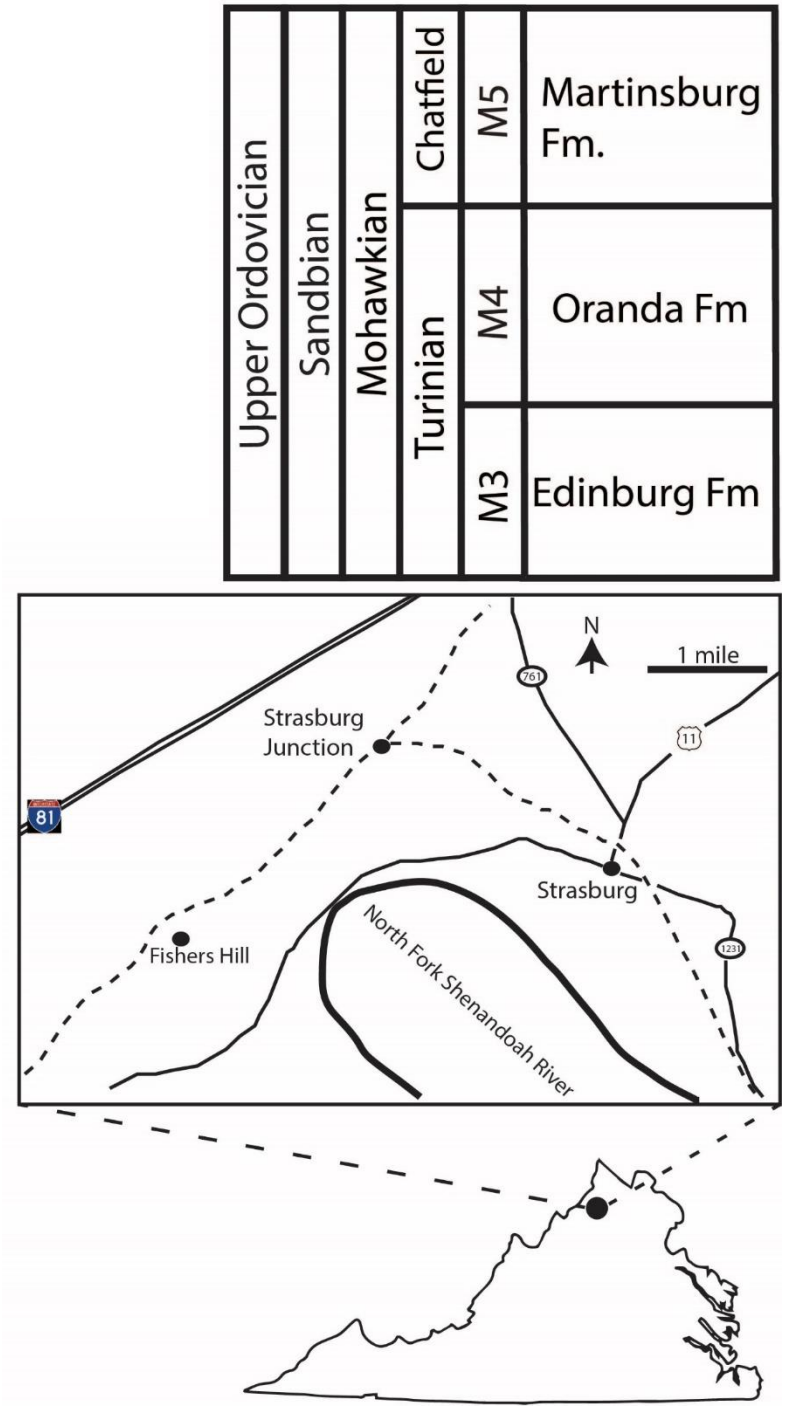

Figure 10: Locality map for Strasburg Junction

Modified from Jacobs & Carlucci (2019)

Segmented volumes for ferrous and siliceous material were refined by removing small (<100 voxel) island volumes and were then partitioned into distinct regions-of-interest (ROIs), using 6-connectivity (voxels considered to be connected if sharing faces rather than only edges or vertices) for both purposes. Individual fossils and other objects were identified among these ROIs by visual inspection in 3D representations of voxels and against individual 2D projections of CT imagery. In cases where a fragmentary or incompletely resolved fossil fell into multiple non-connected ROIs, those ROIs were merged into one; in cases where a single ROI contained multiple contiguous objects, it was manually partitioned.

Each object resolved in the segmented volumes was measured for minimum, maximum, and mean three-dimensional Feret diameter (Feret, 1930; Walton, 1948). Fossils that could be confidently identified to at least the phylum level were scored for additional taxon-specific features and anatomical measurements (see Table 5).

After each core had been imaged with μCT, it was macerated in 10% acetic acid to dissolve calcareous material until fully disaggregated and no longer visibly evolving gas bubbles. Insoluble residues were washed with water and sonicated in 30-second intervals, iterating until the supernatant ran clear. This washing process was then repeated using Calgon solution (0.052 M $Na_6(PO_3)_6$, 0.286 M $NaHCO_3$) as a deflocculant, sonicating as before, until all loose clay was removed. Cleaned residues were then washed over a 250 μm sieve, allowed to dry, and picked for identifiable fossils.

Fossils recovered from residues were photographed using a GIGAmacro high-resolution robotic imaging system. For large specimens, additional photographs were taken under a reflected light microscope to record features not visible in top-down view.

This imagery was processed and analyzed with FIJI/ImageJ software, using the Trainable Weka Segmentation plugin to identify fossils against the image background (Arganda-Carreras et al., 2017, 2022; Schindelin et al., 2012). Each fossil was measured for minimum and maximum two-dimensional Feret diameter as well as taxon-specific measurements corresponding to those taken from μCT imagery (see Table 5) (Feret, 1930; Walton, 1948).

Taxon		**Measurements**
Trilobita	Cranidium	Maximum width (tr.) of occipital lobe*, maximum width (tr.) between eyes**, total length (sag.)
	Thoracic segment	Maximum width (tr.) of axial ring, width (tr.) between fulcra of left and right pleurae, length (sag.) of axial ring
	Pygidium	Maximum width (tr.) of first axial ring, total length (sag.)
Bryozoa		Growth form: dendroid or lacy
Gastropoda		Presence/absence of outer walls of whorls, total height of shell, height of last complete whorl, width of last complete whorl, half-angle of teleoconch***
Ostracoda		Body length (a.-p.), body height (d.-v.), articulation/disarticulation, presence/absence of lateral spine

Table 5: Anatomical Measurements by Taxon and Sclerite

Measurements taken from CT and residue imagery for each of several common taxa. The main sclerites of trilobites (excluding hypostomes and librigenae) were assigned different sets of measurements due to fundamental differences in structure. Lengths, widths, and heights are measured in mm; angles are measured in degrees; other category variables were recorded as Booleans.

* Raphiophorids have an effaced prosopon with indistinct furrows, making identification of the occipital lobe difficult in CT especially. For this family of trilobites, occipital width was instead measured as the full width (tr.) of the sclerite from gena to gena at the occiput.

** For eyeless trilobites of the families Metagnostidae and Raphiophoridae, interocular distance was excluded.

*** This is the angle formed at the apex between the axis of coiling and a line tangent to the outer walls of the body whorls.

Results

CT objects

A total of 582 objects were resolved in CT imagery, 460 as a low-opacity siliceous phase and 122 as a high-opacity ferrous phase; of these, 241 siliceous objects and 14 ferrous objects were identifiable to at least a coarse taxonomic level (phylum or, for arthropods, class), with the remaining 219 and 108 respectively left unidentified.

Siliceous fossils were dominated by trilobites, of which slightly more than half (126/225) could not be confidently assigned to a family. Trilobites identified included members of the families Asaphidae (c.f. *Isotelus*), Cheiruridae (*Ceraurus*), Metagnostidae (*Trinodus*), Pterygometopidae (*Calyptaulax*), Raphiophoridae (*Ampyx*, *Lonchodomas*), and Remopleurididae (*Remopleurides*), all of which are previously known from this site (Evitt, 1961; Whittington & Evitt, 1953). Non-trilobite material consisted of thin-branching and lacy bryozoans and a single ostracod. Ferrous fossils were largely gastropods, with 2 bivalves also identified, 1 apparent thin-branching bryozoan, and 1 infilling of a raphiophorid cranidium. (Table 6)

Residue objects

Residues yielded 1349 recognizable objects, 1222 preserved as silica and 125 as iron minerals (pyrite, hematite, and/or limonite). The remaining 2 were other materials, one appearing to be a crystal of muscovite; neither was identifiable as a fossil. Nearly all siliceous fossils were identifiable to at least a coarse taxonomic level, with only 48 left unidentified; however, 113 of the iron-preserved objects could not be identified.

Siliceous objects in residue were made up largely of trilobites, fragments of thin-branching bryozoans, and ostracods. All trilobite genera represented in CT imagery were found also in residues, along with trilobites from the family Odontopleuridae (c.f. *Ceratocephala*). The remainder consisted of thick-branching and lacy bryozoans along with occasional brachiopod fragments. Ferrous fossils were almost all gastropods, though a single bivalve was also recovered. (Table 6)

Taxon		CT	Residues
Asaphidae		6	20
Cheiruridae		2	3
Metagnostidae		6	14
Odontopleuridae		0	18
Pterygometopidae		6	41
Raphiophoridae		57	149
Remopleurididae		22	59
Unknown Trilobita		126	290
Total Trilobita		225	594
Bivalvia		2	1
Brachiopoda		0	5
Bryozoa	Thin-branching	9	304
	Thick-branching	0	49
	Lacy	7	22
Gastropoda		10	11
Ostracoda		1	232
Unknown		327	161

Table 6: Fossils Recovered by Preparation Method and Taxon

Total counts of all objects identified in CT and residue imagery, grouped by taxon. Trilobites are further broken down to the family level. Trilobite material lacking sufficient anatomical features to be confidently assigned to a family was categorized separately.

Analysis

Taxon bias, CT to residue

A contingency table was constructed containing counts of specimens identified in CT, broken down by taxonomic grouping and by presence or absence in residues. The relationship between taxon and recovery was investigated using Pearson's χ^2 test (Pearson, 1900). (Table 7). The only taxonomic group which deviated significantly ($p < 0.05$) from overall likelihood of recovery was Unidentified Trilobita, material clearly from trilobites but lacking anatomical features in CT sufficient to assign it to a family; such fossils identified in CT are disproportionately unlikely to be recovered in residues.

Taxon	Not Recovered	Recovered	Recovered residual	p-value
Asaphidae	3	2	0.213	0.841
Cheiruridae	1	1	0.285	0.673
Metagnostidae	2	4	1.855	0.109
Pterygometopidae	4	1	-0.787	0.457
Raphiophoridae	37	20	-0.376	0.904
Remopleurididae	13	8	0.493	0.813
Unknown Trilobita	71	28	-7.389	0.037
Bivalvia	1	1	0.285	0.673
Bryozoa (thin)	4	4	1.140	0.392
Bryozoa (lacy)	2	4	1.855	0.109
Gastropoda	4	6	2.425	0.101

Table 7: Taxonomic Effects on Recovery

Contingency table containing counts of fossils with distinctive geometry identified in CT imagery and either recovered or not recovered in residue. Residuals of recovered counts are standardized to the expected number of recovered specimens for a taxon; positive residuals indicate disproportionately high likelihood of recovery in residues, while negative values indicate lower-than-average likelihood of recovery.

Statistically significant results ($p < 0.05$) are shaded.

Size bias, CT to residue

The presence of size bias in the likelihood of recovery was evaluated using the Mann-Whitney U-test with a null hypothesis of no difference in medians and a standard threshold of significance at $p = 0.05$ (Mann & Whitney, 1947). In comparisons between fossils identified in both CT and residue and those identified in CT but *not* in residue, there was no statistically significant difference of maximum ($p = 0.544$), minimum ($p = 0.088$), or mean ($p = 0.244$) Feret diameters, nor of elongation factor ($p = 0.159$) defined as the ratio of maximum to minimum Feret diameters. This indicates that for a given fossil identified in CT, none of the respective measures of size or elongation is associated with a differential likelihood of being recovered in residue.

However, when testing overall distributions of size between all fossils identified in CT and all those found in residue, the U-test found a dramatic difference in maximum Feret diameter ($p <<< 0.001$) between the medians of the two groups, with fossils in CT tending to be larger. (Comparisons involving minimum or mean Feret diameter are not possible between CT and residues; see Discussion.) Taken together, this indicates that while size is not correlated with the likelihood of recovery in residue, a larger size is correlated with a greater likelihood of being identified in CT.

Recovery bias overall

Application of Pearson's χ^2 test (Pearson, 1900) to total counts of taxa identified in CT and in residue found strong support ($p < 0.000001$) for different proportional abundances in the two preparation types (Table 8). Raphiophorids, remopleuridids, unidentified trilobites, bivalves and gastropods are significantly ($p < 0.05$) more abundant

in CT than the average of all taxa, while dendroid bryozoans (thin and thick) and ostracods are significantly more abundant in residues.

	CT	Residue	CT residual	Residue residual	p-value
Asaphidae	6	20	0.71459	-0.32633	0.428
Cheiruridae	2	3	1.2243	-0.5591	0.178
Metagnostidae	6	14	1.3721	-0.62657	0.129
Odontopleuridae	0	18	-1.7624	0.80481	0.051
Pterygometopidae	6	41	-0.74094	0.33836	0.408
Raphiophoridae	57	149	3.5984	-1.6432	1.99 E-05
Remopleurididae	22	59	2.146	-0.98001	0.015
Unknown Trilobita	126	290	6.3992	-2.9223	9.92 E-17
Bivalvia	2	1	2.0603	-0.94084	0.023
Brachiopoda	0	5	-0.92886	0.42417	0.306
Bryozoa (thin)	9	304	-6.1245	2.7968	3.26 E-14
Bryozoa (thick)	0	49	-2.9078	1.3279	1.15 E-3
Bryozoa (lacy)	7	22	0.89224	-0.40745	0.322
Gastropoda	10	11	3.3497	-1.5297	2.08 E-4
Ostracoda	1	232	-6.183	2.8236	1.27 E-13

Table 8: Comparison of Taxonomic Abundances

Contingency table containing total counts of taxa identified in CT and in residue imagery. Residuals of recovered counts are standardized to the expected number of recovered specimens for the combination of taxon and preparation; positive CT residuals indicate overrepresentation in CT for that taxon, while positive residue residuals indicate overrepresentation in residues (relative to average proportional abundance for all fossils). Statistically significant results ($p < 0.05$) are shaded.

Size measurement bias

For cranidia and thoracic segments identified both in CT and in residue for which measurements could be made of key anatomical parameters, these measurements were compared. (Only one such pygidium was found.) For each anatomical measurement, the difference between the two is expressed as the ratio of the measurement from CT imagery to the same measurement in the photographed residues (Table 9, Figure 11).

A) Cranidia

Core	Family	CT			Residue			Occ. Ratio	Sag. Ratio
		ID	Occ.	Sag.	ID	Occ.	Sag.		
03-C1	Metagnostidae	009	1.24	2.57	149	1.15	2.12	1.078	1.212
04-C1	Raphiophoridae	026	7.39	4.86	113	6.93	4.72	1.066	1.030
04-C2	Pterygometopidae	028	3.56	7.31	027	3.08		1.156	
05-C4	Cheiruridae	001	2.50	2.54	103	2.11	2.90	1.185	0.876
05-C4	Raphiophoridae	005	2.60	4.16	095	2.27		1.145	
06-C4	Metagnostidae	027	1.33	2.75	070	1.20	2.63	1.108	1.046

B) Thoracic Segments

Core	Family	CT			Residue			Ring Ratio	Fulcrum Ratio
		ID	Ring	Fulc.	ID	Ring	Fulc.		
03-C1	Pterygometopidae	002	1.27	2.42	094	0.94	1.76	1.351	1.375
03-C3	Remopleurididae	004	1.53	2.37	020	1.02	1.34	1.500	1.769
03-C3	Pterygometopidae	005	2.26	4.67	106	2.39	4.70	0.946	0.994
03-C3	Remopleurididae	009	1.25	1.55	024	1.28	1.67	0.977	0.928
03-C3	Remopleurididae	035	1.04	1.68	031	0.94	1.45	1.106	1.159
04-C1	Remopleurididae	005	1.68	2.26	093	1.16	1.61	1.448	1.404
04-C1	Pterygometopidae	012	1.08	3.06	011	1.31	2.64	0.824	1.159
04-C1	Remopleurididae	033	1.46	2.01	081	1.16	1.51	1.259	1.331
05-C4	Pterygometopidae	004	3.08	6.60	086	3.80	6.92	0.810	0.954
06-C3	Remopleurididae	001	1.75	2.61	038	2.22	2.88	0.788	0.906
06-C4	Pterygometopidae	002	2.28	4.93	018	2.76		0.826	
06-C4	Pterygometopidae	006	1.46	4.51	002	2.42	4.97	0.603	0.907

Table 9: Size measurement bias

Selected cranidia and thoracic segments identified and measured in CT and in residue imagery, with key anatomical dimensions measured in both. Listed ratios for each measurement are the ratio of the measurement in CT to the corresponding measurement in residue, quantifying how measurements in CT over- or underestimate actual dimensions as measured from extracted fossils.

A) Occ. = occipital width, Sag. = sagittal length

B) Ring = axial ring width, Fulc. = fulcrum-to-fulcrum distance

Shaded cells indicate measurements on segments with damage to one pleura, obtained by doubling the distance from the feature in question to the midline.

This comparison shows a persistent differential in measurement, albeit limited in confidence by small sample sizes (6 cranidia, 12 thoracic segments). Among cranidia, the occipital width (tr.) of the sclerite is measured as larger in CT than in residue by approximately 5 to 15%. Meanwhile, the difference in measured sagittal length varies somewhat, possibly due to imperfect orientation of the cranidia during imaging (in CT or in residues) causing foreshortening effects. (Figure 11A)

Anatomical measurements of thoracic segments are less consistent between CT and residues. Both the width (tr.) of the axial ring and the width (tr.) between the fulcra of the pleurae in CT are underestimated in some specimens and overestimated in others relative to the corresponding measures in residues. The ratio of each measure in CT relative to the residue is positively correlated between the axial ring and fulcrum widths. (Figure 11B)

Due to the small sample sizes of these comparisons, it is not currently possible to confidently draw conclusions on how reliably equivalent measurements taken from CT and photographed residues are. However, these preliminary results should serve as a note of caution to any analysis that might use them interchangeably.

Discussion

Size limitations

The use of CT and the methods of sample preparation impose bounds on the size of objects identified in this study. Core dimensions (~1.5 cm diameter, ~1-3 cm height) strictly limit the maximum size of fossils and other features of interest; additionally,

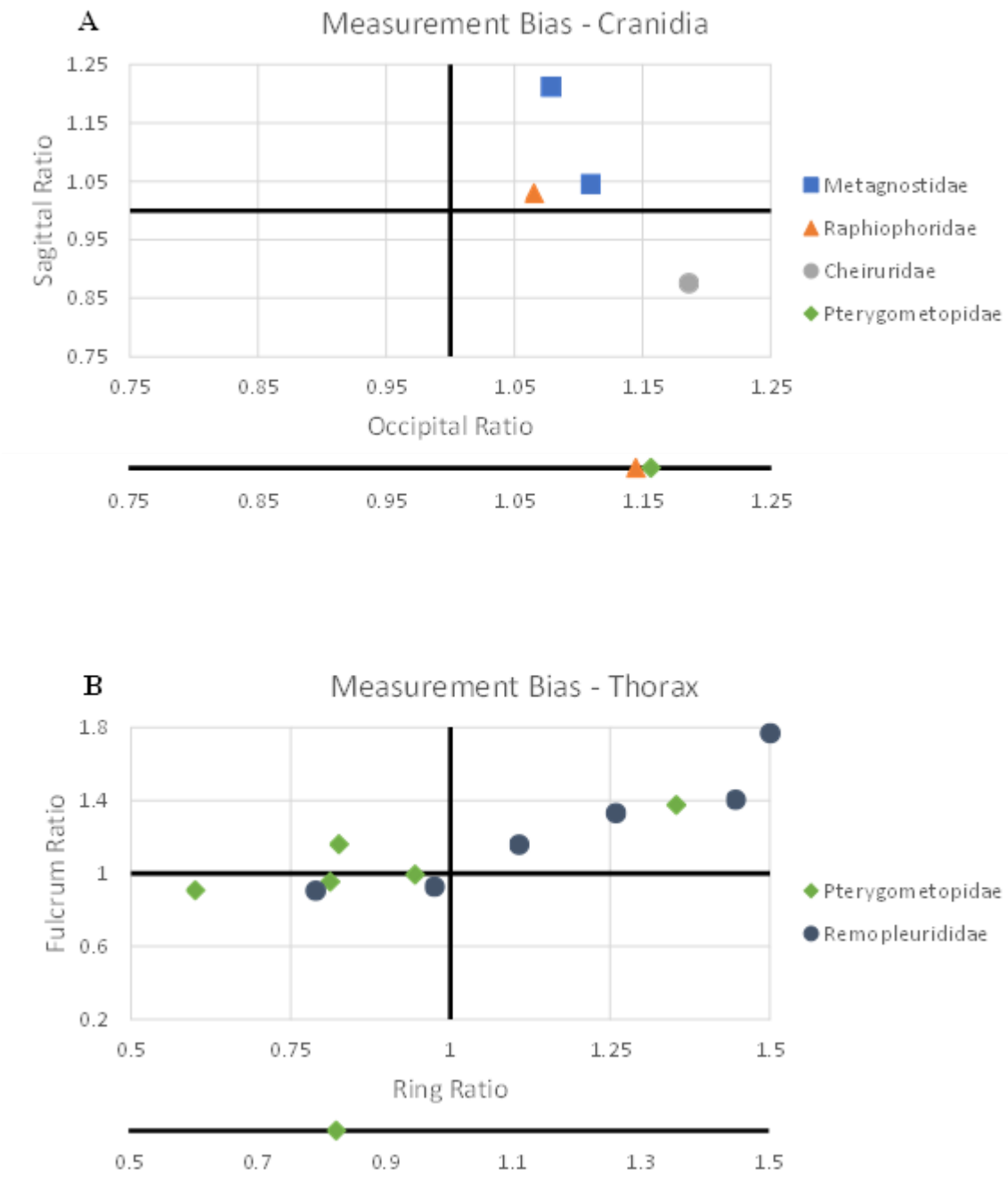

Figure 11: Measurement bias of cranidia and thoracic segments

Ratios of CT measurements to corresponding residue measurements in
A) cranidia: occipital lobe width, sagittal length
B) thoracic segments: axial ring width, fulcrum-to-fulcrum width

objects approaching these dimensions are increasingly likely to be damaged or truncated by the drill used in sampling, biasing both CT and residue against the recovery of particularly large fossils.

The minimum size limit is the result of imaging resolution. CT imagery in this study has a voxel size of approximately 30 μm, while GIGAmacro optical imaging of residues has pixel size on the order of 5 μm. (Neither is near the technical limit of the imaging technique in question or the instruments used, but rather reflects a tradeoff between resolution and time on the instrument required to image the sample.) However, the practical resolution limit at which objects can be identified is significantly larger than the pixel/voxel side length and is highly dependent on object shape and the amount of background noise. Objects smaller than ~1 mm in CT or ~0.5 mm in residue imagery were not reliably identified.

Both maximum and minimum size limitations can cause apparent taxonomic biases as a knock-on effect. Very large taxa, such as the trilobite *Isotelus* (Asaphida: Asaphidae) are found in this study only as fragmentary material since their sclerites are too large to easily fit within a sample core. Meanwhile, very small taxa, such as ostracods, are abundant in residues but nearly absent from CT data due to their small body size making them more susceptible to noise; other organisms with a large maximum dimension but narrow body width, such as dendroid bryozoans, can suffer from this effect as well if they cannot be distinguished from abiotic features with similar geometry.

Size bias

We hypothesized at the outset of this study that body size would be negatively associated with likelihood of recovery in residues; larger fossils may be more susceptible to breakage, and larger organisms with thicker skeletal elements may not silicify through entirely and rather produce a brittle outer husk. However, the results of this study do not support this possible effect. While fossils recovered in residue have a smaller median

body size than those resolved in CT, this appears to be due not to preferential breakage of larger fossils during washing but rather disproportionate non-resolution of smaller fossils in CT imaging. Rather than CT acting as a baseline to test the biases of acid maceration based on body size, the results of this study suggest maceration has less size bias than CT.

Limitations of size comparisons

Comparisons of fossil size between CT imagery and residues suffer from two key limitations. Breakage during washing can alter the measured size of fossils, and may not be immediately apparent if the broken area has suffered pre-burial damage or is poorly resolved due to noise. (Noise may also render part of a fossil unrecognizable in CT, giving a false appearance of pre-burial breakage.) While this is relevant to the central research question of this study, it can interfere with correlating objects in CT imagery to their counterparts in residue, causing some to be recorded as not recovered in residue, when in fact they were recovered but not *recognizably* so.

The other issue of size comes from automated measures of size. Maximum and minimum widths of segmented regions are measured automatically in Dragonfly and FIJI as Feret diameter (Feret, 1930; Walton, 1948). While these measurements are taken of 3-D objects in CT, however, the corresponding measurements of objects in residue are not of the 3-D objects themselves, but rather of 2-D projections of 3-D objects (that is, the top-down view of the fossils in a gridded picking tray). Since these objects naturally come to rest in a stable position, their true minimum diameter is typically nearly normal to the plane of the image; any minimum diameter taken is therefore likely larger than the true minimum diameter of the residue object being imaged and cannot be compared with

the minimum diameter of the corresponding CT object. Maximum diameters can be affected as well, if the true maximum diameter of the residue object is inclined relative to the plane of the image, but this difference is usually fairly minor. For the purposes of this study, comparisons between automated measures of size in CT and residue were restricted to maximum diameters.

Taxon bias

The finding that unidentified trilobite fossils resolved in CT are significantly less likely than the average to be recovered in residue is perhaps to be expected. Fragmentation and incomplete preservation are likely and common causes for trilobite material to lack identifying characteristics, and both are likely to promote breakage and degradation during washing by compromising the structural integrity of the sclerite. This may also influence likelihood of recovery by impeding identification of the fossil in residue; a fragment of cuticle lacking identifying characteristics is less likely to be recognized as corresponding to an object observed in CT, and minor breakage is likely to disrupt recognizable aspects of its outline and other key features.

The overrepresentation relative to the average of pyritized taxa (gastropods and bivalves) in CT may be the result of the high contrast between iron-bearing phases and the matrix making such fossils easier to resolve in CT than otherwise-comparable siliceous fossils. Alternatively, this may represent preferential breakage of pyritized material during washing due to differences in replacement texture. Ostracods, meanwhile, are almost certainly overrepresented in residue due to their small size making them difficult to resolve in CT. Branching bryozoans may also suffer from this, but their numbers are likely inflated by fragmentation of large individuals into many smaller ones.

Ostracods persistently not resolved

While ostracods are abundant in many sample residues, they are nearly absent from CT imagery, with only a single individual identified in the latter. This can be attributed to their small size rendering them vulnerable to obliteration by imaging artifacts and other noise and their morphological simplicity leaving them "featureless", without recognizable anatomical markers (Williams & Vannier, 1995).

Ostracods from these residues are typically found as single valves, though articulated individuals are not uncommon. Most bear little ornamentation and have a smooth outer surface, while some have laterally projecting spines finely preserved. Fragmentary individuals are fairly rare, which may indicate that they are resistant to breakage during washing or that those that do fragment typically do so beyond recognition; discerning which is the case is beyond the scope of this work.

Taxon-specific breakage: remopleuridid thoracic segments

Remopleuridids, a family of small micropygous asaphid trilobites with large eyes, narrow (tr.) pleurae, and an inferred nektonic lifestyle, are abundant in many samples from this study, principally as the type genus *Remopleurides*. Another genus, *Robergia*, is known from the Liberty Hall facies, but identifiable material in this study is more consistent with *Remopleurides* (Read, 1982).

Their effaced cranidia and librigenae (complete with genal spines) are fairly common, as are their thoracic segments, while their small four-forked pygidia are quite rare in both CT and residues. *Remopleurides* thoracic segments have a distinctive geometry; they are highly arched with a wide axis and very small abaxial-posteriorly

angled paddle-shaped pleural lobes (hence the generic epithet, Latin for “oar flanks”) with an extensive doublure. This doublure makes the thoracic pleurae effectively bilayered across most of its area, reinforcing it against stresses and likely increasing the resilience of these parts of the sclerite during washing.

This anatomical feature may explain a pattern observed in this study. Remopleuridid thoracic segments observed in CT were typically complete, but residues in which *Remopleurides* were present tended to contain abundant isolated thoracic pleurae recognizable by their geometry but unattached to any axial material. While pre-burial breakage cannot be definitively ruled out in this case, it is possible for fragmentation of recognizable remopleuridid thoracic segments (whether complete or partial) to preferentially destroy the axis of these sclerites, leaving behind the more resistant pleurae without sufficient anatomical features to pair them with their correspondents in CT data.

Taxon-specific breakage: raphiophorid cranidia

Raphiophorids are abundant in several of the sampled horizons and have the highest total sclerite count of all trilobite groups considered. Like many other trinucleoids these epifaunal trilobites are eyeless, with long hollow genal spines and thin cuticle with an effaced prosopon, and usually bear long, gently curved glabellar spines; both glabellar and genal spines were likely used in social interactions with conspecifics (Knell & Fortey, 2005; Vannier et al., 2019).

In samples containing raphiophorids, cranidia and librigenae (particularly the distinctive fishhook-shaped librigenae of *Lonchodomas carinatus*) are generally common

and recognizable, and pygidia and thoracic segments somewhat less so. While this general pattern of abundance is qualitatively consistent between CT imagery and residues, there is a marked difference in the preservational quality of raphiophorid cranidia specifically. Cranidia tend to be fairly complete when identified in CT, with the glabella intact and usually only minor damage to the fixigenae. In residues, however, cranidia are frequently found in highly fragmentary condition, with the base of the glabellar spine and surrounding cuticle forming a cup-like structure but the rest of the sclerite entirely missing. This breakage pattern is likely the result of the thin cuticle and the absence of deep furrows reinforcing the sclerite; since the cuticle is thicker where the glabella is extended out to form the spine, this remnant is less subject to breakage.

Isolated spines similarly suffer breakage during extraction. It is not generally possible to definitively distinguish between genal and glabellar spines from the raphiophorids present here if the spine base is not preserved; the notable exception is, again, *L. carinatus* due to the unique and distinctive geometry of its genal spines. Long (> 1cm) spines from large individuals are clearly visible in CT imagery, occasionally including the base or tip, but found only as shorter fragments in residue. This is easily attributable to the highly elongated shape and very thin cross-sectional area of these spines.

Taxon-specific breakage: bryozoans

Like other silicified fossils in these samples, recovered bryozoans tend to be preserved through highly fabric-specific replacement of original skeletal material rather than infilling of interior spaces. The result of this preservational style is bryozoans consisting of thin crusts of silicified cuticle with void space (originally filled by micrite,

but lost during maceration) within; neither the interiors of dendroid forms nor the fenestrae of lacy forms are filled with diagenetic silica. Bryozoans preserved in this hollow fashion are fragile and susceptible to crushing stresses, especially dendroid forms with highly elongated geometry, and commonly break apart during washing.

Due to their modular growth patterns, bryozoans can be challenging to digitally reassemble; they exhibit frequent self-similarity, with multiple parts of a single colony following the same general growth form to the point of near-interchangeability when piecing together a fragmented specimen (Key et al., 2016; Sánchez et al., 2004). However, some specimens, even when highly fragmented during washing, can be effectively correlated to whole objects from CT imagery.

Fenestrate bryozoans with a lacy growth form are generally better suited to this approach due to their more constrained geometry and greater abundance of well-constrained recognizable loci (Type I landmarks in the morphometric sense) than bryozoans with thin- or thick-branching dendroid growth forms (Slice et al., 2009). Such lacy bryozoans are not particularly abundant in sampled materials, but a single colony fragment identified in CT (01-C4-001) was identified in residue as four separate smaller fragments (01-R4-002, 01-R4-005, 01-R4-010, 01-R4-044) recognizable by their pattern of anastomosing, representing in total nearly all of the CT object. (Figure 12)

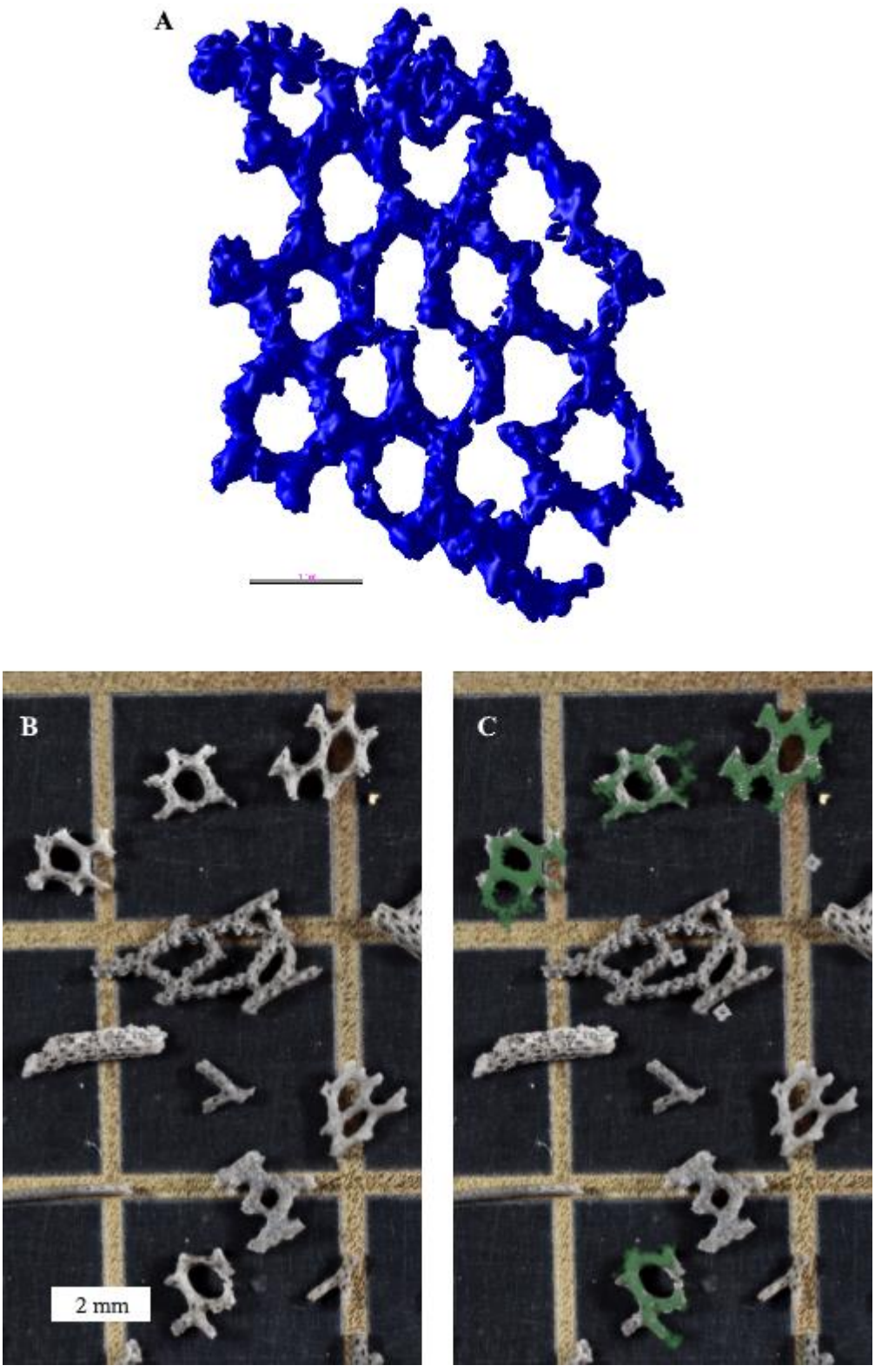

Figure 12: A lacy fenestrate bryozoan in CT and in residue

A) CT render of fenestrate bryozoan (01-C4-001), scale bar approx. 1 mm
B) Recovered fossils from core 01-C4, scale bar 2 mm
C) Same as B) but with overlay of CT imagery on fragments (01-R4-002, 005, 010, 044) corresponding to 01-C4-001.

Orientation of fossils in CT

Previous work on the Edinburg Formation has found evidence of transport prior to burial based on preferential size-sorting of different sclerites within trilobite taxa (Whittington & Evitt, 1953). Such transport might plausibly also directionally sort sclerites along a preferred orientation, and this effect is observed in some cores in this study.

Of the 15 cores imaged, two (01-C1, 05-C1) showed signs of directional sorting, with closely packed fossils with platy geometry preferentially aligned with the orientation of bedding. The contents of most cores (01-C2, 01-C4, 03-C1, 03-C3, 03-C4, 04-C2, 04-C3, 05-C4, 06-C1, 06-C3) were sparse, with no sign of preferred orientation of grains. One core (01-C3) appeared to have undergone pervasive and disseminated fabric-nonspecific silicification, obliterating any signals of directional sorting.

Patterns of pyritization

While the main focus of this study is on silicified fossils, a second remineralized preservational style, pyritization, is present in the Edinburg Formation. Pyrite and pseudomorphs of iron oxides and oxyhydroxides after pyrite are known from the Liberty Hall facies of the Edinburg reflecting fossil replacement, disseminated growth within sediment or along fractures, and occasionally large euhedral grains within voids (Penick, 1987). In material from this study, both fabric-specific and fabric-nonspecific pyritization is observed.

Remineralization in the studied rocks is highly taxon-specific. Bryozoans, brachiopods, and arthropods (trilobites and ostracods) are preserved through silicification, while mollusks (gastropods and bivalves) are preserved through pyritization. Rare exceptions to this rule include occasional pyrite infilling of space within silicified trilobite sclerites and branching pyritized objects (resolved in CT but not recovered in residue) that may be dendroid bryozoans. Residues from sample 06-C3 contained pyritized objects which based on their regular porous texture may be fragmentary echinoderm ossicles, most likely crinoid brachials, but definitive identification is not possible at this time.

Fossils preserved through pyritization in this study consist almost universally of replaced skeletal material rather than internal molds or other space-filling pyrite growth. Both bivalve and gastropod shells are preserved through fine-grained replacement, with little to no overgrowth (Figure 13); however, subsequent oxidation of early pyrite to iron oxides/oxyhydroxides may have obscured the original diagenetic texture. One internal mold of a gastropod shell was recovered from residues, alongside several other gastropods from the same sample preserved in the more common shell-replacement style.

Two instances of unambiguous pyrite infilling of silicified trilobite material were observed. In one case, a raphiophorid cranidium observed in CT imagery (05-C4-005, 05-C4-047) was found to contain space-filling iron minerals within its hollow glabellar spine and in parts of the glabella itself. (Figure 14) This specimen was identified in residues as an iron-stained partial cranidium missing the anterior aspect of the glabella and spine base (05-R4-095) and separately, a short section of a hollow spine with the interior

infilled with pyrite since altered to hematite (05-R4-052), apparently having fragmented during washing.

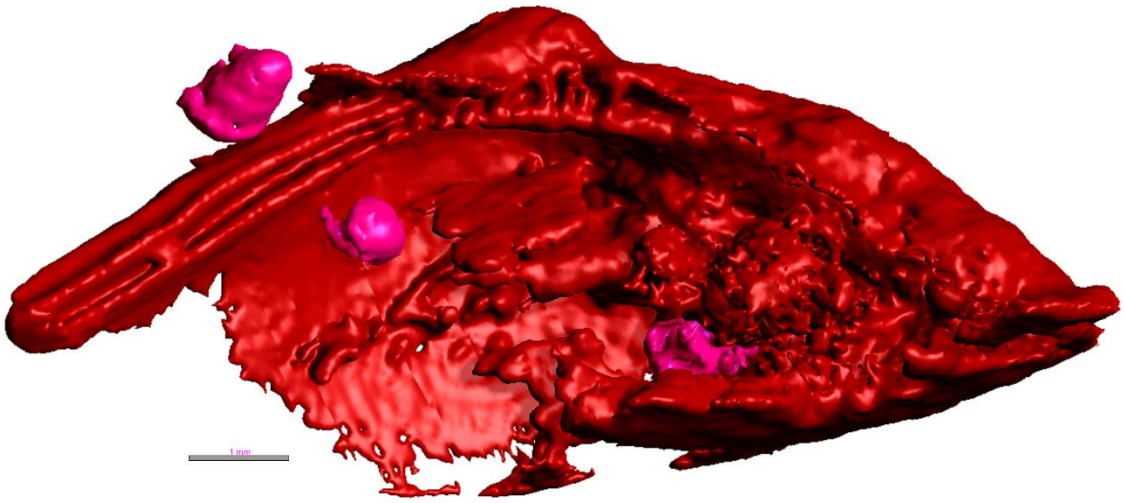

Figure 13: CT renders of pyritized mollusks

A large bivalve (03-C3-064, red) in the family Nuculanidae containing disseminated iron mineralization along with three small gastropods (03-C3-060, 03-C3-062, 03-C3-065, pink). Sampling of the core has truncated this specimen at the bottom right of the image.

A more dramatic example is that of three articulated *Remopleurides* thoracic segments (03-R3-009), the middle segment bearing an axial spine and the posterior segment incomplete. (Figure 15) The silicified cuticle is patchily preserved or abraded in places along the ventral surface of the axial spine and on the dextral pleurae of the anterior and middle segments, and hematite (originally pyrite) infilling is clearly visible in between; iron staining is also noticeable in patches on both dorsal and ventral surfaces of the segments. It is unknown whether this pyritization is related to the remarkable articulation of this specimen (all other trilobite material was fully disarticulated), but both could stem from a shared cause. Particularly rapid burial after death might have promoted remineralization starting while the cadaver was still partially articulated, cementing

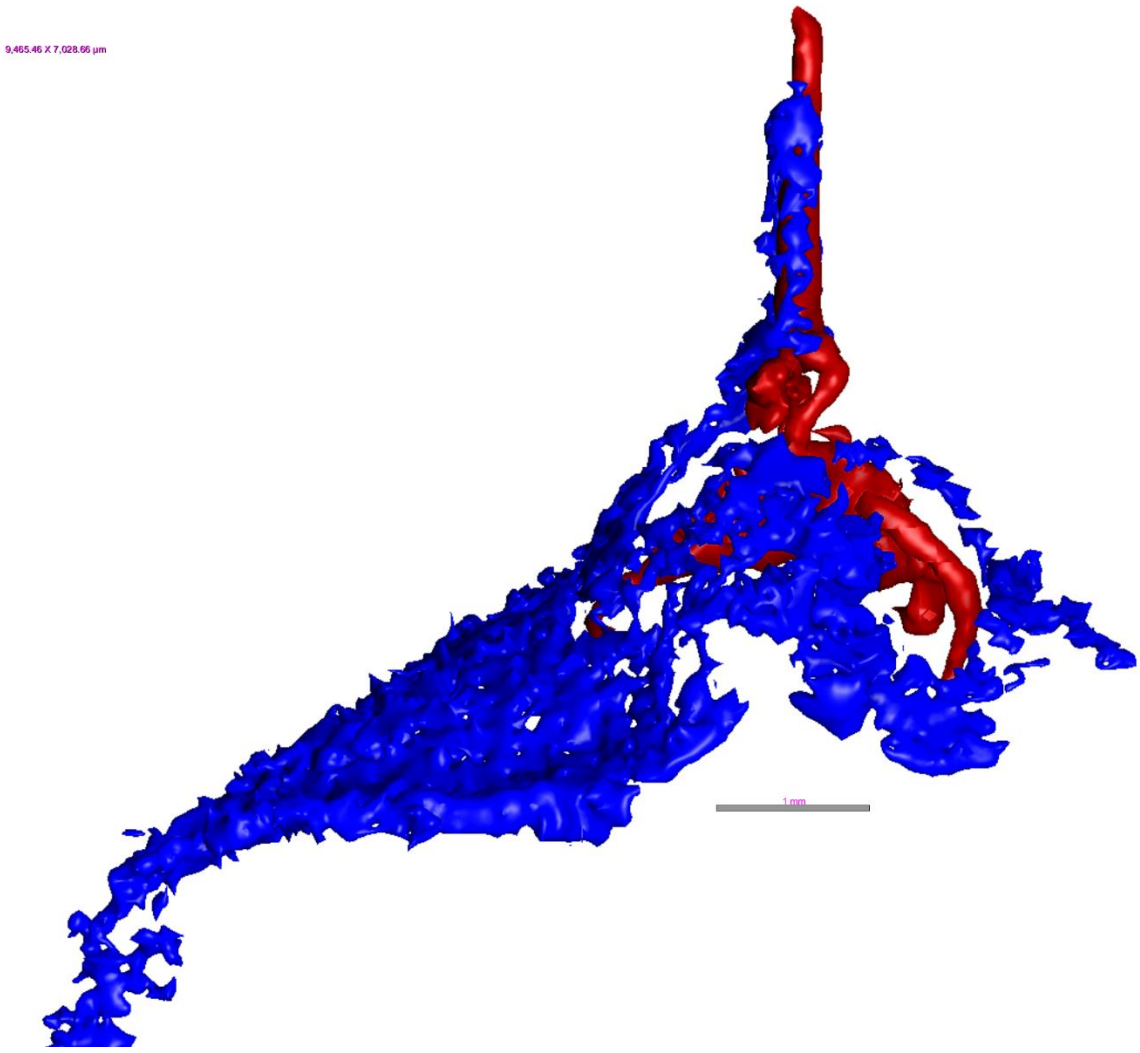

Figure 14: CT render of raphiophorid cranidium

Dorso-posterior view. Preservation includes both silica remineralization (05-C4-005, blue) and pyrite infilling (05-C4-047, red).
Scale bar approx. 1 mm

sclerites together, and an influx of sediment sufficient for such burial could bring it into the bacterial sulfate reduction (BSR) zone while still containing abundant organic matter to feed this process (Muscente et al., 2016; Schiffbauer et al., 2014). It is of note that this specimen was not resolved in CT imagery, and subsequent attempts to find signs of it failed as well. This is attributable to the beam hardening artifacts caused by large grains of high-density iron minerals, which tend to obliterate subtler signals immediately

Figure 15: Articulated thoracic segments of *Remopleurides*

Note iron mineralization as reddish staining at left. Scale bar = 1 mm

adjacent to them; since the thin cuticle of the specimen appears to be filled in largely with iron minerals, it likely cannot be resolved in the imagery available. (Cone artifacts near the top and bottom of the core may have played a role as well.)

Pyrite was also present as isolated granules within the matrix, based on CT imagery. The paragenesis of this disseminated pyrite is unclear, and it is not immediately apparent whether it formed during early burial or later in diagenesis. Long (>1 cm), arcuate tubes and streamers of partially or weakly pyritized sediment were also observed

in CT imagery, possibly reflecting burrows, worm tubes, or other biogenic structures (though no taxonomic assignment is possible); with one exception, these features were not recovered in residue and apparently disintegrated during dissolution due to their poorly cemented structure.

Most pyritized objects, whether fossils or not, appear to have been secondarily oxidized to hematite and/or limonite during diagenesis, either completely or as partial alteration rinds around unaltered cores. All iron-containing phases were resolved well against calcareous and argillaceous matrix materials, but distinguishing between them in CT is not feasible in this study due to the relatively small difference in X-ray opacity between them (relative to the much larger differences between iron minerals and matrix) and the presence of beam-hardening artifacts around all high-opacity objects. Fragments of both pyrite and hematite (easily distinguished by their respectively metallic and earthy lusters) were observed during washing.

Preservational/preparational incomplete gastropod preservation

Pyritized gastropods have previously been reported from the Liberty Hall facies in projects using acid maceration (Jacobs & Carlucci, 2019). Gastropods from that previous work and those from the current study tend to be preserved through fine-grained replacement of shell material and also share an unusual pattern of incomplete preservation: the columella and the sutures between adjoining whorls are well-preserved, but the outer (abaxial) walls of the whorls are patchy or absent.

Based solely on fossils extracted through acid maceration, it is difficult to say whether this incomplete condition reflects a pattern of original remineralization or

breakage during recovery. Since the outer walls of the shell are more exposed to abrasion, crushing, and tumbling during washing, the observed preservation might plausibly result from damage preferentially to these areas during specimen preparation. However, CT imagery clearly shows this style of incomplete preservation in gastropods still within the sampled rocks, indicating that it is a feature of diagenetic remineralization (Figure 16).

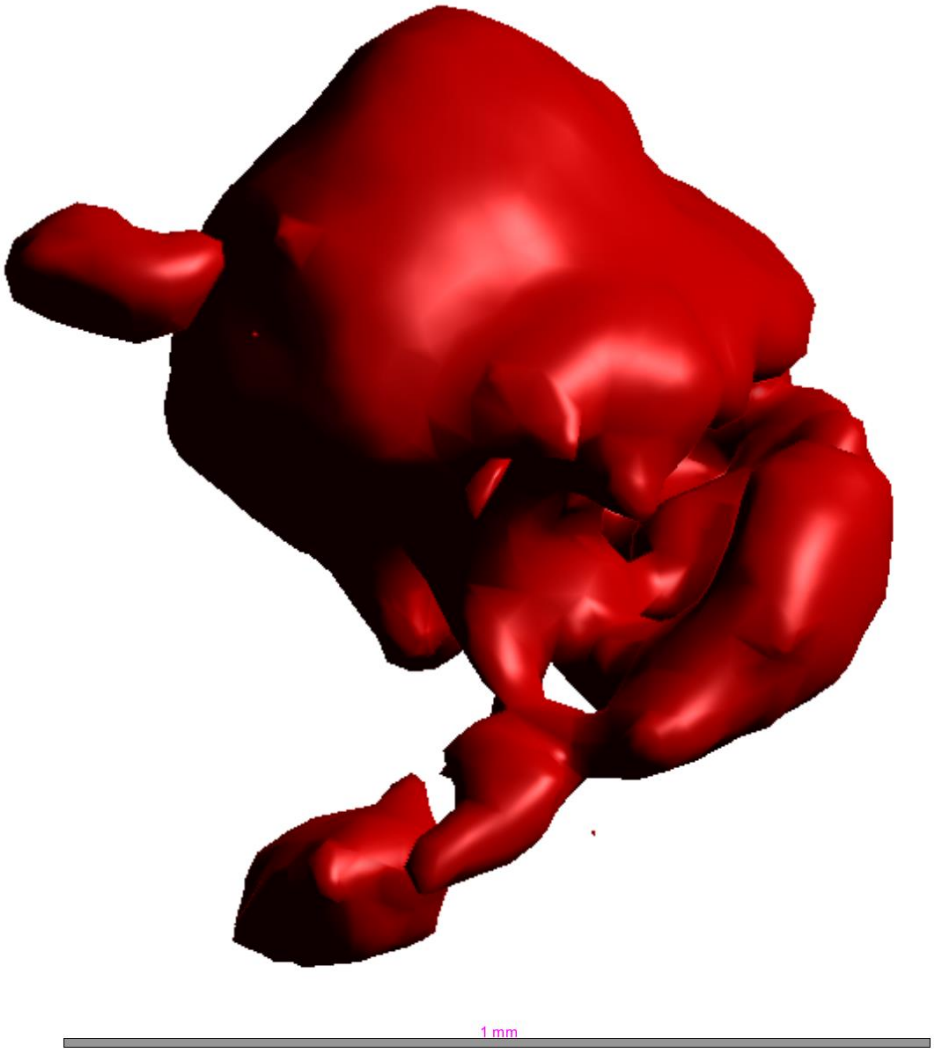

Figure 16: CT render of a pyritized gastropod (06-C3-033)

Apex at top of image; note incomplete preservation of whorl outer wall. Scale bar approximately 1 mm.

Brachiopods incompletely preserved

Brachiopods in these samples are quite uncommon. All brachiopod material recovered from residues is highly fragmentary and identifiable only by ornamentation (ridging) rather than overall valve morphology. Interestingly, all such material is quite thin, likely preserving either a single layer of shell or an alteration crust formed by incomplete remineralization of only the outermost surface of a brachiopod valve.

No brachiopods were identified in CT imagery; since surface texture of fossils is indistinct and poorly resolved due to noise in the data, this is not unexpected given the condition of brachiopods from residue.

Whether the scarcity and poor preservation of brachiopods in study materials reflect preservational bias or original paleoecological structure is not immediately clear. Previous descriptions of the Edinburg Formation note that faunal assemblages found within it vary markedly among sites, and record brachiopods from the underlying Lincolnshire Limestone that are absent in the Edinburg in sections where both are exposed (Cooper & Cooper, 1946). Since the Lincolnshire is interpreted as a subtidal ramp deposit while the Edinburg is a deep-ramp to basin, it is possible that brachiopods from these localities were restricted to medium depth environments and disappeared from these sections due to regional transgression in foreland basins associated with the Taconic Orogeny (Read, 1980, 1982; Read & Eriksson, 2016). If this is the case, the rare and poorly preserved brachiopod material recorded in this study may have been transported downslope from shallower settings; there is evidence based on trilobite sclerite ratios of pre-burial transport among some biota in the Edinburg (Whittington & Evitt, 1953).

Clay content and washing

A noteworthy factor controlling patterns of fossil recovery is the clay content of the rocks sampled. The Liberty Hall facies represents deep-ramp to basinal environments with low depositional energy, resulting in relatively high amounts of clay, both as argillaceous limestone (including the materials in this study) and as shaley interbeds (Cooper & Cooper, 1946). Clays have two physical properties affecting the recovery of silicified fossils under these methods: insolubility in acidic aqueous solutions and a tendency to flocculate. Dissolution of the whole rock leaves behind not only the silica and iron sulfides/oxides/oxyhydroxides making up remineralized fossils, but also chemically resistant clays; if this clay fraction is significant, fossils may remain caked in a layer of clay that obscures surface detail or even embedded within lumps of clay that prevent recovery entirely.

Purely mechanical means are ineffective at removing this clay residue, since clay particles readily flocculate due to electrostatic forces resulting from their platy geometry and unusual anisometric charge distribution (van Olphen, 1964). Layers of clay on extracted grains tend to resist being suspended in the supernatant through gentle washing, and agitation intense enough to remove them would likely destroy the brittle fossils to which they adhere. Chemical methods, however, can loosen clays and allow them to be washed away. The deflocculant Calgon (sodium hexametaphosphate/polyphosphate) efficiently promotes the suspension of clays through substitution and complexing of cations, reducing the tendency of clay grains to cling to each other and to other objects of interest (Abdulkarim et al., 2021; Andreola et al., 2004). However, this process still requires substantial washing, with repeated changes of supernatant alternated with

immersion in a sonic bath to loosen clay and promote its interaction with Calgon in solution.

The fragility of silicified fossils unavoidably means that they may be chipped, fragmented, or destroyed even by gentle sonication, and this risk increases with the intensity and total duration of sonication. For this reason, the mineralogical bulk composition of the sampled limestone exerts an influence on the recovery of silicified fossils through acid maceration; clay-poor sediment will require little or no sonication, while clay-rich sediment must be washed and sonicated for longer durations or else risk leaving significant amounts of clay behind, leading to greater loss of fossils either within resistant lumps of clay or through breakage during washing. The choice of acid can become relevant as well when dissolving argillaceous limestones; hydrochloric acid and formic acid may promote flocculation of clays, a shortcoming apparently not shared by acetic acid (st. Clair, 1935; Yang et al., 2012). The use of appropriate reagents to minimize flocculation can help reduce the total washing and sonication times necessary, avoiding breakage of recovered fossils.

Conclusions

Key takeaways

The geosciences have made extensive use of μCT in the decades since its invention, ranging from quantitative hydrological characterization of pore space to nondestructive imaging of unique fossils to mapping fractures, sedimentation, and mineralization in three dimensions (Bendle et al., 2015; Cnudde et al., 2006; Cnudde & Boone, 2013; Elkhoury et al., 2019; Markussen et al., 2019; Mees et al., 2003;

Schiffbauer et al., 2020). We here report an additional application of this method to assess bias in differential preservation and preparation of silicified fossils in limestone extracted through acid maceration, as well as recovering information on depositional textures which is lost during dissolution.

While the main goal of this study was to quantify the effects of taxonomic affinity and body size on the likelihood of recovery, it is the qualitative results that may have the broadest relevance to further work. Breakage remains an unavoidable concern with acid maceration, but the degree to which breakage rates depend on body size and taxonomic factors likely varies substantially between deposits. This variation can stem not only from easily observable sedimentological features such as grain size and composition but also from redox chemistry and solute profiles of pore fluids during burial and early diagenesis, which can be challenging to infer from samples without more in-depth geochemical analyses. Original shell composition, both in terms of organic content and aragonitic versus calcitic (high- or low-magnesium) mineralogy is likely relevant due to its influence on the spontaneity and kinetics of silicification chemistry.

Information on the breadth of variation is limited but suggests a wide range of possible taxonomic outcomes based on sample lithology. Previous studies have found aragonitic taxa to be silicified in some deposits but excluded from silicification in others, an observation relevant to settings dominated by mollusks or corals (Cherns et al., 2010; Cherns & Wright, 2000; Holdaway & Clayton, 1982; James G. Schmitt, 1981; Pruss et al., 2015; Wright et al., 2003). It is currently unclear whether oceanic concentrations of Mg^{2+} play a role in whether or not aragonitic organisms readily silicify. The source of diagenetic silica may exert control on patterns of silicification as well; deposits with a

similar taxonomic composition of silicified and non-silicified faunas (evincing the absence of taxonomic bias in silica replacement) are often associated with bentonites, suggesting that taxon-selective silicification may be more common with silica derived from other sources, such as sponge spicules or diatomaceous oozes (Laufeld & Jeppsson, 1976; Pruss et al., 2015).

CT imagery should not be considered an unbiased inventory of the rock's original contents prior to dissolution, nor should recovered residues be treated as a way to "ground truth" interpretations of CT. Rather, these two methods are complementary, each with a different set of biases and limitations, and neither recovering all information originally present. CT allows for the documentation and description of features, such as partially mineralized burrows and preferential orientation of fossil grains, which may be common in studied rocks but are universally lost during dissolution through the removal of grains from their depositional context. Residues from acid maceration, meanwhile, can recover fossils in a broader size range (potentially both larger and smaller) and with greater taxonomic certainty due to improved fidelity of surface and textural features.

Further study

Directions for ongoing research include the investigation of other common destructive preparation methods as well as expanding analyses to other deposits with different lithology or preservation diagenesis in order to broaden applicability beyond a specific instance of silicification. Closer study of the geochemistry and timing of silicification in the Edinburg Formation may also be important to contextualize results from this study.

Acid maceration is a common and longstanding chemical preparation method, but its use is limited to chemically susceptible rocks containing resistant grains (in practice, limestones containing siliceous, phosphatic, or ferrous fossils). With few exceptions (e.g., calcite-cemented fossiliferous sandstones) clastic rocks cannot be prepared in this way. The use of CT, however, is not limited by sample mineralogy or composition, so long as the features of interest are distinguished from the matrix by detectable differences in X-ray opacity or textural changes sufficient for phase-contrast imaging; by pairing μCT with other common destructive preparation methods, this imaging technique can provide relevant context to studies of broader types of samples.

One such preparation method is petrographic thin section analysis, ubiquitous in sedimentology and petrography of all kinds. By grinding a hand sample down to a very thin (~30 μm) layer recording a single plane through the original rock, textural and mineralogical features of the sample can be studied in detail and, with the use of standardized point-counting techniques, in a quantitative way permitting direct comparison of sample composition (mineralogical and paleoecological) across a geographic area or along a stratigraphic section. The cost of this method is the loss of the third dimension in the sample; textural anisotropy (e.g., cross-bedding, directional sorting) may be difficult or impossible to record, taxonomic precision is limited because individual fossil grains cannot be identified by morphological features, large grains may be overrepresented since they are more likely to be intercepted by a plane through a sample (or even intercepted twice separately depending on their geometry), and grains composed of opaque minerals can require additional analysis to identify. Some of these limitations can be corrected by pairing thin section analysis with μCT, selecting a

projection in CT imagery as a “virtual thin section” corresponding to the plane of the thin section then made from the sample. Such an approach provides three-dimensional context to grains intercepted by the plane of sectioning, allowing potentially for better recovery of textural features and greater confidence in the identification of fossils; this technique has been successfully applied in sedimentological research on glaciolacustrine deposits, and holds promise for the investigation of fossiliferous rocks (Bendle et al., 2015).

The results of this study are strongly controlled by the characteristics of the rocks sampled; biases measured by this paired analysis are specific to the preservational style of the Liberty Hall member of the Edinburg Formation. Further lithological analysis of these limestones and the timing and biogeochemistry of early diagenetic remineralization within them may help to explain patterns of recovery by the methods applied here. Given the possible link between bentonite-derived silica and taxon-nonspecific silicification, investigation of the source of diagenetic silica in the Edinburg via mass spectrometry may yield useful insights; likely origins of this silica include sponge spicule oozes and the Millbrig bentonite (Mitchell et al., 2004; Pruss et al., 2015; Sell et al., 2013).

Going forward, μCT has the potential to inform and act as a key control on analyses of chemically extracted/prepared fossils. The results of this study should serve in equal measure as a roadmap and a cautionary tale; researchers applying our methods should be aware of the drawbacks of CT as well as its strengths, taking advantage of the otherwise-lost information it recovers while not discounting the degree to which traditional acid maceration methods complement its deficiencies.

Chapter 4: Paleoecology interpreted through paired preparation methods

Introduction

Biofacies analysis is a discipline linking sedimentology and paleoecology, characterizing past environments not by the organisms that lived in them but by the distinctive assemblages of fossils and other biological features found within the corresponding rock units (Imbrie, 1955). Living biota and fossil assemblages are separated by biases in preservation, which may magnify the apparent importance of taxa with high preservation potential or cause keystone species with small populations and little mineralization to occur only as isolated specimens with little relevance to stratigraphic categories. These preservational effects can be compounded by further biases imposed during sample preparation, preferentially recovering some taxa over others based on differences in body size, original mineralogy, or differential remineralization.

The early stages of biofacies analysis are particularly vulnerable to such biases because of the degree to which further steps depend on their results. Initial statistical methods tend to be exploratory in nature, generating multiple categories to describe the variation observed across the samples studied; confirmatory tests are then applied to determine the proportion of variation explained by the grouping and to sort new samples within the previously established categories (Huntley, 2011). However, if the samples are affected by pervasive taxonomic bias these categories may not be meaningful. Multiple related biofacies corresponding to distinct paleoenvironments might be wrongly grouped together if taxa unique to one are poorly preserved and therefore rarely recovered. Taxa

that are overrepresented by a high potential for recovery or pre-burial sorting may come to dominate the classification scheme, obscuring differing patterns in less abundant taxa by their sheer numbers (Westrop, 1986). If potential biases are not taken into account when performing exploratory tests, downstream analyses in the workflow can be compromised.

Developing a classification scheme for biofacies based on the relative abundance of taxa across sampled units typically begins with representing samples as points in an n-dimensional space, where n is the number of informative taxa in the study. (A taxon is informative for these purposes if it appears in multiple samples; a taxon found only in a single sample gives no information on how similar or dissimilar that site is to others.) Each Cartesian coordinate of a point corresponds to that sample's measured abundance of a different taxon, whether as raw counts, abundance categories, log-transformed counts, or similar. Samples with similar taxonomic composition will be near to each other within the space, and samples with different makeup will be relatively further away; this is the basis for further analysis to group samples by mutual similarity.

Since high-dimensional spaces cannot be visualized, the resulting point cloud must be subjected to an ordination to isolate variation within a dataset in fewer dimensions. One of the simplest such methods is principal component analysis (PCA), which performs a rigid rotation of the point cloud (change of basis) to find new axes along which is distributed as much as possible of the variation within the data set (Pearson, 1901). While reliable and serviceable for most applications of this type, PCA has been largely supplanted by newer methods that isolate more variation into two dimensions at the cost of deforming the point cloud. These include principal coordinate

analysis (PCoA) and the related iteratively computed method non-metric multidimensional scaling (NMDS) (Kruskal, 1964a, 1964b; Torgerson, 1958). These methods are suitable for data sets that may not meet the preconditions for PCA, which requires that input data be continuous and normally distributed, criteria rarely met by ecological observations; taxon counts or abundance scores are invariably discrete, and the relationship between observed abundance and frequency of observations cannot be relied on to follow a normal distribution. By comparing abundance rank rather than abundance itself, NMDS also avoids potential over-weighting of relatively common taxa, which can occur in PCA and PCoA.

However, applying alternatives to PCA does introduce potential weaknesses into the analysis. Due to the relative position of data points influencing how the cloud is deformed in these ordinations, and especially due to the iterative nature of NMDS potentially amplifying small variations, these methods are especially sensitive to bias and errors in the original data.

The choice of ordinations for exploratory analysis of ecological and especially paleoecological data remains a somewhat contentious open problem. Various studies have applied multiple ordination methods to single data sets in order to assess their consistency and reliability, but their relative performance seems to depend on the characteristics of the data sets and the types of questions being asked (Clapham, 2011; Huntley, 2011; Jackson, 1993; Minchin, 1987). Ultimately, which ordination is used is often a matter of preference and familiarity, within the bounds imposed by the ordination's prior assumptions and how the characteristics of the data set compare to them.

Paleoecology through CT

Work concomitant to this study has investigated potential taxonomic and body-size biases of preservation and preparation in fossils imaged using micro-computed X-ray tomography (μCT) and extracted using acid maceration. While that analysis focused on biases affecting differential recovery of fossils by the methods paired, the results gathered also contain a wealth of paleoecological information on the sampled horizons. By analyzing biofacies and ecological similarity across samples using taxon abundances derived from CT imagery and from disaggregated maceration residues, the potential effects of these recovery biases on paleoecological reconstructions can be assessed.

Methodology

Materials

Hand samples were collected from six distinct fossiliferous horizons at the Strasburg Junction railcut in Shenandoah County, Virginia, from rocks of the Liberty Hall member of the Edinburg Formation. (Figure 10) Cylindrical cores approximately 2 cm in diameter and 1 to 4 cm in height were drilled from these samples, approximately normal to the orientation of bedding. Fifteen of these cores, representing five of the six horizons, were selected for further study.

Hand sample material from the five horizons studied was visually examined to characterize variation in lithology across sampled material. Color, texture, apparent layering or directional sorting, the presence of grains (biological or otherwise) and fossil taxa recognizable on fresh and weathered surfaces, and the appearance of the weathering

rind were all recorded for the samples from which the cores were cut, as well as for additional material collected from the same horizons.

Sample preparation

Selected cores were scanned using a Zeiss Xradia 510 Versa X-ray microscope to produce three-dimensional images of the cores and their contents, with an approximate voxel length of 30 μm along all three axes. This μCT imagery was processed using the Ring Removal and Median filters in ORS Dragonfly software (*Dragonfly*, 2022). Regions of high and low density relative to the surrounding matrix (representing silicified and pyritized fossils respectively) were manually segmented in Dragonfly, using multiple brightness bands in different regions of cores when necessary due to persistent radial and longitudinal variation in baseline brightness of the matrix.

After imaging, cores were digested in 10% acetic acid to remove the calcareous matrix. The resulting disaggregated sediment was repeatedly washed first with water and then with Calgon solution (0.052 M $Na_6(PO_3)_6$, 0.286 M $NaHCO_3$) to loosen insoluble clays and promote their suspension in the supernatant. In between successive washes, sediment was sonicated for 30 seconds to assist in the removal of clays. Once the supernatant remained visibly clear after sonication, the remaining sediment (consisting mainly of silica and iron minerals, with minor amounts of resistant clay) was rinsed in a 250 μm sieve, dried on filter paper, and picked for fossils under a binocular microscope. Fossils recovered from sample residues were then photographed using a GIGAmacro automated camera system to capture, stack, and stitch specimen imagery.

Data collection

For each core, CT imagery and residues were counted for the total abundance of fossil taxa. Trilobites were identified to the family level based on their general geometry, furrow pattern, and, in residues, their prosopon. Trilobite material not reliably assignable to a single family was treated as a separate category. Prosopon and other textural features were not well-resolved in CT due to noise in the imagery, and so were not generally considered for taxonomic assignment in counts based on CT results. Bryozoans were classified by growth form either as thin-branching, thick-branching, or lacy/fenestrate. Ostracods, gastropods, and bivalves were not further classified due to the absence of reliably identifiable taxonomically relevant features and their generally small sample size.

Two versions of abundance counts were taken for each core CT data set and residue. For the total count or loose count, all taxonomically identifiable fossils were counted, including isolated thoracic segments and librigenae and broken-off pleurae for trilobites and all bryozoan fragments containing at least one zooecium, but excluding unidentifiable fragments of arthropod sclerite. For the minimum distinct individual (MDI) count or strict count, only fossils representing whole individuals were counted; this included trilobite cranidia or pygidia with a largely complete axial lobe, all ostracods with over 50% of a valve present, gastropods with a recognizably complete apex (not necessarily including the protoconch), and bivalves or brachiopods with extensive fragments of shell or the umbo preserved, but excluded all bryozoans due to the modular nature of their growth. For each core studied, therefore, four different counts were

produced, pairing a preparation method (CT or acid maceration) with a counting method (loose or strict).

Using *R* statistical software, all four datasets were subjected to NMDS in three dimensions following the Bray-Curtis dissimilarity index, using the *metaMDS* function provided in the *vegan* package (Bray & Curtis, 1957; Dixon, 2003; Kruskal, 1964b; R Core Team, 2017). In all cases, sites with no counted fossils under the count criteria were excluded from the analysis. The resulting ordination scores for each of the samples and taxa present in them along the first two NMDS axes were visualized as scatter plots. Variation along the third axis was not assessed.

Further paleoecological analysis of taxon abundances within and between samples was performed using PAST statistical software, calculating various diversity metrics and assessing compositional similarity between samples (Hammer et al., 2001; Hammer & Harper, 2022).

Results

A total of 1218 fossils were identified in residues, of which 355 met strict-count criteria. Analysis of CT imagery resolved 254 identifiable fossils, of which 75 were included in the strict count. (Tables 6, 10)

Taxon	CT strict	Residues strict
Asaphidae	0	0
Cheiruridae	2	2
Metagnostidae	6	11
Odontopleuridae	0	2
Pterygometopidae	6	12
Raphiophoridae	35	71
Remopleurididae	7	7
Unknown Trilobita	6	4
Total Trilobita	62	109
Bivalvia	2	1
Brachiopoda	0	3
Gastropoda	10	13
Ostracoda	1	229

Table 10: Strict counts of recovered fossils

Strict counts for CT and residue include only fossils likely representative of distinct individuals.

Residues

Trilobite sclerites were abundant in residues, especially raphiophorids (*Lonchodomas* and *Ampyx*) with many cranidia and librigenae present and thoracic segments and pygidia somewhat rarer. Pterygometopids (*Calyptaulax*) and remopleuridids (*Remopleurides*) were moderately abundant, represented mainly by fragments of thoracic segments. Asaphids (c.f. *Isotelus*) were present only as large fragments of cuticle and the occasional partial librigena, differentiable from similar raphiophorid material by their much greater size. Odontopleurids (c.f. *Ceratocephala*) were represented mainly by spinose marginal spines, with complete sclerites much rarer. Cheirurids (*Ceraurus*) were much rarer, while agnostids (*Trinodus*) were rare as well and unsurprisingly represented exclusively by cranidia and pygidia. (The phylogenetic

position of agnostids remains controversial, considered either as a basal group of trilobites or as non-trilobite artiopods. Within the scope of this study, they are grouped with trilobites *sensu stricto*.)

Nearly half (290 of 594) of total trilobite components could not be confidently assigned to a family; since this pool consisted overwhelmingly of isolated spines, librigenae, thoracic segments, or fragments thereof rather than largely complete cranidia or pygidia whose features would aid in classification, a considerably smaller fraction (4 of 109) of the strict-count trilobites remained unidentified.

Occasional rhynchonelliform brachiopods were found in residues as well, mostly as flaky fragments of shell. Ostracods were highly abundant and included articulated specimens as well as some valves with intact lateral spines; fragmentary valves were less common. In contrast to other fossils preserved through silica replacement, gastropods (both as replaced shells and as internal molds) and a single bivalve were found preserved through pyritization followed by secondary conversion to hematite and other iron (oxy-) hydroxides.

Tomography

Specimens identified in CT imagery were also dominated by trilobites, with raphiophorids again being most common. Remopleuridids were fairly abundant as well, though represented largely by thoracic segments. Pterygometopids, agnostids, and cheirurids were less abundant, and as in residues, asaphids were represented solely by librigenae, large cuticle fragments, and a single thoracic segment. No recognizable odontopleurids were resolved, likely due to their small body size and very fine diagnostic features. Over half (126 of 225) of trilobites in the loose count were not identifiable to the

family level, though as with the residues, this proportion dropped considerably (6 of 62) in the strict count. Since prosopon and other textural features are not reliably resolved in CT due to issues of noise, identification relied solely on general morphology, interfering with the identification of thoracic segments in particular due to their scarcity of morphological characters relative to cranidia and pygidia.

Ostracods were nearly absent from CT data, apparently due to their small body size, thin cuticle, and lack of readily identifiable anatomical features. Bryozoans were more rarely resolved and tended to be large (~5 mm) fragments of either thin-branching dendroid or planar lacy forms rather than the smaller (~1 mm) fragments found in residue, suggesting breakage during maceration and washing; unlike the purely silicified bryozoans recovered from residues, at least one apparent pyritized bryozoan was observed in CT. No brachiopods were identified. Bivalves and gastropods were occasionally resolved, always in pyritized form.

Taxa across horizons

Considering CT and residue results together, taxon assemblages were fairly consistent within horizons and exhibited apparent variation across horizons. The fauna of Horizon 01 were starkly different from the other samples, dominated by bryozoans and with trilobites nearly absent. Horizons 03 and 04 were rich in raphiophorids and ostracods, with significant remopleuridids and pterygometopids as well. Horizons 05 and 06 were dominated by raphiophorids, with some pterygometopids and bryozoans also present.

Hand sample lithology

Hand sample observations revealed two starkly different apparent lithologies. Rocks from Horizon 01 were coarse-grained, with a sparry or dismicritic texture likely indicative of recrystallization during early diagenesis. Sparse fossils and possible intraclasts visible on fresh surfaces were weakly aligned with the direction of original bedding, suggesting directional sorting during deposition.

Horizons 03, 04, 05, and 06, conversely, were fine-grained with only occasional sparry or hematitic grains; fossils, where visible on fresh or weathered surfaces, were oriented randomly to original bedding. Rocks from these horizons also displayed heavy rinds on weathered surfaces, frequently stained rusty orange to pale yellow with iron oxides/oxyhydroxides. Arthropods, brachiopods, and occasional crinoid ossicles were found weathering out; however, no crinoids were recovered in either CT or residues (with the possible exception of irregular pyritized-hematitic grains with a regularly porous texture in residues from sample 06-C3, which may represent crinoid brachials). The apparent absence of crinoid material in residues may result from echinoderms' textural resistance to remineralization, since echinoderm ossicles often develop syntaxial calcite cements very early in diagenesis, imposing a kinetic barrier on replacement mineralization and limiting silicification to thin superficial crusts (Butts, 2007, 2014).

Quantitative Analyses

NMDS performed on the four datasets converged readily, producing ordinations with acceptable stress scores (< 0.1). Plotting individual samples and taxon loadings produced representations of assemblage disparity over sampled material (Figures 17, 18).

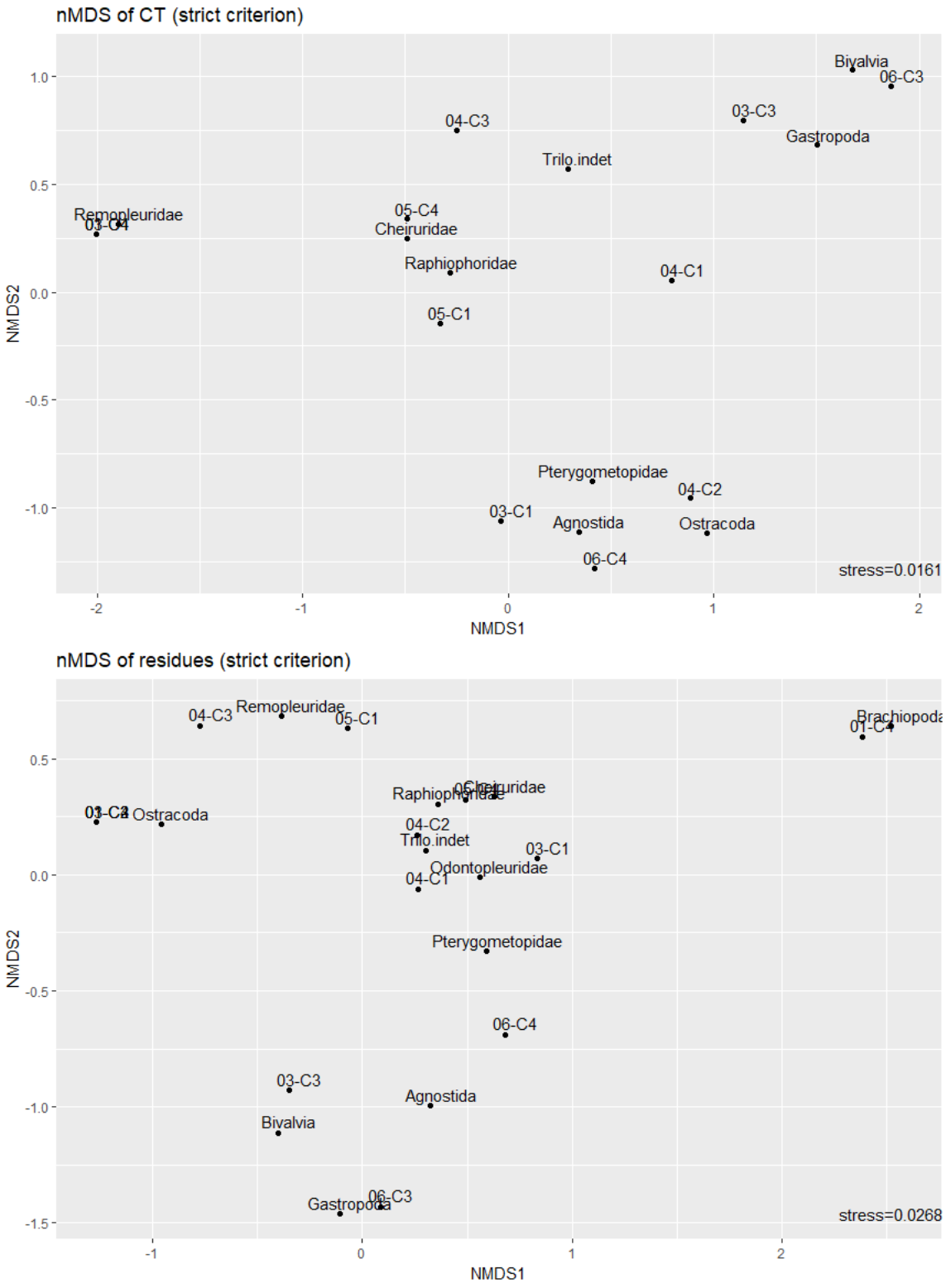

Figure 17: nMDS ordinations of strict counts of taxa in CT and residue

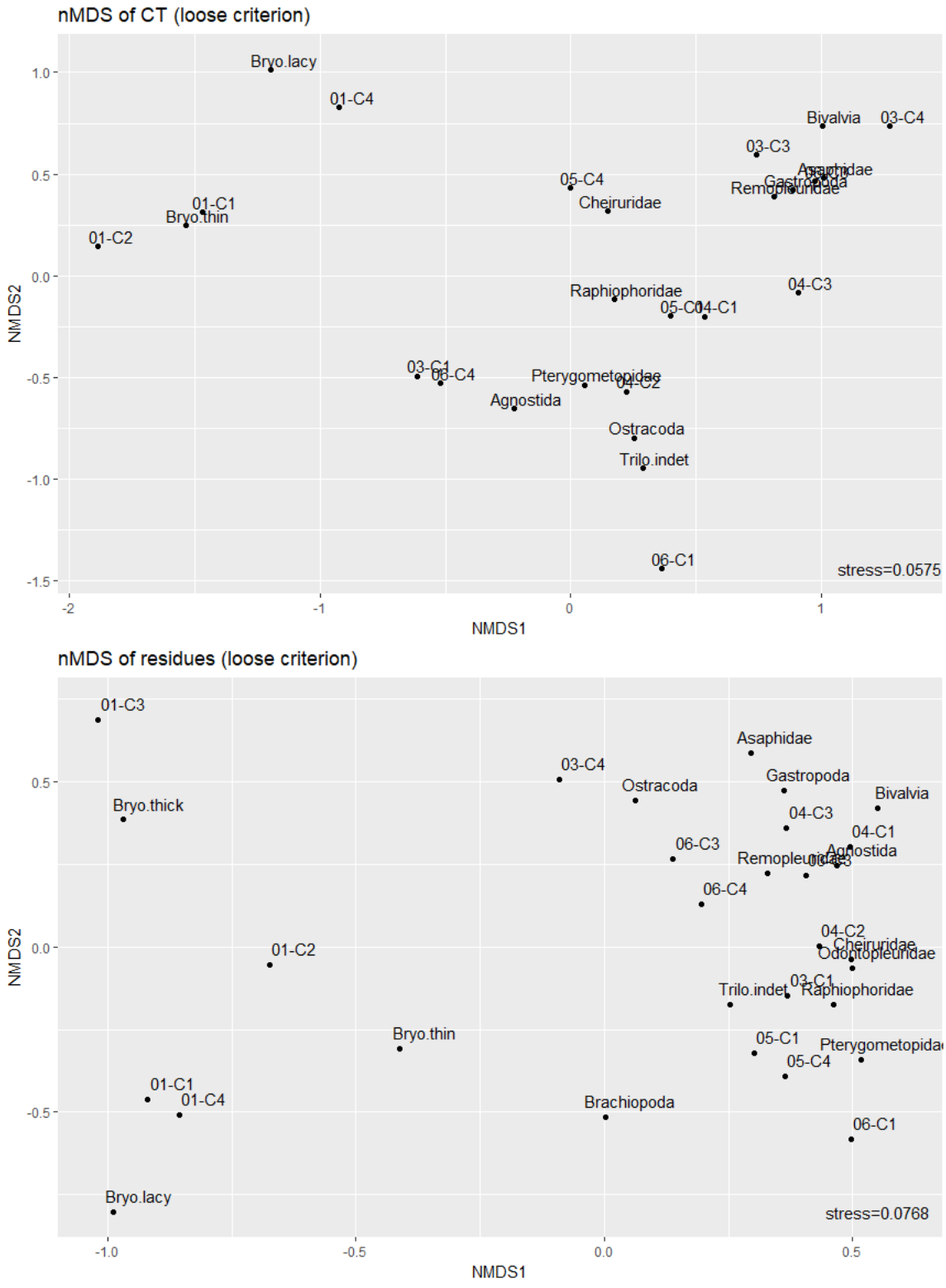

Figure 18: nMDS ordinations of loose counts of taxa in CT and residue

Ordinations on the strict-count data are of questionable utility due to the exclusion of bryozoans, which constituted nearly all fauna in Horizon 01 samples, and due also to the drastically lower number of trilobites after excluding thoracic segments, librigenae, and fragmentary material. The relative distributions of samples and taxa in CT and residue strict-count ordinations have little in common with either each other or with loose-count ordinations; conversely, loose-counted CT and residues follow generally similar patterns and form the basis for paleoecological conclusions drawn from this study.

Taxon loadings in all four ordinations consistently grouped bivalves and gastropods nearby each other, which may reflect either a shared infaunal environment or instead early burial conditions conducive to pyritization in those deposits; however, the low abundance of bivalves (2 in CT, 1 recovered from residues, always alongside multiple gastropods) makes this apparent association tenuous. It is noteworthy that disseminated pyritization in the form of non-fossil granules was present in several samples (e.g., 05-C4) that contained no mollusks, suggesting that early diagenetic conditions are not the sole control of the measured abundance of pyritized fauna.

Loose-count ordinations

Loose counts of both CT and residues tended to group medium-sized benthic trilobites (raphiophorids, pterygometopids, and cheirurids) together along with unidentified trilobite material (most of which likely derived from one of those families), with pelagic trilobites (remopleuridids) plotting closer to gastropods and bivalves. Asaphids, likely represented here by the extremely large benthic trilobite *Isotelus*, consistently fall near the latter cluster but are represented only by fragments of cuticle.

The ordination position of agnostids, whose life habit remains controversial (Fortey & Owens, 1999), is inconsistent between CT and residues, falling near the benthic and pelagic trilobite clusters in those analyses respectively. In both cases, they are closely accompanied by ostracods (which can occupy pelagic or benthic niches and whose life habit was not interpreted in this study). Due to the extreme disparity between identification in CT and recovery in residues of ostracods, their location within the ordination for CT data is likely not informative.

Thin-branching and lacy bryozoans plotted together, forming a cluster far away from other taxa. Thick-branching bryozoans fell further away from the other two morphotypes in the residue ordination and were not detected in CT.

Samples from individual horizons tended to fall near each other in loose association. Two main clusters are apparent in both CT and residue loose counts: one characterized by low NMDS1 scores and dominated by bryozoans, and one with higher NMDS1 scores and dominated by arthropods (trilobites and ostracods).

Diversity metrics in CT and residue

For each sample, Simpson's dominance index *D* was computed for both CT and residue taxon totals, with 95% confidence intervals based on 9999 bootstrap replicates. The results of this analysis differed notably between the two; CT dominance values fell in a tight band between 0.25 and 0.40 (excepting three outliers with $n<3$), while residue

dominance values had a bimodal distribution with one group of values between 0.40 and 0.65 and another falling between 0.15 and 0.30. (Figure 19)

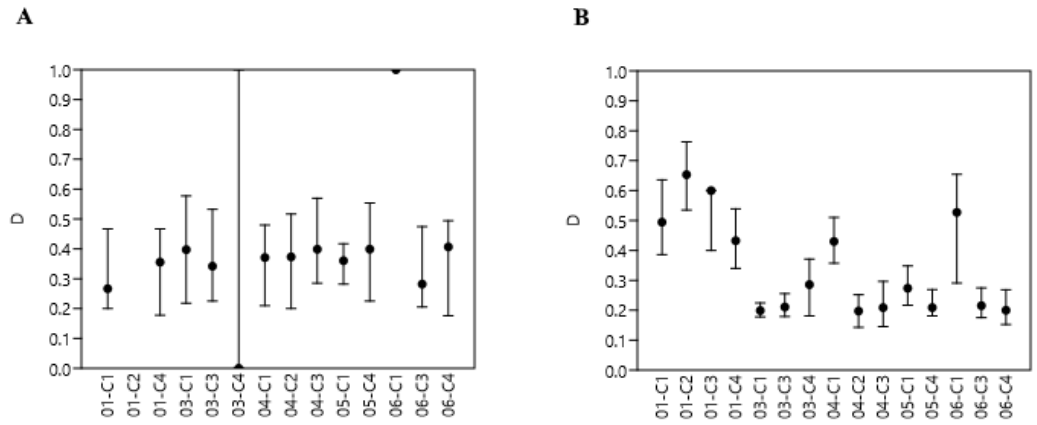

Figure 19: Simpson's dominance (D) for samples

Error bars denote 95% CIs
A) CT loose counts
B) Residue loose counts

Rarefaction curves were calculated for both CT and residue counts of each sample using PAST (Hammer & Harper, 2022). (Figure 20). Curves were visually inspected for the presence of an inflection point as a rough qualitative assessment of sampling completeness; a sample's curve "leveling off" (sudden decrease in slope) is considered indirect evidence that taxa in the true population are well-represented in the sample (Raup, 1975; Sanders, 1968). This inflection point was observed in residue counts from most samples, but less frequently in CT counts. This suggests that the smaller total counts of individuals in CT imagery are leading to the non-recovery of rarer taxa. Such undersampling is a liability of ecological analyses based on those samples.

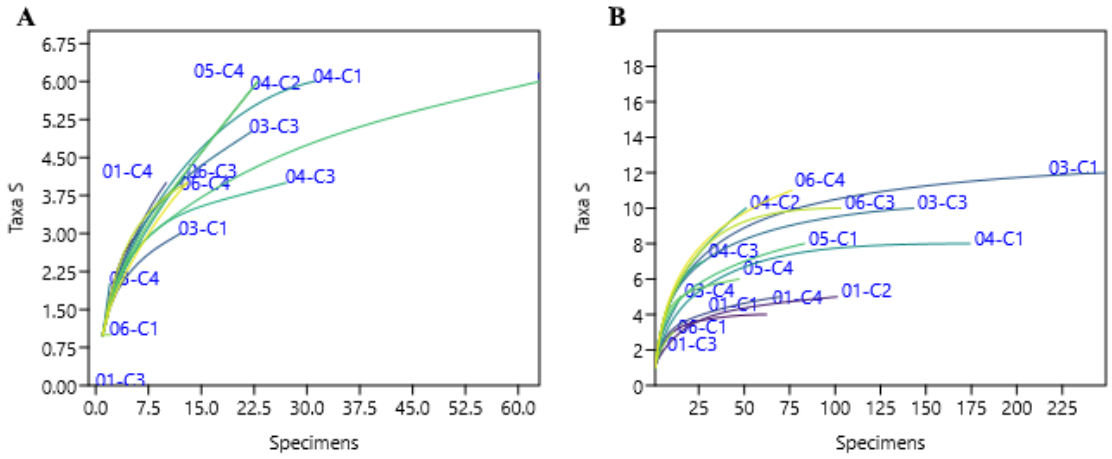

Figure 20: Rarefaction curves of sample abundances

A) CT loose counts

B) residue loose counts

Sample cluster analysis

Multivariate cluster analyses were performed in PAST to provide alternate metrics of similarity in the paleoecological composition of the samples, using the Bray-Curtis dissimilarity index as before (Bray & Curtis, 1957; Hammer & Harper, 2022). Dendrograms with branch length scaled to dissimilarity were constructed for CT loose counts, residue loose counts, and a combined dataset treating CT and residue loose counts for each sample as two separate sites. (Figure 21)

Cluster analysis of CT counts grouped samples from Horizon 04, and treated Horizon 05 similarly, but scattered samples from Horizons 03 and 06 across the tree. Using residue data, Horizon 05 formed a cluster as before but Horizon 04 split, with cores 04-C2 and 04-C3 remaining close but 04-C1 further removed; Horizons 03 and 06 were dispersed as in the CT tree. In both trees, samples from Horizon 01 were far removed from other samples, tending to form a cluster basal to the rest of the samples.

The combined tree retains the general close groupings of the two individual trees due to sharing the same dissimilarity metric. (Figure 22) Notably, even for horizons (01, 04, 05) whose samples tended to cluster in both the CT and residue trees, those clusters are not terribly closely related in the overall analysis; there are few clear patterns in this tree, but CT samples tend to cluster more closely with other CT samples, and residue samples with residue samples, than do CT and residue counts of the same sample or even of samples from the same horizon.

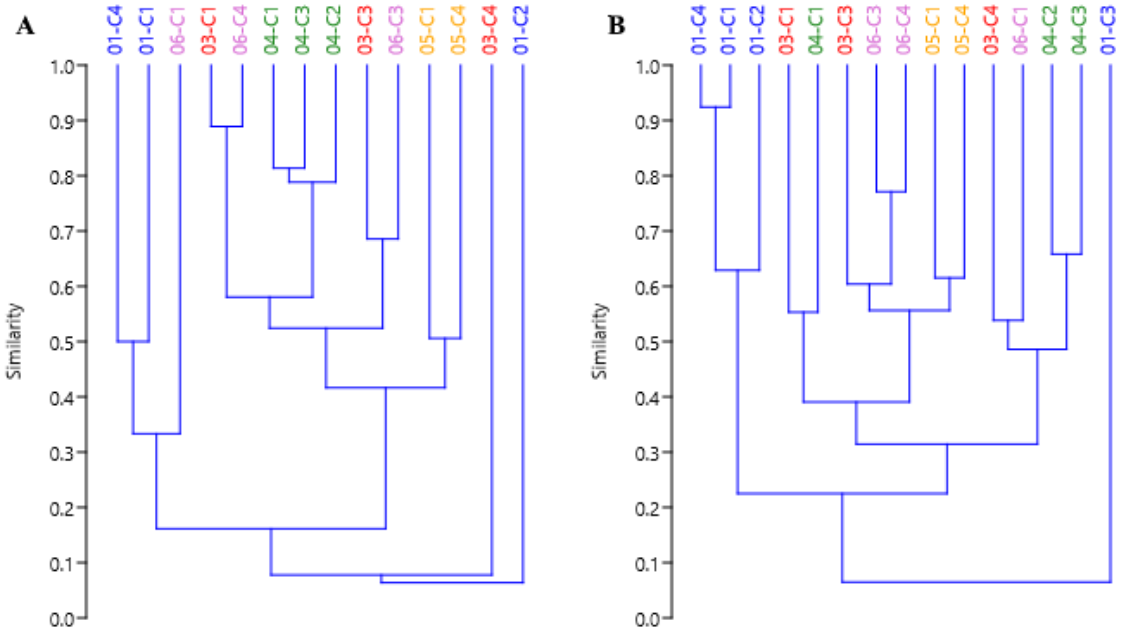

Figure 21: Bray-Curtis similarity dendrograms of sample abundances

A) CT loose counts
B) residue loose counts

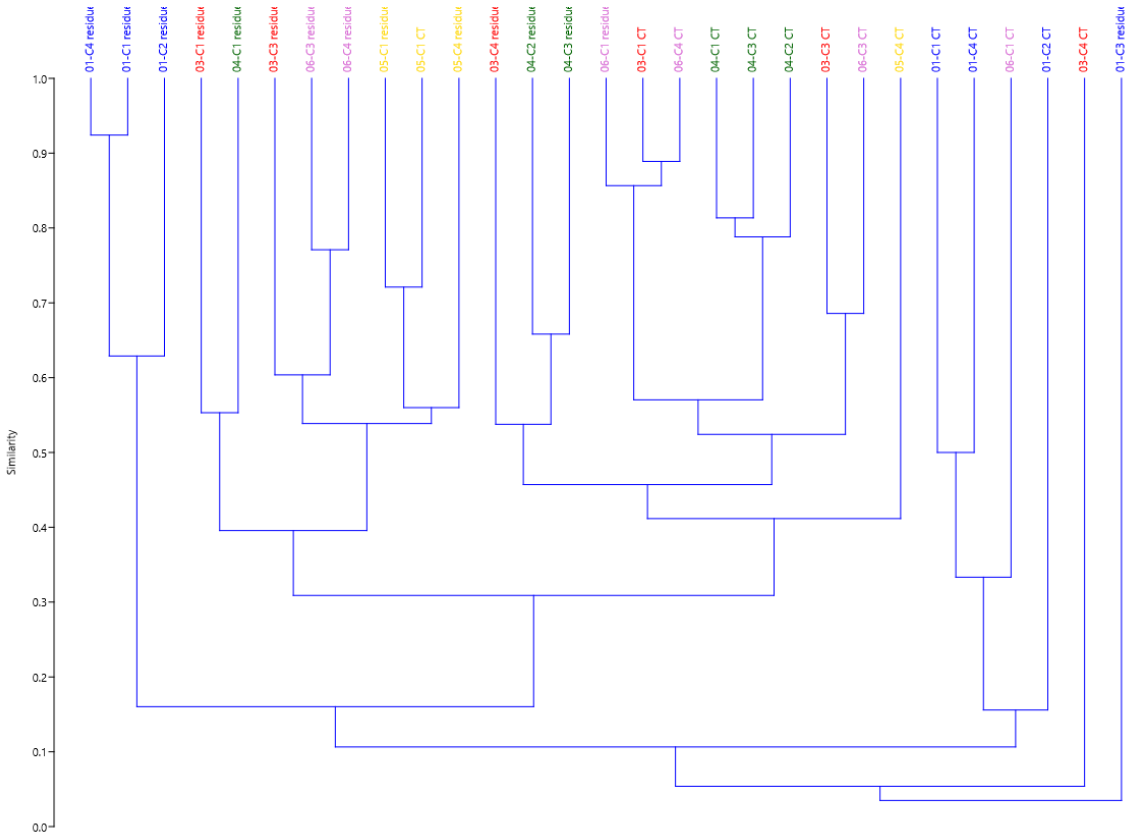

Figure 22: Bray-Curtis similarity dendrogram of CT and residue sample abundances

Discussion

Biofacies interpretation

The clearest division within the studied samples, in hand sample lithology, in residues, and in CT, is between the rocks of Horizon 01 and those of other strata. These samples are markedly different in their texture from the other samples, with a crystalline appearance nearly reminiscent of gabbro suggesting post-burial recrystallization of an originally micritic matrix; grains visible in hand sample were also aligned albeit weakly with the direction of original bedding, suggesting directional sorting during transport. CT imagery of these samples supports this observation, as large lacy bryozoans with

approximately planar geometry were similarly oriented. All Horizon 01 samples lacked the abundant trilobites of other material and instead contained mainly bryozoans and sparse fragmentary trilobite material, and their location in both loose-count NMDS ordinations reflects this, falling near the three bryozoan morphotypes and away from all other taxa and samples. These lines of evidence point potentially towards bioclastic debris being transported from upslope into a setting poor in autochthonous skeletal material.

Interpreting distinctions among other sampled horizons is not as clear. In nMDS ordinations, the two samples from Horizon 05 plot close together near medium-sized benthic trilobites, but samples from Horizon 04 are more widely distributed between this region and the cluster of remopleuridids and mollusks. Samples from Horizon 03 tend to fall nearer the latter cluster but are not closely grouped themselves. Samples from Horizon 06 are more widely scattered across the general area associated with the various trilobites.

Variation in the relative abundance of pelagic versus benthic trilobites may reflect changes in benthos; since pelagic and planktic taxa are not facies-dependent, the rate at which their remains accumulate in sediment can remain fairly constant even while benthic communities wax and wane with changes in water depth, bottom-water chemistry, or sediment input (Munnecke & Servais, 2008). As (pelagic) remopleuridids often co-occur with (semi-infaunal) bivalves and gastropods in these samples, this could hint at shifts in benthic community structure, though the sampling in this study is insufficient to rigorously test for this possibility.

Two samples are notable as apparent anomalies across both residue and CT loose-counts. Unlike other samples from Horizon 03, sample 03-C1 plotted near medium benthic trilobites rather than remopleuridids. This is consistent with the highly abundant raphiophorids resolved in CT and recovered in residues for this core, in contrast to the remopleuridid-dominated sample 03-C3 and depauperate 03-C4.

Both loose-count ordinations also placed 06-C1 as an outlier to the rest of the trilobite-dominated material. This is likely an artifact of small sample size rather than any true feature of community structure, however, due to the very few fossils of any sort resolved or recovered from this sample.

The results of the cluster analyses largely recapitulate those of the NMDS: strong distinction between Horizon 01 and all other samples, weak clustering of Horizon 04 and Horizon 05, and broad dispersal of samples from Horizon 03 and Horizon 06. A key conclusion from this analysis specifically is the persistent dissimilarity between CT and residue counts from the same sample. Abundance data from CT and residues should not be directly compared in any paleoecological analysis; any ecological similarity or dissimilarity is likely to be drowned out by a strong signal of recovery bias between the two methods, a conclusion that should be intuitive in this case.

Diversity and Dominance Between Preparatory Methods

Simpson's dominance index *D*, the likelihood of a sample that two randomly selected individuals from it will be of the same taxon, is a simple metric of diversity (Simpson, 1949). As applied to samples in this study, it illustrates a shortcoming of CT for the purposes of this analysis. While dominance remained consistently low across

samples in counts based on CT data, the corresponding residues showed far more variability between samples. Based on counts from the residues, high dominance values were found mainly in samples from Horizon 01, while low dominance values characterized samples from the other horizons in residue. Some samples from other horizons did have high dominance values, but this is likely the result of small sample size. This is consistent with the conclusions of other analyses from NMDS to hand sample inspection, which readily distinguished Horizon 01 from the others; it is therefore noteworthy that CT data did not replicate this distinction.

Drawbacks of CT

The application of CT to biofacies analysis is subject to inherent limitations of the imaging method. The single greatest liability is likely the restriction on sample size imposed by the internal dimensions of the microscope itself; only small (< ~3 cm) hand samples can be imaged in typical instruments. Some CT instruments such as those used in medicine can accommodate larger samples, but are typically optimized to image lower-density biological materials rather than higher-density (and therefore higher-opacity to X-rays) geological materials and may not obtain good contrast between calcareous and siliceous features. Medical CT instruments tend to suffer from coarser voxel resolution as well, as they are designed to image larger samples.

Even if larger instruments are available, interactions between the beam and the sample can also limit the thickness of rock that can be reliably imaged; attenuation and hardening of the beam by the outer layers of larger hand samples can leave the interior dark and poorly resolved. Increasing beam intensity can better resolve interior features to an extent at the cost of producing cupping artifacts, leaving the outer layers overexposed

and complicating interpretation of that volume. Aggressive filtering of CT imagery can correct for these artifacts to an extent but tends to produce new sets of artifacts in the process, potentially injecting additional bias into the data (Jung et al., 2011; Kyriakou et al., 2009; Orhan et al., 2020; Park et al., 2015).

The degree to which imaging artifacts obscure features of interest is influenced also by heterogeneity within the material; regions of drastically higher X-ray opacity (such as iron minerals) are highly disruptive to segmentation based on less dramatic opacity differences (as between silicified fossils and micritic matrix) (Bam et al., 2019; Remeysen & Swennen, 2006). It may be more feasible to resolve features in larger samples if the rocks in question have not undergone any pyritization during diagenesis, but it is not necessarily possible to know beforehand if this is the case.

Issues of sample volume resulting from reliance on CT are for these reasons a serious impediment to interpreting biofacies through this approach. Working with small individual pieces rather than bulk samples reduces the number of fossils recovered from each sample, exposing small-scale heterogeneity within sampled beds and causing rare taxa to often be missed entirely. The results of rarefaction analyses of sample counts (Figure 20) are consistent with such undersampling. The absence of inflection points in the majority of CT curves suggest that uncommon taxa in this study are not recovered in CT imagery; curves from corresponding residues indicate generally more complete sampling, but still insufficient in less fossiliferous cores.

Breakage effects

Fossils can be damaged during maceration and washing by being tumbled against other grains or against the wall of the vessel, and may also crumble if supporting calcareous material is dissolved away. Breakage during preparation can cause taxa to be undercounted due to wholesale destruction of individuals or damage to them sufficient to make them no longer recognizable, but can also paradoxically cause some taxa to be overcounted by turning one fossil into many still-recognizable fragments.

Dendroid and lacy/foliaceous bryozoans in the macerates generally appear as small (~ 1 mm) fragments, with larger pieces comparatively rarer. However, it is apparent from CT data in the Horizon 01 samples that at least some were originally preserved as larger branches or sheets and were further fragmented during sample preparation. Since bryozoans with these growth forms are typically found as fragments rather than as nearly complete colonies, it is difficult to draw a distinction between large and small fragments in a sample when calculating abundance. Alternate methods of counting colonial animals with modular growth forms are possible, such as the number of zooids or the total area of the outline, but these are subject to body-size effects within such taxa and are not directly comparable to counts of non-colonial animals.

The difference between many small fragments originally from one larger bryozoan colony and similar fragments from a total of three colonies is not readily apparent. In this circumstance, CT does provide a distinct advantage by enabling counts of the original fossils before breakage multiplied their number.

Conclusions

Broad categories of biofacies are fairly consistent between residue- and CT-derived taxon abundances as interpreted using NMDS. While total counts for CT are much lower than those of residues, relative abundances in the former largely recapitulate the latter with some notable exceptions; ostracods are almost absent from CT data due to issues of resolution even when highly abundant in residues, and bryozoan counts tend to be much higher in residues than in CT due to breakage transforming one large fragment into many small fragments. For this reason alone, any application of CT data to describe paleoecological structure should be undertaken with caution. Ordinations used in paleoecology are sufficiently complex that such biases in recovery can, by introducing error and uncertainty upstream, irreparably taint conclusions drawn downstream.

Overall, the use of CT counts to characterize biofacies is of uncertain value. Sample volume constraints make bulk samples unfeasible, and the cost of instrument time can be a roadblock to large-scale use. However, this approach may see niche use when chemical preparation is dangerous or impractical due to matrix or fossil mineralogy, or when studying sponges, bryozoans, corals, or other modular organisms for which fragmentation during washing can obscure or inflate the number of individuals present. Samples best-suited to this approach will be densely fossiliferous (mitigating the limitation of sample volume), bear taxa with morphological features conducive to identification in CT, and contain grains more susceptible to dissolution than the matrix or cement joining them together. Such rocks should also have a strong contrast in density (and therefore X-ray opacity) between grains and matrix, but with relatively low density overall to minimize beam hardening artifacts. These criteria are fairly constraining, but

materials meeting them are not unheard of. Conodonts and other phosphatic fossils, for example, are occasionally known from silicified sediments, and characterizing taxonomic assemblages using μCT imaging may constitute a welcome alternative to digestion with the notoriously toxic and hazardous hydrofluoric acid normally used to liberate fossils from siliceous cements (Green, 2001).

While μCT imaging of fossils in matrix is capable of resolving morphological features of interest, its application towards paleoecological questions is less promising. Analyzing original rock contents as a means of detecting breakage during preparation may be valuable as a control on fragmentary abundance counts, but limitations of sample size and the potential for taxonomic bias to affect ordinations present serious pitfalls to analysis or characterization of biofacies. It can, however, be useful in establishing broad categories if not finer gradations between related assemblages, which may yet be of value.

Chapter 5: Conclusions

Key takeaways

Intense parasitism in Pleistocene Leukoma

In most taxa and samples evaluated, parasitic pits attributable to infestation by digenean metacercariae are fairly rare. The very high prevalence and intensity on *Leukoma* from Pleistocene shell beds stands in stark contrast to patterns in other taxa and in Recent shell beds, but is consistent with rates observed in live-collected *Leukoma* from a comparable environment. This suggests not only taxonomic selectivity of infestation (possibly related to the semi-infaunal lifestyle of *Leukoma*) but also some type of environmental control on trematode parasitism. Since both the glacial retreat of the latest Pleistocene and anthropogenic climate change in the present have resulted in episodes of rapid sea level rise, increases in parasitism pressure may be related to the flooding of coastal environments and the invasion of new territory by shallow marine biota; this potential effect and its implications for marine fisheries in the near future are under investigation by several wide-ranging programs of research (Huntley et al., 2014; Scarponi et al., 2017).

Differential information recovery of CT and maceration

Quantitative comparison of fossils recovered from the same sample by μCT and acid maceration quickly encounters complications, since both are subject to incompleteness and biases in recovery; neither method can truly be used as a control by which to test the results of the other. However, the two preparation methods are

complementary in qualitative descriptions, preserving different types of information useful to the characterization of sample materials.

CT utility for paleoecology limited

While μCT can be useful for describing textural features and poorly mineralized fossils in rocks, it is not well-suited to descriptions of paleoecology. Limitations of sample size along with disproportionate non-recovery of small and morphologically simple taxa prevent all but the starkest differences in community makeup from being confidently recognized. Though μCT may have some niche utility for describing biofacies in rocks with unusual mineralization, destructive chemical or mechanical preparation remains preferable for most such studies.

Cautionary Tales

Don't trust radiocarbon ages of marine shells

Radiocarbon dating is widely used to constrain the ages of organic materials from the Late Pleistocene and Holocene. However, it relies on several assumptions including that during the life of the organism, the isotopic composition of carbon within its tissues and skeleton reflected that of the atmosphere. This is generally true for terrestrial organisms but not necessarily of marine biota, which often experience a reservoir effect due to sourcing their carbon from the ocean rather than directly from the atmosphere (Stuiver et al., 1998). Complicating this for the purposes of this study is the tendency of mollusks to build their shells from a mixture of dissolved inorganic carbon (DIC) and metabolic carbon derived from their diet; these pools of carbon may have different isotopic profiles (Bauer et al., 1998; Dillaman & Ford, 1982; Mook & Vogel, 1968;

Tanaka et al., 1986). Assessing and correcting for this reservoir effect is not trivial and the magnitude of the correction is highly regional, varying significantly even within ocean basins (Kovanen & Easterbrook, 2002; Yoneda et al., 2007).

In the case of bivalves from Whidbey Island (Chapter 2), attempts to document variation in age among sample materials quickly encountered complications from said reservoir effect. Material from shell beds thought to date from the latest Pleistocene frequently returned ^{14}C ages of roughly 1000 years, while shells from death assemblages (known to contain material less than 50 years in age due to the presence of the recently introduced purple mahogany clam *Nuttallia obscurata*) often came out around 300 years. While previous work has quantified the reservoir effect in the northeast Pacific (Kovanen & Easterbrook, 2002), even corrected ages might not be reliable in this case. The glaciomarine setting of the shell beds and high input of terrigenous sediment raise questions about the strength of the terrestrial (atmospheric) component of shell carbonate; the bivalve taxa in question are suspension or deposit feeders from shallow marine environments and may, during periods of high input from the landmass, have consumed much higher quantities of terrigenous organic matter than under modern conditions, producing a stronger terrestrial signal in the metabolic carbon component. The strength of this effect is challenging to estimate.

Ultimately, concerns about the ages of materials in this study proved to be a distraction from its core goals. Without extensive remapping of shell beds at the site or seeking out alternative ways of dating the deposits (work outside the immediate scope of this project), better constraints on the ages of study materials remain out of reach. Previous mapping of the sedimentary facies has assigned the glaciomarine shell beds of

Whidbey Island to the Late Pleistocene, and in the absence of definitive evidence to the contrary we will follow this interpretation (Domack, 1983).

CT underperforms in resolving fossils in compositionally heterogeneous rocks

The difference between idealized and actual study materials looms large over CT studies of fossils from the Edinburg Formation (Chapters 3 and 4). Modern CT methods are capable of distinguishing between mineral phases based on relatively small density differences, easily theoretically separating calcite from common opal and other low-density silica phases (and possibly even differentiating calcite from dolomite). In practice, textural variation in sample materials can hamper this. The hand samples taken from the Liberty Hall facies of the Edinburg are untidy mixtures of micrite, clays, fine sand, silicified fossils, and pyrite and its oxidation products, and are frequently cut through by veins and fractures. Disseminated mineralization is prominent in some samples and nonexistent in others. This degree of compositional heterogeneity adds a good deal of noise into CT data, blurring outlines of fossil grains and interfering with the identification of smaller features.

A very good reason to use mesh filter baskets in coffeemakers

One final warning from this program of study pertains to the brewing of coffee rather than any paleontological topic. The processing of disaggregated sediment as part of the studies on silicified fossils (Chapters 3 and 4) required that wet residues be turned out from their sieves onto filter paper for drying. However, large (~25 cm diameter) circles of filter paper proved difficult and expensive to procure, and so commercial coffee filters were used instead. (These paper filters, of a “basket” type, were made available as

departmental office supplies.) Since the material of these filters was to a food-service standard rather than laboratory grade, some stray fibers and other foreign materials were found in sediment dried on these filters; however, all such contaminants were easily distinguished from the clay and silica of the research materials.

Of particular note are two unidentified insects found in residues. While they are poorly preserved (desiccated, directionally compressed as if between two layers, appendages only partly preserved, and with a dull gray cuticle potentially suggesting chemical bleaching) it is immediately apparent from their preservational style and their taxonomic placement in the Insecta that they are not Ordovician in age but rather modern contaminants. It is unlikely that they fell into the beakers during the maceration process or onto the sieve during drying, as these procedures were all carried out inside a fume hood and no stray insects were noted in the laboratory; in any case, this would not explain their compression. The inescapable conclusion is that these insects were present on the coffee filters used to dry the sediment, having either been trapped on them during manufacturing or flattened between adjacent filters during packaging.

Those squeamish (the author included) about the possibility of introducing insect material into the office coffee pot should therefore consider avoiding paper filters entirely and instead opt for reusable wire mesh filter baskets. Further investigation of insect contaminants on filters is beyond the scope of this research.

BIBLIOGRAPHY

Abdulkarim, M., Grema, H. M., Adamu, I. H., Mueller, D., Schulz, M., Ulbrich, M., Miocic, J. M., & Preusser, F. (2021). Effect of Using Different Chemical Dispersing Agents in Grain Size Analyses of Fluvial Sediments via Laser Diffraction Spectrometry. *Methods and Protocols*, *4*(3), 44. https://doi.org/10.3390/mps4030044

Abel, R., Laurini, C., & Richter, M. (2012). A palaeobiologist's guide to "virtual" micro-CT preparation. *Palaeontologia Electronica*, *15*(2). https://doi.org/10.26879/284

Addino, M., Lomovasky, B. J., Cremonte, F., & Iribarne, O. (2010). Infection by gymnophallid metacercariae enhances predation mortality of SW Atlantic stout razor clam Tagelus plebeius. *Journal of Sea Research*, *63*(2), 102–107. https://doi.org/10.1016/j.seares.2009.11.001

Andreola, F., Castellini, E., Manfredini, T., & Romagnoli, M. (2004). The role of sodium hexametaphosphate in the dissolution process of kaolinite and kaolin. *Journal of the European Ceramic Society*, *24*(7), 2113–2124. https://doi.org/10.1016/S0955-2219(03)00366-2

Arganda-Carreras, I., Kaynig, V., Rueden, C., Eliceiri, K. W., Schindelin, J., Cardona, A., & Sebastian Seung, H. (2017). Trainable Weka Segmentation: a machine learning tool for microscopy pixel classification. *Bioinformatics*, *33*(15), 2424–2426. https://doi.org/10.1093/bioinformatics/btx180

Arganda-Carreras, I., Rueden, C., Colina, J. S., Schindelin, J., Arzt, M., Cardona, A., Eglinger, J., Hiner, M., Tinevez, J.-Y., Freydiere, P., Meijering, E., & Helfrich, S. (2022). *fiji/Trainable_Segmentation: Trainable_Segmentation-3.3.2*. https://doi.org/10.5281/ZENODO.5849093

Arnold, J. B., Daroczi, G., Werth, B., Weitzner, B., Kunst, J., Auguie, B., Rudis, B., Wickham, H., Talbot, J., & London, J. (2021). *ggthemes: Extra Themes, Scales and Geoms for "ggplot2"* (4.2.4).

Bam, L. C., Miller, J. A., Becker, M., & Basson, I. J. (2019). X-ray computed tomography: Practical evaluation of beam hardening in iron ore samples. *Minerals Engineering*, *131*, 206–215. https://doi.org/10.1016/j.mineng.2018.11.010

Bauer, J. E., Druffel, E. R. M., Wolgast, D. M., Griffin, S., & Masiello, C. A. (1998). Distributions of dissolved organic and inorganic carbon and radiocarbon in the eastern North Pacific continental margin. *Deep Sea Research Part II: Topical Studies in Oceanography*, *45*(4–5), 689–713. https://doi.org/10.1016/S0967-0645(97)00098-2

Bendle, J. M., Palmer, A. P., & Carr, S. J. (2015). A comparison of micro-CT and thin section analysis of Lateglacial glaciolacustrine varves from Glen Roy, Scotland.

Quaternary Science Reviews, *114*, 61–77. https://doi.org/10.1016/j.quascirev.2015.02.008

Bray, J. R., & Curtis, J. T. (1957). An Ordination of the Upland Forest Communities of Southern Wisconsin. *Ecological Monographs*, *27*(4), 325–349. https://doi.org/10.2307/1942268

Bush, S. L., Santos, G. M., Xu, X., Southon, J. R., Thiagarajan, N., Hines, S. K., & Adkins, J. F. (2013). Simple, Rapid, and Cost Effective: A Screening Method for 14 C Analysis of Small Carbonate Samples. *Radiocarbon*, *55*(2), 631–640. https://doi.org/10.1017/S0033822200057787

Butts, S. H. (2007). Silicified Carboniferous (Chesterian) Brachiopoda of the Arco Hills Formation, Idaho. *Journal of Paleontology*, *81*(1), 48–63.

Butts, S. H. (2014). Silicification. *The Paleontological Society Papers*, *20*, 15–34. https://doi.org/10.1017/S1089332600002783

Butts, S. H., & Briggs, D. E. G. (2010). Silicification Through Time. In P. A. Allison & D. J. Bottjer (Eds.), *Taphonomy: Process and Bias Through Time* (2nd ed., pp. 411–434). Springer Dordrecht. https://doi.org/10.1007/978-90-481-8643-3_11

Cherns, L., Wheeley, J. R., & Wright, V. P. (2010). Taphonomic Bias in Shelly Faunas Through Time: Early Aragonitic Dissolution and Its Implications for the Fossil Record. In P. A. Allison & D. J. Bottjer (Eds.), *Taphonomy* (Vol. 32, pp. 79–105). Springer. https://doi.org/10.1007/978-90-481-8643-3_3

Cherns, L., & Wright, V. P. (2000). Missing molluscs as evidence of large-scale, early skeletal aragonite dissolution in a Silurian sea. *Geology*, *28*(9), 791–794. https://doi.org/10.1130/0091-7613(2000)28<791:MMAEOL>2.0.CO;2

Clapham, M. E. (2011). Ordination Methods and the Evaluation of Ediacaran Communities. In M. Laflamme, J. D. Schiffbauer, & S. Q. Dornbos (Eds.), *Quantifying the Evolution of Early Life* (pp. 3–21). https://doi.org/10.1007/978-94-007-0680-4_1

Cnudde, V., & Boone, M. N. (2013). High-resolution X-ray computed tomography in geosciences: A review of the current technology and applications. *Earth-Science Reviews*, *123*, 1–17. https://doi.org/10.1016/j.earscirev.2013.04.003

Cnudde, V., Masschaele, B., Dierick, M., Vlassenbroeck, J., Hoorebeke, L. van, & Jacobs, P. (2006). Recent progress in X-ray CT as a geosciences tool. *Applied Geochemistry*, *21*(5), 826–832. https://doi.org/10.1016/j.apgeochem.2006.02.010

Cooper, B. N., & Cooper, G. A. (1946). Lower middle Ordovician stratigraphy of the Shenandoah valley, Virginia. *Bulletin of the Geological Society of America*, *57*, 35–114.

Cremonte, F., & Ituarte, C. (2003). Pathologies elicited by the gymnophallid metacercariae of Bartolius pierrei in the clam Darina solenoides. *Journal of the Marine Biological Association of the United Kingdom*, *83*(2), 311–318. https://doi.org/10.1017/S0025315403007136h

de Baets, K., Dentzien-Dias, P., Upeniece, I., Verneau, O., & Donoghue, P. C. J. (2015). Constraining the Deep Origin of Parasitic Flatworms and Host-Interactions with Fossil Evidence. In K. de Baets & D. T. J. Littlewood (Eds.), *Fossil Parasites* (pp. 93–135). https://doi.org/10.1016/bs.apar.2015.06.002

de Baets, K., & Huntley, J. W. (Eds.). (2021a). *The Evolution and Fossil Record of Parasitism: Coevolution and Paleoparasitological Techniques* (Vol. 50). Springer International Publishing. https://doi.org/10.1007/978-3-030-52233-9

de Baets, K., & Huntley, J. W. (Eds.). (2021b). *The Evolution and Fossil Record of Parasitism: Identification and Macroevolution of Parasites* (Vol. 49). Springer International Publishing. https://doi.org/10.1007/978-3-030-42484-8

de Baets, K., Huntley, J. W., Klompmaker, A. A., Schiffbauer, J. D., & Muscente, A. D. (2021). The Fossil Record of Parasitism: Its Extent and Taphonomic Constraints. In K. de Baets & J. W. Huntley (Eds.), *The Evolution and Fossil Record of Parasitism* (Vol. 2, pp. 1–50). Springer Cham. https://doi.org/10.1007/978-3-030-52233-9_1

Dillaman, R. M., & Ford, S. E. (1982). Measurement of calcium carbonate deposition in molluscs by controlled etching of radioactively labeled shells. *Marine Biology*, *66*(2), 133–143. https://doi.org/10.1007/BF00397186

Dixon, P. (2003). VEGAN, a package of R functions for community ecology. *Journal of Vegetation Science*, *14*(6), 927–930. https://doi.org/10.1111/j.1654-1103.2003.tb02228.x

Domack, E. W. (1983). Facies of Late Pleistocene Glacial-Marine Sediments on Whidbey Island, Washington: An Isostatic Glacial-Marine Sequence. In B. F. Molnia (Ed.), *Glacial-Marine Sedimentation* (pp. 535–570). Springer US. https://doi.org/10.1007/978-1-4613-3793-5_13

Dragonfly (2022.1.0.1249). (2022). Object Research Systems (ORS), Inc. https://www.theobjects.com/dragonfly/index.html

Elkhoury, J. E., Shankar, R., & Ramakrishnan, T. S. (2019). Resolution and Limitations of X-Ray Micro-CT with Applications to Sandstones and Limestones. *Transport in Porous Media*, *129*(1), 413–425. https://doi.org/10.1007/s11242-019-01275-1

Evitt, W. R. (1961). Early Ontogeny in the Trilobite Family Asaphidae. *Journal of Paleontology*, *35*(5), 986–995.

Feret, L. R. (1930). La grosseur des grains des matières pulvérulentes. *Premières Communications de La Nouvelle Association Internationale Pour l'Essai Des Matériaux, Groupe D*, *2*, 428–436.

Forsyth, R. (1997). An introduction to introduced marine molluscs in the Pacific Northwest. *Of Sea and Shore*, *19*(4).

Fortey, R. A., & Owens, R. M. (1999). Feeding habits in trilobites. *Palaeontology*, *42*(3), 429–465. https://doi.org/10.1111/1475-4983.00080

Garnier, S., Ross, N., Rudis, B., Sciaini, M., Camargo, A. P., & Scherer, C. (2021). *viridis: Colorblind-Friendly Color Maps for R* (0.6.2).

Gillespie, G. E., Parker, M., & Merilees, W. (1999). *Distribution, Abundance, Biology and Fisheries Potential of the Exotic Varnish Clam (Nuttallia obscurata) in British Columbia*.

Grant, R. E. (1989). Extraction of fossils from carbonates by acid. *The Paleontological Society Special Publications*, *4*, 237–243. https://doi.org/10.1017/S2475262200005190

Green, O. R. (2001). Extraction Techniques for Phosphatic Fossils. In *A Manual of Practical Laboratory and Field Techniques in Palaeobiology* (pp. 318–330). Springer Netherlands. https://doi.org/10.1007/978-94-017-0581-3_27

Hammer, Ø., & Harper, D. A. T. (2022). *PAST* (4.10).

Hammer, Ø., Harper, D. A. T., & Ryan, P. D. (2001). PAST: Paleontological Statistics Software Package for Education and Data Analysis. *Palaeontologia Electronica*, *4*(1), 1–9.

Holdaway, H. K., & Clayton, C. J. (1982). Preservation of shell microstructure in silicified brachiopods from the Upper Cretaceous Wilmington Sands of Devon. *Geological Magazine*, *119*(4), 371–382. https://doi.org/10.1017/S0016756800026285

Holland, S. M., & Patzkowsky, M. E. (1996). Sequence stratigraphy and long-term paleoceanographic change in the Middle and Upper Ordovician of the eastern United States. In B. J. Witzke, G. A. Ludvigson, & Jed Day (Eds.), *Paleozoic sequence stratigraphy; views from the North American Craton* (Vol. 306, pp. 117–130). Geological Society of America. https://doi.org/10.1130/0-8137-2306-X.117

Hudson, P. J., Dobson, A. P., & Lafferty, K. D. (2006). Is a healthy ecosystem one that is rich in parasites? *Trends in Ecology & Evolution*, *21*(7), 381–385. https://doi.org/10.1016/j.tree.2006.04.007

Huntley, J. W. (2007). Towards establishing a modern baseline for paleopathology: trace-producing parasites in a bivalve host. *Journal of Shellfish Research*, *26*(1), 253–259.

Huntley, J. W. (2011). Exploratory Multivariate Techniques and Their Utility for Understanding Ancient Ecosystems. In M. Laflamme, J. D. Schiffbauer, & S. Q. Dornbos (Eds.), *Quantifying the Evolution of Early Life* (pp. 23–48). https://doi.org/10.1007/978-94-007-0680-4_2

Huntley, J. W., & de Baets, K. (2015). Trace Fossil Evidence of Trematode—Bivalve Parasite—Host Interactions in Deep Time. *Advances in Parasitology*, *90*, 201–231. https://doi.org/10.1016/bs.apar.2015.05.004

Huntley, J. W., de Baets, K., Scarponi, D., Linehan, L. C., Epa, Y. R., Jacobs, G. S., & Todd, J. A. (2021). Bivalve Mollusks as Hosts in the Fossil Record. In K. de Baets & J. W. Huntley (Eds.), *The Evolution and Fossil Record of Parasitism* (pp. 251–287). https://doi.org/10.1007/978-3-030-52233-9_8

Huntley, J. W., Fürsich, F. T., Alberti, M., Hethke, M., & Liu, C. (2014). A complete Holocene record of trematode–bivalve infection and implications for the response of parasitism to climate change. *Proceedings of the National Academy of Sciences*, *111*(51), 18150–18155. https://doi.org/10.1073/pnas.1416747111

Huntley, J. W., & Scarponi, D. (2012). Evolutionary and ecological implications of trematode parasitism of modern and fossil northern Adriatic bivalves. *Paleobiology*, *38*(1), 40–51. https://doi.org/10.1666/10051.1

Huntley, J. W., & Scarponi, D. (2015). Geographic variation of parasitic and predatory traces on mollusks in the northern Adriatic Sea, Italy: implications for the stratigraphic paleobiology of biotic interactions. *Paleobiology*, *41*(1), 134–153. https://doi.org/10.1017/pab.2014.9

Imbrie, J. (1955). Biofacies Analysis. In A. Poldervaart (Ed.), *Crust of the Earth: A Symposium* (pp. 449–464). Geological Society of America. https://doi.org/10.1130/SPE62-p449

Jackson, D. A. (1993). Multivariate analysis of benthic invertebrate communities: the implication of choosing particular data standardizations, measures of association, and ordination methods. *Hydrobiologia*, *268*(1), 9–26. https://doi.org/10.1007/BF00005737

Jacobs, G. S., & Carlucci, J. R. (2019). Ontogeny and shape change of the phacopid trilobite Calyptaulax. *Journal of Paleontology*, *93*(6), 1105–1125. https://doi.org/10.1017/jpa.2019.38

James G. Schmitt, D. W. B. (1981). Patterns of Silicification in Permian Pelecypods and Brachiopods from Wyoming. *SEPM Journal of Sedimentary Research*, *51*(4), 1297–1308. https://doi.org/10.1306/212F7E91-2B24-11D7-8648000102C1865D

Jonsson, P. R., & Andé, C. (1992). Mass mortality of the bivalve Cerastoderma edule on the Swedish west coast caused by infestation with the digenean trematode Cercaria

cerastodermae. *Ophelia*, *36*(2), 151–157. https://doi.org/10.1080/00785326.1992.10430365

Jung, Y.-J., Yun, T.-S., Kim, K.-Y., & Choo, J.-H. (2011). Image Calibration Techniques for Removing Cupping and Ring Artifacts in X-ray Micro-CT Images. *Journal of the Korean Geotechnical Society*, *27*(11), 93–101. https://doi.org/10.7843/kgs.2011.27.11.093

Ketcham, R. A., & Carlson, W. D. (2001). Acquisition, optimization and interpretation of X-ray computed tomographic imagery: applications to the geosciences. *Computers & Geosciences*, *27*(4), 381–400. https://doi.org/10.1016/S0098-3004(00)00116-3

Key, M. M., Wyse Jackson, P. N., & Felton, S. H. (2016). Intracolony variation in colony morphology in reassembled fossil ramose stenolaemate bryozoans from the Upper Ordovician (Katian) of the Cincinnati Arch region, USA. *Journal of Paleontology*, *90*(3), 400–412. https://doi.org/10.1017/jpa.2016.66

Knell, R. J., & Fortey, R. A. (2005). Trilobite spines and beetle horns: sexual selection in the Palaeozoic? *Biology Letters*, *1*(2), 196–199. https://doi.org/10.1098/rsbl.2005.0304

Kovanen, D. J., & Easterbrook, D. J. (2002). Paleodeviations of radiocarbon marine reservoir values for the northeast Pacific. *Geology*, *30*(3), 243–246. https://doi.org/10.1130/0091-7613(2002)030<0243:PORMRV>2.0.CO;2

Kozloff, E. N. (2000). *Seashore life of the northern Pacific coast: An illustrated guide to northern California, Oregon, Washington, and British Columbia*. University of Washington Press.

Kruskal, J. B. (1964a). Multidimensional scaling by optimizing goodness of fit to a nonmetric hypothesis. *Psychometrika*, *29*(1), 1–27. https://doi.org/10.1007/BF02289565

Kruskal, J. B. (1964b). Nonmetric multidimensional scaling: A numerical method. *Psychometrika*, *29*(2), 115–129. https://doi.org/10.1007/BF02289694

Kuris, A. M., Hechinger, R. F., Shaw, J. C., Whitney, K. L., Aguirre-Macedo, L., Boch, C. A., Dobson, A. P., Dunham, E. J., Fredensborg, B. L., Huspeni, T. C., Lorda, J., Mababa, L., Mancini, F. T., Mora, A. B., Pickering, M., Talhouk, N. L., Torchin, M. E., & Lafferty, K. D. (2008). Ecosystem energetic implications of parasite and free-living biomass in three estuaries. *Nature*, *454*(7203), 515–518. https://doi.org/10.1038/nature06970

Kyriakou, Y., Prell, D., & Kalender, W. A. (2009). Ring artifact correction for high-resolution micro CT. *Physics in Medicine and Biology*, *54*(17), N385–N391. https://doi.org/10.1088/0031-9155/54/17/N02

Laufeld, S., & Jeppsson, L. (1976). Silicification and bentonites in the Silurian of Gotland. *Geologiska Föreningen i Stockholm Förhandlingar*, *98*(1), 31–44. https://doi.org/10.1080/11035897609454336

Legendre, P. (2018). *lmodel2: Model II Regression* (1.7-3).

Leslie, S. A. (1995). *Upper Middle Ordovician conodont biofacies and lithofacies distribution patterns in eastern North America and northwestern Europe: Evaluations using the Deicke, Millbrig and Kinnekulle potassium-bentonite beds as time planes*.

Leung, T. L. F. (2017). Fossils of parasites: what can the fossil record tell us about the evolution of parasitism? *Biological Reviews*, *92*(1), 410–430. https://doi.org/10.1111/brv.12238

Maliva, R. G., & Siever, R. (1988). Mechanism and Controls of Silicification of Fossils in Limestones. *The Journal of Geology*, *96*(4), 387–398. https://doi.org/10.1086/629235

Mann, H. B., & Whitney, D. R. (1947). On a Test of Whether one of Two Random Variables is Stochastically Larger than the Other. *The Annals of Mathematical Statistics*, *18*(1), 50–60. https://doi.org/10.1214/aoms/1177730491

Markussen, Ø., Dypvik, H., Hammer, E., Long, H., & Hammer, Ø. (2019). 3D characterization of porosity and authigenic cementation in Triassic conglomerates/arenites in the Edvard Grieg field using 3D micro-CT imaging. *Marine and Petroleum Geology*, *99*, 265–281. https://doi.org/10.1016/j.marpetgeo.2018.10.015

Mees, F., Swennen, R., Geet, M. van, & Jacobs, P. (2003). Applications of X-ray computed tomography in the geosciences. *Geological Society, London, Special Publications*, *215*(1), 1–6. https://doi.org/10.1144/GSL.SP.2003.215.01.01

Minchin, P. R. (1987). An evaluation of the relative robustness of techniques for ecological ordination. In I. C. Prentice & E. Maarel (Eds.), *Theory and models in vegetation science* (pp. 89–107). Springer Netherlands. https://doi.org/10.1007/978-94-009-4061-1_9

Mitchell, C. E., Adhya, S., Bergström, S. M., Joy, M. P., & Delano, J. W. (2004). Discovery of the Ordovician Millbrig K-bentonite Bed in the Trenton Group of New York State: Implications for regional correlation and sequence stratigraphy in eastern North America. *Palaeogeography, Palaeoclimatology, Palaeoecology*, *210*(2–4), 331–346. https://doi.org/10.1016/j.palaeo.2004.02.037

Mook, W. G., & Vogel, J. C. (1968). Isotopic Equilibrium between Shells and Their Environment. *Science*, *159*(3817), 874–875. https://doi.org/10.1126/science.159.3817.874

Morris, S. C. (1981). Parasites and the fossil record. *Parasitology*, *82*(3), 489–509. https://doi.org/10.1017/S0031182000067020

Mouritsen, K. N., & Poulin, R. (2002). Parasitism, community structure and biodiversity in intertidal ecosystems. *Parasitology*, *124*(7), 101–117. https://doi.org/10.1017/S0031182002001476

Mouritsen, K. N., & Poulin, R. (2005). Parasites boosts biodiversity and changes animal community structure by trait-mediated indirect effects. *Oikos*, *108*(2), 344–350. https://doi.org/10.1111/j.0030-1299.2005.13507.x

Munnecke, A., & Servais, T. (2008). Palaeozoic calcareous plankton: evidence from the Silurian of Gotland. *Lethaia*, *41*(2), 185–194. https://doi.org/10.1111/j.1502-3931.2008.00113.x

Muscente, A. D., Laflamme, M., Schiffbauer, J. D., Broce, J. S., O'Donnell, K. H., Boag, T. H., Meyer, M., Hawkins, A. D., Huntley, J. W., & Xiao, S. (2016). EXCEPTIONALLY PRESERVED FOSSIL ASSEMBLAGES THROUGH GEOLOGIC TIME AND SPACE. *Gondwana Research*, *48*, 164–188. https://doi.org/10.1130/abs/2016AM-282405

Nebelsick, J. H. (2004). Taphonomy of Echinoderms: introduction and outlook. In T. Heinzeller & J. H. Nebelsick (Eds.), *Echinoderms: Munchen* (pp. 471–477). CRC Press. https://doi.org/10.1201/9780203970881

Oksanen, J., Blanchet, F. G., Friendly, M., Kindt, R., Legendre, P., McGlinn, D., Minchin, P. R., O'Hara, R. B., Simpson, G. L., Solymos, P., Stevens, M. H. H., Szoecs, E., & Wagner, H. (2022). *vegan: Community Ecology Package* (2.6-2).

Orhan, K., de Faria Vasconcelos, K., & Gaêta-Araujo, H. (2020). Artifacts in Micro-CT. In K. Orhan (Ed.), *Micro-computed Tomography (micro-CT) in Medicine and Engineering* (pp. 35–48). Springer International Publishing. https://doi.org/10.1007/978-3-030-16641-0_4

Padilla, C. B., Páramo, M. E., Noè, L., Gómez Pérez, M., & Luz Parra, M. (2010). Acid Preparation of Large Vertebrate Specimens. *The Geological Curator*, *9*(3), 85–92.

Paladini, G., Longshaw, M., Gustinelli, A., & Shinn, A. P. (2017). Parasitic Diseases in Aquaculture: Their Biology, Diagnosis and Control. In B. Austin & A. Newaj-Fyzul (Eds.), *Diagnosis and Control of Diseases of Fish and Shellfish* (pp. 37–107). John Wiley & Sons, Ltd. https://doi.org/10.1002/9781119152125.ch4

Park, H. S., Chung, Y. E., & Seo, J. K. (2015). Computed tomographic beam-hardening artefacts: mathematical characterization and analysis. *Philosophical Transactions of the Royal Society A: Mathematical, Physical and Engineering Sciences*, *373*, 1–11. https://doi.org/10.1098/rsta.2014.0388

Pearson, K. (1900). On the criterion that a given system of deviations from the probable in the case of a correlated system of variables is such that it can be reasonably supposed to have arisen from random sampling. *The London, Edinburgh, and Dublin Philosophical Magazine and Journal of Science*, *50*(302), 157–175. https://doi.org/10.1080/14786440009463897

Pearson, K. (1901). On lines and planes of closest fit to systems of points in space. *The London, Edinburgh, and Dublin Philosophical Magazine and Journal of Science*, *2*(11), 559–572. https://doi.org/10.1080/14786440109462720

Penick, D. A. (1987). Pyrite and other Minerals from Bargers Quarry. *Rocks & Minerals*, *62*(2), 109–113. https://doi.org/10.1080/00357529.1987.11762637

Polenz, M., Schasse, H. W., & Petersen, B. B. (2005). *Geologic map of the Freeland and northern part of the Hansville 7.5-minute Quadrangles, Island County, Washington*.

Polenz, M., Slaughter, S. L., & Thorsen, G. W. (2006). *Geologic map of the Coupeville and part of the Port Townsend North 7.5-minute quadrangles, Island County, Washington*.

Pruss, S. B., Payne, J. L., & Westacott, S. (2015). Taphonomic bias of selective silicification revealed by paired petrographic and insoluble residue analysis. *Palaios*, *30*(8), 620–626. https://doi.org/10.2110/palo.2014.105

R Core Team. (2017). *R: A Language and Environment for Statistical Computing* (3.4.1). R Foundation for Statistical Computing.

Raup, D. M. (1975). Taxonomic diversity estimation using rarefaction. *Paleobiology*, *1*(4), 333–342. https://doi.org/10.1017/S0094837300002633

Read, J. F. (1980). Carbonate Ramp-to-Basin Transitions and Foreland Basin Evolution, Middle Ordovician, Virginia Appalachians. *AAPG Bulletin*, *64*(10), 1575–1612.

Read, J. F. (1982). Geometry, facies, and development of Middle Ordovician carbonate buildups, Virginia Appalachians. *AAPG Bulletin*, *66*(2), 189–209.

Read, J. F., & Eriksson, K. A. (2016). Paleozoic Sedimentary Successions of the Virginia Valley & Ridge and Plateau. In C. M. Bailey, W. C. Sherwood, L. S. Eaton, & D. S. Powars (Eds.), *The Geology of Virginia*. Virginia Museum of Natural History.

Remeysen, K., & Swennen, R. (2006). Beam hardening artifact reduction in microfocus computed tomography for improved quantitative coal characterization. *International Journal of Coal Geology*, *67*(1–2), 101–111. https://doi.org/10.1016/j.coal.2005.10.001

Rogers, R. R., Curry Rogers, K. A., Bagley, B. C., Goodin, J. J., Hartman, J. H., Thole, J. T., & Zatoń, M. (2018). Pushing the record of trematode parasitism of bivalves upstream and back to the Cretaceous. *Geology*, *46*(5), 431–434. https://doi.org/10.1130/G40035.1

Ruiz, G. M., & Lindberg, D. R. (1989). A fossil record for trematodes: extent and potential uses. *Lethaia*, *22*(4), 431–438. https://doi.org/10.1111/j.1502-3931.1989.tb01447.x

Sánchez, J. A., Lasker, H. R., Nepomuceno, E. G., Sánchez, J. D., & Woldenberg, M. J. (2004). Branching and Self-Organization in Marine Modular Colonial Organisms: A Model. *The American Naturalist*, *163*(3), E24–E39. https://doi.org/10.1086/382139

Sanders, H. L. (1968). Marine Benthic Diversity: A Comparative Study. *The American Naturalist*, *102*(925), 243–282. https://doi.org/10.1086/282541

Scarponi, D., Azzarone, M., Kowalewski, M., & Huntley, J. W. (2017). Surges in trematode prevalence linked to centennial-scale flooding events in the Adriatic. *Scientific Reports*, *7*(1), 5732. https://doi.org/10.1038/s41598-017-05979-6

Schiffbauer, J. D., Selly, T., Jacquet, S. M., Merz, R. A., Nelson, L. L., Strange, M. A., Cai, Y., & Smith, E. F. (2020). Discovery of bilaterian-type through-guts in cloudinomorphs from the terminal Ediacaran Period. *Nature Communications*, *11*(1), 205. https://doi.org/10.1038/s41467-019-13882-z

Schiffbauer, J. D., Xiao, S., Cai, Y., Wallace, A. F., Hua, H., Hunter, J., Xu, H., Peng, Y., & Kaufman, A. J. (2014). A unifying model for Neoproterozoic–Palaeozoic exceptional fossil preservation through pyritization and carbonaceous compression. *Nature Communications*, *5*(1). https://doi.org/10.1038/ncomms6754

Schindelin, J., Arganda-Carreras, I., Frise, E., Kaynig, V., Longair, M., Pietzsch, T., Preibisch, S., Rueden, C., Saalfeld, S., Schmid, B., Tinevez, J.-Y., White, D. J., Hartenstein, V., Eliceiri, K., Tomancak, P., & Cardona, A. (2012). Fiji: an open-source platform for biological-image analysis. *Nature Methods*, *9*(7), 676–682. https://doi.org/10.1038/nmeth.2019

Schladitz, K. (2011). Quantitative micro-CT. *Journal of Microscopy*, *243*(2), 111–117. https://doi.org/10.1111/j.1365-2818.2011.03513.x

Sell, B., Ainsaar, L., & Leslie, S. (2013). Precise timing of the Late Ordovician (Sandbian) super-eruptions and associated environmental, biological, and climatological events. *Journal of the Geological Society*, *170*(5), 711–714. https://doi.org/10.1144/jgs2012-148

Simpson, E. H. (1949). Measurement of Diversity. *Nature*, *163*(4148), 688–688. https://doi.org/10.1038/163688a0

Slice, D. E., Bookstein, F. L., Marcus, L. F., & Rohlf, F. J. (2009, February 12). *A Glossary for Geometric Morphometrics*. Https://Sbmorphometrics.Org/Glossary/Gloss1.Html.

Slowikowski, K., Schep, A., Hughes, S., Dang, T. K., Lukauskas, S., Irisson, J.-O., Kamvar, Z. N., Ryan, T., Christophe, D., Hiroaki, Y., Gramme, P., Abdol, A. M.,

Barrett, M., Cannoodt, R., Krassowski, M., Chirico, M., & Aphalo, P. (2021). *ggrepel: Automatically Position Non-Overlapping Text Labels with "ggplot2"* (0.9.1).

Southon, J., & Santos, G. M. (2007). Life with MC-SNICS. Part II: Further ion source development at the Keck carbon cycle AMS facility. *Nuclear Instruments and Methods in Physics Research Section B: Beam Interactions with Materials and Atoms*, *259*(1), 88–93. https://doi.org/10.1016/j.nimb.2007.01.147

st. Clair, D. W. (1935). The Use of Acetic Acid to Obtain Insoluble Residues. *SEPM Journal of Sedimentary Research*, *5*, 146–149. https://doi.org/10.1306/D4268F3B-2B26-11D7-8648000102C1865D

Stuiver, M., & Polach, H. A. (1977). Discussion Reporting of 14 C Data. *Radiocarbon*, *19*(3), 355–363. https://doi.org/10.1017/S0033822200003672

Stuiver, M., Reimer, P. J., & Braziunas, T. F. (1998). High-Precision Radiocarbon Age Calibration for Terrestrial and Marine Samples. *Radiocarbon*, *40*(3), 1127–1151. https://doi.org/10.1017/S0033822200019172

Tanaka, N., Monaghan, M. C., & Rye, D. M. (1986). Contribution of metabolic carbon to mollusc and barnacle shell carbonate. *Nature*, *320*, 520–523. https://doi.org/10.1038/320520a0

Todd, J. A., & Harper, E. M. (2011). Stereotypic boring behaviour inferred from the earliest known octopod feeding traces: Early Eocene, southern England. *Lethaia*, *44*(2), 214–222. https://doi.org/10.1111/j.1502-3931.2010.00237.x

Toombs, H. A., & Rixon, A. E. (1959). The Use of Acids in the Preparation of Vertebrate Fossils. *Curator*, *2*(4), 304–312. https://doi.org/10.1111/j.2151-6952.1959.tb00514.x

Torgerson, W. S. (1958). *Theory and Methods of Scaling*. Wiley.

van Olphen, H. (1964). Internal mutual flocculation in clay suspensions. *Journal of Colloid Science*, *19*(4), 313–322. https://doi.org/10.1016/0095-8522(64)90033-9

Vannier, J., Vidal, M., Marchant, R., el Hariri, K., Kouraiss, K., Pittet, B., el Albani, A., Mazurier, A., & Martin, E. (2019). Collective behaviour in 480-million-year-old trilobite arthropods from Morocco. *Scientific Reports*, *9*(1), 14941. https://doi.org/10.1038/s41598-019-51012-3

Vodrážka, R. (2009). A New Method for the Extraction of Macrofossils From Calcareous Rocks Using Sulphuric Acid. *Palaeontology*, *52*(1), 187–192. https://doi.org/10.1111/j.1475-4983.2008.00829.x

Walossek, D., Repetski, J. E., & Müller, K. J. (1994). An exceptionally preserved parasitic arthropod, Heymonsicambria taylori n.sp. (Arthropoda incertae sedis: Pentastomida), from Cambrian – Ordovician boundary beds of Newfoundland,

Canada. *Canadian Journal of Earth Sciences*, *31*(11), 1664–1671. https://doi.org/10.1139/e94-149

Walton, W. H. (1948). Feret‘s Statistical Diameter as a Measure of Particle Size. *Nature*, *162*, 329–330. https://doi.org/10.1038/162329b0

Westrop, S. R. (1986). Taphonomic versus ecologic controls on taxonomic relative abundance patterns in tempestites. *Lethaia*, *19*(2), 123–132. https://doi.org/10.1111/j.1502-3931.1986.tb00722.x

Whittington, H. B., & Evitt, W. R. I. (1953). Silicified Middle Ordovician Trilobites. *Geological Society of America Memoirs*, *59*, 1–137. https://doi.org/10.1130/MEM59

Wickham, H. (2016). *ggplot2: Elegant Graphics for Data Analysis*. Springer-Verlag.

Wickham, H., Chang, W., Henry, L., Pedersen, T. L., Takahashi, K., Wilke, C., Woo, K., Yutani, H., & Dunnington, D. (2022). *ggplot2: Create Elegant Data Visualisations Using the Grammar of Graphics* (3.3.6).

Williams, M., & Vannier, J. M. C. (1995). Middle Ordovician Aparchitidae and Schmidtellidae: the significance of ‘featureless’ ostracods. *Journal of Micropalaeontology*, *14*(1), 7–24. https://doi.org/10.1144/jm.14.1.7

Wright, P., Cherns, L., & Hodges, P. (2003). Missing molluscs: Field testing taphonomic loss in the Mesozoic through early large-scale aragonite dissolution. *Geology*, *31*(3), 211–214. https://doi.org/10.1130/0091-7613(2003)031<0211:MMFTTL>2.0.CO;2

Yang, F. ., Nasr-El-Din, H. A., & Al-Harbi, B. . (2012, February). Acidizing Sandstone Reservoirs Using HF and Formic Acids. *SPE International Symposium and Exhibition on Formation Damage Control*. https://doi.org/10.2118/150899-MS

Yoneda, M., Uno, H., Shibata, Y., Suzuki, R., Kumamoto, Y., Yoshida, K., Sasaki, T., Suzuki, A., & Kawahata, H. (2007). Radiocarbon marine reservoir ages in the western Pacific estimated by pre-bomb molluscan shells. *Nuclear Instruments and Methods in Physics Research Section B: Beam Interactions with Materials and Atoms*, *259*(1), 432–437. https://doi.org/10.1016/j.nimb.2007.01.184

Yousuf, M. A., & Asaduzzaman, M. (2009). An Efficient Ring Artifact Reduction Method Based on Projection Data for Micro-CT Images. *Journal of Scientific Research*, *2*(1), 37–45. https://doi.org/10.3329/jsr.v2i1.2645

Zhang, Z., Strotz, L. C., Topper, T. P., Chen, F., Chen, Y., Liang, Y., Zhang, Z., Skovsted, C. B., & Brock, G. A. (2020). An encrusting kleptoparasite-host interaction from the early Cambrian. *Nature Communications*, *11*(1), 2625. https://doi.org/10.1038/s41467-020-16332-3

VITA

Gabriel S. Jacobs is a native of Evanston, IL, and credits his Chicagoland upbringing with exposing him to the Field Museum of Natural History and inspiring a lifelong fascination with the history and prehistory of the natural world. Before attending Mizzou as a doctoral student, he earned a B.S. from the University of Chicago (2013) and a M.S. from Midwestern State University (2017). He's pretty sure that writing this all up took six months off his life.

His research interests include trilobites, silicification, silicified trilobites, and even parasitic interactions, and he spends his free time with video games, home cooking, and sci-fi/fantasy novels. He has previously kept honeybees and always looks a little blurry.

In keeping with his career interests in education and outreach, he has accepted an engagement as a visiting Lecturer in Geology at Cornell College for the 2022-23 school year.

Eamus Catuli, Urbs In Horto, Illegitimi Non Carborundum.